SHEAR WAVE VELOCITY ANALYSIS BY SURFACE WAVE METHODS IN THE BOSTON AREA

Author: Siyu Liu

SHEAR WAVE VELOCITY ANALYSIS BY SURFACE WAVE METHODS IN THE BOSTON AREA

Siyu Liu

A thesis

submitted to the Faculty of

the department of Earth and Environmental Sciences

in partial fulfillment

of the requirements for the degree of

Master of Science

Boston College
Morrissey College of Arts and Sciences
Graduate School

April, 2017

SHEAR WAVE VELOCITY ANALYSIS BY SURFACE WAVE METHODS IN THE BOSTON AREA

Siyu Liu

Advisor: Prof. John E. Ebel, Ph.D.

ABSTRACT

As the best seismic indicator of shear modulus, shear-wave velocity is an important property in engineering problems in near-surface site characterization. Several surface-wave methods have been developed to obtain the subsurface shear-wave velocity structure. This thesis compared three surface-wave methods, Spectral Analysis of Surface Waves (SASW) (Nazarian et al., 1983), Multichannel Analysis of Surface Waves (MASW) (Park et al., 1999), and Refraction Microtremor (ReMi) (Louie, 2001), to determine which method gives the best estimation of the 1-D shear-wave velocity profile of near-surface soils. We collected seismic data at three sites in the greater Boston area where there are direct measurements of shear-wave velocities for comparison. The three methods were compared in terms of accuracy and precision. Overall, the MASW and the ReMi methods have comparable quality of accuracy, whereas the SASW method is the least accurate method with the highest percentage differences with direct measurements. The MASW method is the most precise method among the three methods with the smallest standard deviations. In general, the MASW method is concluded to be the best surface-wave method in determining the shear-wave velocities of the subsurface structure in the greater Boston area.

TABLE OF CONTENTS

LIST OF TABLES

LIST OF FIGURES

ACKNOWLEDGMENT

I offer my sincere appreciation to Professor John E. Ebel, my advisor and mentor, who have been supportive through my research with expert advice and encouragement. He has shown me, by his example, what a good scientist should be. I would also like to thank Professor Alan K. Kafka and Professor Seth Kruckenberg, who have provided me extensive professional guidance of scientific research as my academic committee members. This work would not have been well-accomplished without the financial support from the Boston College department of Earth and Environmental Sciences of a full scholarship with a teaching assistantship, the Linehan Fund and the Skehan Fund.

I cannot express enough thanks to those with whom I have had the pleasure to work during this thesis project. I am especially grateful to Professor Alfredo Urzua for providing me with crucial information and unlimited helpful material. Thank you Vincent Murphy for your warm support of helping me accomplish a high-quality thesis and your parental care for my life. I would also like to thank Parker Aubin, Marshall Pontrelli and Marina Borja for their wonderful collaboration, and all my colleagues at Boston College for their continued support and companion.

I would like to express my deepest gratitude to my family. Knowing that their love and support are always there with me saved me uncountable times from falling apart. Thank you Shenglin Zheng and Shufan Feng for always saving the protected time for me to rest and take a breath. Your supportive companion provides me more than friends could function. Most importantly, I would like to thank the best musician in my heart, band Guckkasten, for transferring to me endless inspiration through their music and their motivating spiritual world.

INTRODUCTION

Shear modulus is one of the most pivotal parameters in engineering problems involving the mechanical behavior of rock and soil. Shear-wave velocity (Vs) is the best seismic indicator of shear modulus. A number of in-situ test methods have been developed to measure the variation of shear-wave velocity with depth in soil, such as crosshole seismic velocity measurements using body waves. Previous research of surface-wave methods, such as Spectral Analysis of Surface Waves (SASW) (Nazarian et al., 1983), Multichannel Analysis of Surface Waves (MASW) (Park et al., 1999), and Refraction Microtremor (ReMi) (Louie, 2001), has shown that inverting surface waves for subsurface shear-wave velocities is a good way to obtain subsurface shear-wave velocities. Compared to body-wave methods, surface-wave methods are noninvasive and can be employed more rapidly and economically.

The major objective of this thesis is to compare the three surface-wave analysis methods SASW, MASW, and ReMi for determining the shear-wave velocity structure of surficial soil layers in the greater Boston area, focusing specifically on the 1D shear-wave velocity profile (Vs profile) with depth. Considering the shear-wave velocities derived from direct measurements as the target values against which the surface-wave velocity profiles are to be compared, this thesis seeks to determine which of these three

methods gives the best estimate of the shear-wave velocity profile with the smallest uncertainty.

Shear modulus characterizes the softness of the ground, which affects the level of ground shaking during an earthquake. Softer soil contributes to greater shaking or amplification of the seismic waves produced by an earthquake (https://training.fema.gov/emiweb/earthquake/NEH0102320.htm). Shear modulus is an important property for site classification, seismic hazard analysis, site seismic response analysis, and soil–structure interaction (Wair et al., 2012). As the best seismic indicator of shear modulus, shear-wave velocity is closely related to the rigidity of sediments (Castellaro et al., 2008) and plays an important role in a variety of applications in near-surface site characterization, including geotechnical applications of earthquake site response, dynamic soil-structure interaction, nondestructive pavement testing, evaluation of ground modification, etc. (Foti et al., 2014). Therefore, it is of vital importance to investigate how well different methods determine a local shear-wave velocity profile. The SASW, MASW and ReMi methods are tested and compared in this thesis project.

Surface waves, commonly known as ground roll in reflection seismology, are seismic waves that propagate horizontally along the earth's surface (Sheriff and Geldart, 1995). This thesis focuses on one kind of surface wave, the Rayleigh wave, because it is detected by vertical-component seismometers, which are commonly used in shallow seismic profiles. Rayleigh waves of lower frequencies have relatively longer wavelengths than higher-frequency Rayleigh waves. The penetration depth of Rayleigh waves

depends on wavelength. Rayleigh waves of longer wavelengths penetrate deeper into the Earth than waves of shorter wavelengths. Because the velocity of seismic waves usually increases with depth, the longer wavelength (lower frequency) waves can travel faster than the shorter wavelength (higher frequency) waves. Due to this property, surface waves are dispersive, with group velocity changing with frequency. The dispersion property is an important feature of surface waves and is caused by variations with depth of the S-wave velocity. Therefore, observations of surface-wave dispersion can be used to estimate variations of shear-wave velocity with depth (Park et al., 1999; Stokoe et al., 1994).

Compared to conventional body-wave methods (for example, S-wave refraction, reflection, or downhole and crosshole surveys) to estimate shear-wave velocity for shallow soil layers, the surface-wave methods have several apparent advantages. In comparison to reflection surveys, the field data acquisition is easier because surface waves always have the strongest energy on the seismograms. Furthermore, the surface-wave methods are noninvasive and do not require boreholes to implement them. In addition, with surface wave methods, a large area can be covered within a relatively short time period, and the data processing procedure is straightforward. Surface-wave methods are, therefore, highly cost-effective and time efficient. There are many published comparisons of surface-wave methods. However, not many of them include comparisons with crosshole surveys, and still fewer are in New England. Therefore, detailed comparisons of shear-wave velocity estimation methods need be conducted in

subsoil areas up to a few tens of meters in depth in New England to verify the accuracy of these methods in this region.

1.0 METHODS

1.1 Surface-wave methods

This section introduces the three surface-wave methods that are compared in this thesis, namely: Spectral Analysis of Surface Waves (SASW), Multichannel Analysis of Surface Waves (MASW), and Refraction Microtremor (ReMi).

1.1.1 Spectral Analysis of Surface Waves (SASW) (Nazarian et al., 1983)

As shown in **Figure 1**, the SASW method uses the spectral analysis of surface waves (also called ground roll in exploration seismology) generated by active sources and recorded repeatedly by a pair of seismometers at small (1 m) to large (500 m) distances (Nazarian and Desai, 1993). The single pair of receivers is configured and reconfigured as many times as necessary to sample the desired wavelength range. The phase velocities are derived in the frequency domain to produce a dispersion curve by computing the phase difference between waveforms recorded by each seismometer pair for each source activation (Gucunski and Woods, 1991).

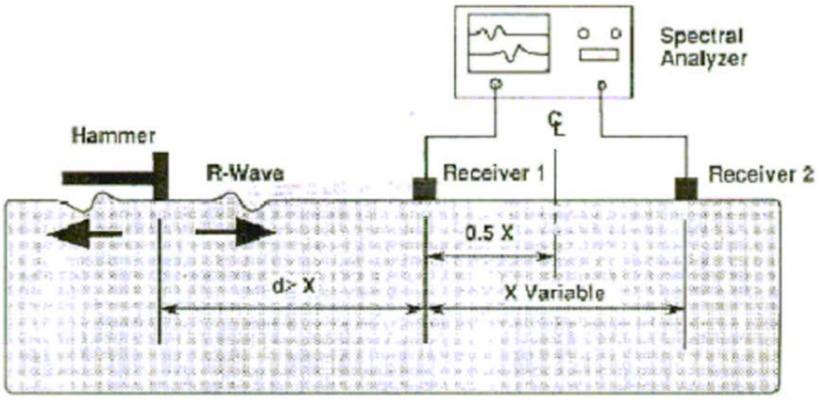

Figure 1: Schematic diagram of SASW data acquisition (Malhotra and Carino, 1991)

1.1.2 Multichannel analysis of surface waves (MASW) (Park et al., 1998, 1999)

Changing receiver positions as required in the SASW method is time consuming. Moreover, because the periodicity of the phase shift between the two receivers leads to "unwrapped" phase on the cross-power spectrum that is used to calculate the Rayleigh phase velocity, the interpretation of SASW data requires subjective judgment and cannot be easily automated (Foti et al., 2014). In response to the shortcomings of SASW, the MASW technique (Park et al., 1999) was developed to enhance the accuracy of the results from the analysis with multiple receivers. As shown in **Figure 2**, the basic field configuration and acquisition routine for MASW is generally the same as that used in conventional common midpoint (CMP) body-wave reflection surveys. It utilizes data from multichannel shot gathers, usually with 24 or 48 geophones. The most common techniques to process the MASW data are transform-based approaches. Field data collected in the time-space domain are transformed into a domain where the phase velocities associated with different frequencies are easily chosen by picking the spectral

maxima. The MASW data are transformed into the frequency-wavenumber domain for the dispersion analyses in this thesis.

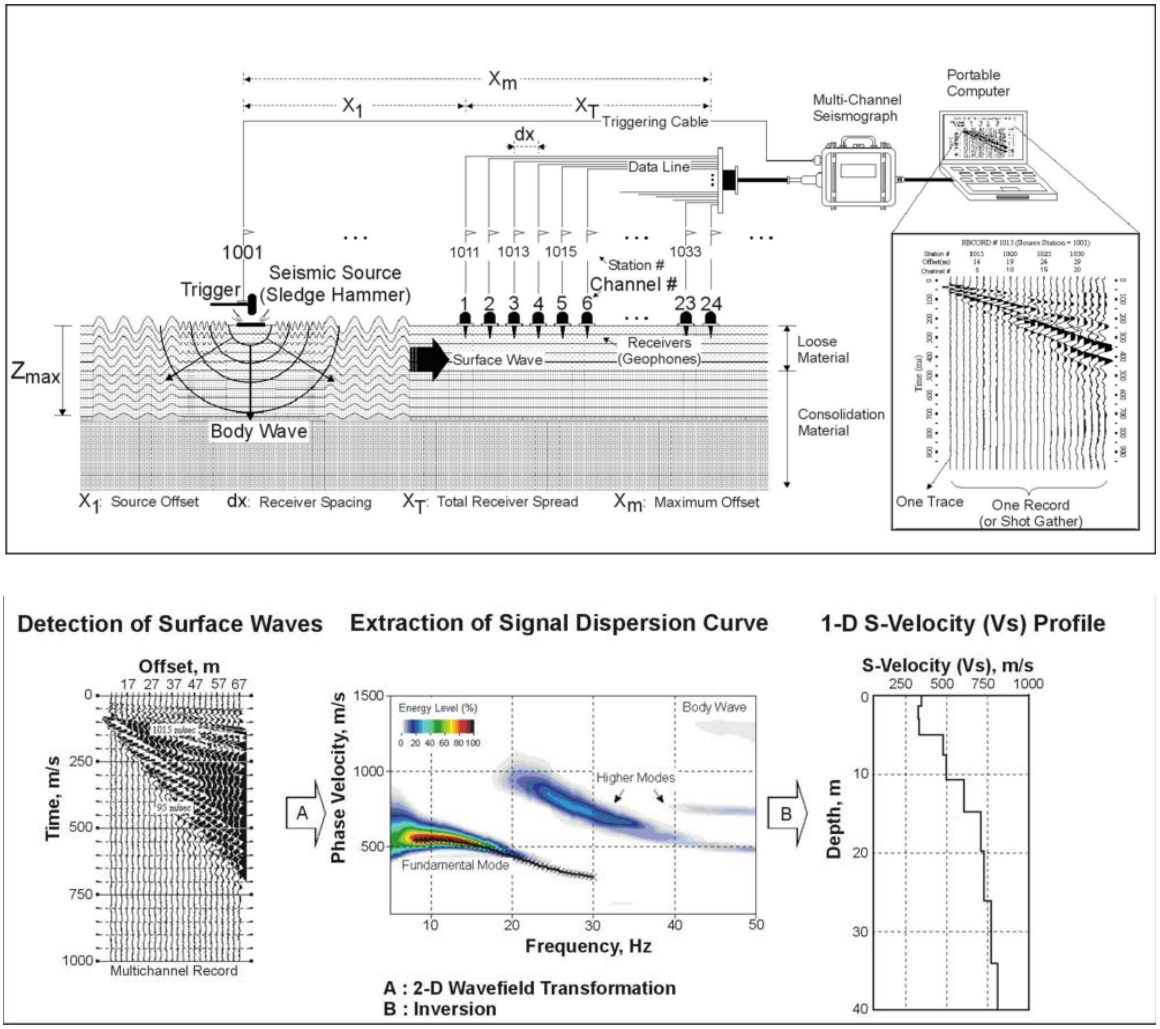

Figure 2: Field configuration and signal processing diagram for MASW (http://www.zapatainc.com)

1.1.3 Refraction Microtremor (ReMi) (Louie, 2001)

The ReMi method is a passive surface-wave method that collects the ambient noise in a relatively low-frequency range which is generally dominated by surface-wave components. The noise may be generated by human activities such as road traffic and industrial activities, by atmospheric movements, and/or by natural sources. ReMi uses

the same field setting as a shallow P-wave refraction survey to record surface waves at low frequencies (e.g. <10 Hz) and to large depths (e.g. >30 m) (Strobbia and Cassiani, 2011). After transforming the time series to the frequency-slowness domain to separate the Rayleigh waves from other seismic arrivals (e.g., body waves), the dispersion curve can be picked on the slowness-frequency image at the frequencies where surface-wave dispersion amplitudes appear (Louie, 2001). The dispersion curve is then used to estimate the Vs profile.

1.2 Data acquisition

In field data acquisition, surface waves can be generated using controlled sources (e.g., sledge hammer) or noise sources (e.g., a vehicle travelling along the length of the array). In this project, the SEISTRONIX Exploration Seismographic system was used for data acquisition. A sledge hammer was used as the source to collect active data for this thesis. Passive-source surveys using the surface waves in ambient background noise also were conducted. The data were collected in Canton, at the Fore River bridge and at Winchester High School.

Geophones were deployed with either spikes or tripods (**Figure 3**) depending on the condition of the site. Geophones with spikes have better coupling with the soil because the spikes are fully inserted into the soil and are less influenced by wind or human disturbance than when the geophones are set on the ground. At sites that are made up of soft soil, the geophones with spikes were planted into the ground (in Canton, Line 1 in Fore River, and Line 2 in Winchester). However, at sties that are made up of compressed gravels (Line 2 in Fore River) or at a paved area (Line 1 in Winchester), it is

hard to insert spikes into the ground. At these places, the data were collected with geophones mounted on tripods.

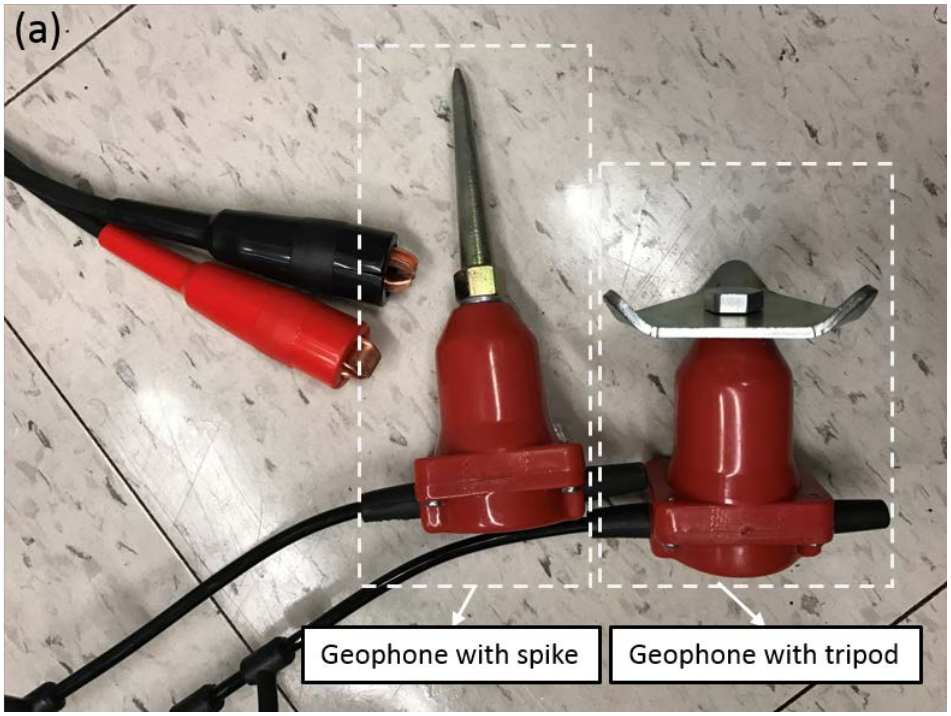

(b) Geophone with spike

(c) Geophone with tripod

Figure 3: These are examples of geophones with spikes or tripods. (a) These photographs show a geophone with a spike base and a geophone with a tripod base. (b) Examples of the installation of a geophone with a spike base, where the spikes have been pushed into the ground. (c) Examples of geophones with tripods that have been installed on a paved surface.

1.3 Data processing

The processing of surface-wave data can be divided into three parts: preprocessing, dispersion analysis, and modeling. Preprocessing includes transforming the data format from .dat to .sg2 or .sgy, calibrating the geometry parameters and deleting bad traces.

The dispersion analysis is the process of obtaining a dispersion curve, which is a plot of phase velocity versus frequency, from field data. After transforming the field data into a dispersion spectrum using 2D Fourier transforms, the dispersion curve is obtained by picking the energy peaks on the dispersion spectrum. One pick makes up one dispersion point. Connecting all the dispersion points on one spectrum yields the

dispersion curve. In this thesis, the fundamental-mode Rayleigh wave is the signal that is to be analyzed. At any given frequency the fundamental-mode travels the slowest among the different modes of Rayleigh waves. Correspondingly, the dispersion points are picked on the energy peak that has the lowest velocity among the local peaks seen on the dispersion spectrum.

The dispersion curve is used in the forward modeling of the shear-wave velocity models. Then the models are input into the iterative inversion process to obtain the best estimate of the shear-wave velocity profile. With an initial earth model that consists of a set of S-wave velocities, layer thicknesses, and Poisson's ratios and density values, one for each depth for which the earth model is being computed, the inversion process uses a least-square approach to converge to a best estimate model of the S-wave velocity with depth (Park et al., 1999).

1.4 Processing software

There are two software packages that were used in this thesis to process the surface-wave data, the Surface module of Geogiga Seismic Pro by Geogiga Technology Corp. for the active methods (MASW and SASW), and SeisOpt by Optim for the passive method (ReMi). Each of these packages is described in the following subsections.

1.4.1 Surface module of Geogiga Seismic Pro

In the Surface module of Geogiga Seismic Pro, after importing the field data into the program and pre-processing the data, the dispersion spectrum is calculated from a frequency-wavenumber 2-D Fourier transform of the data (**Figure 4**).

As defined in the user's manual of the software, the HV curve denotes a curve of depth versus phase velocity. The HV curve is generated by $D_i = \alpha \cdot \lambda_i$, where D is the profile depth, α is the default conversion factor which is set to equal to 0.5, and $\lambda = v/f$ is the wavelength of the Rayleigh wave.

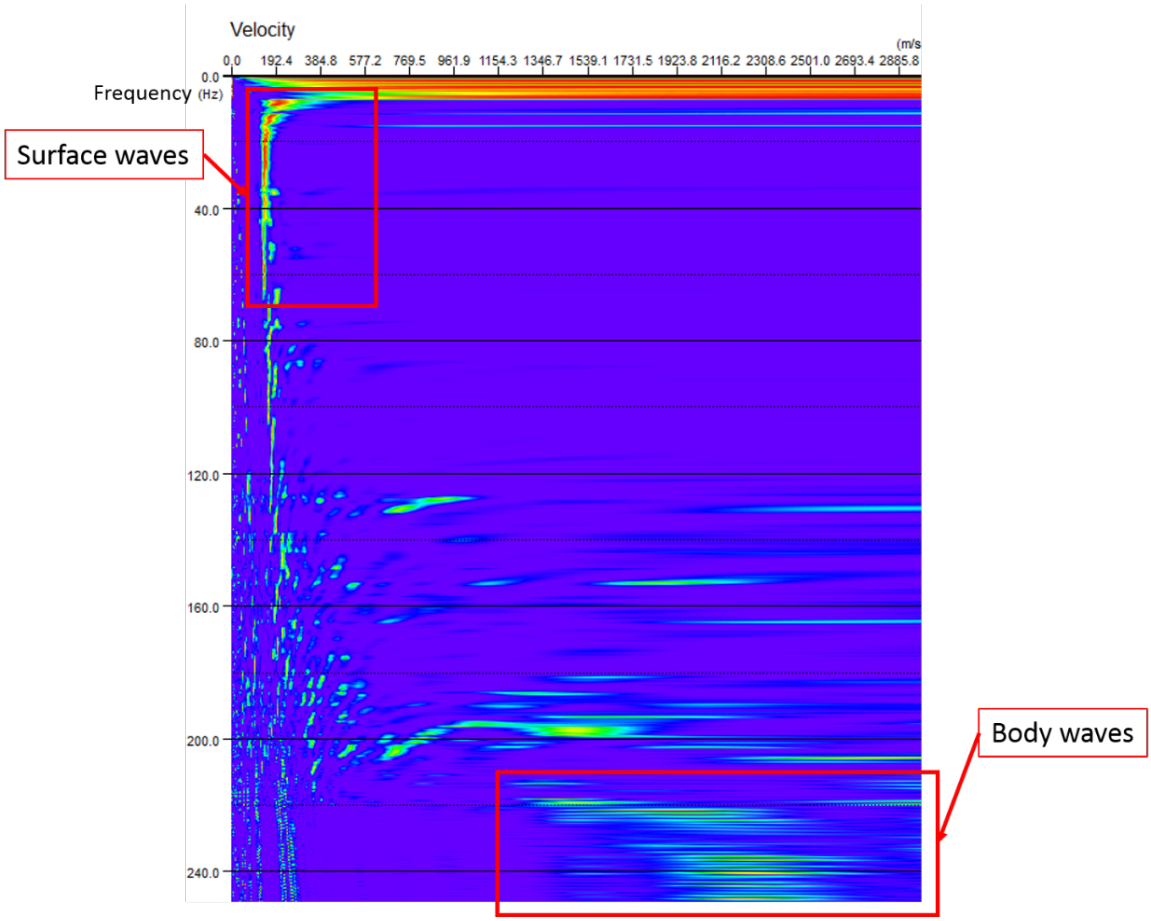

Figure 4: Example of a dispersion spectrum. The surface wave energy is isolated from that of the body waves on the dispersion spectrum. The horizontal axis is phase velocity in m/s; the vertical axis is frequency in Hz.

Figure 5 shows an example of how the fundamental-mode Rayleigh-wave dispersion curve is picked on the dispersion spectrum using the continuous picking option. This option uses using a combination of manually picking and automatic picking. The start point (point A in **Figure 5**) and the end point (point B in **Figure 5**) of the

dispersion curve are determined by the user. By clicking on the start point and dragging the mouse along the energy peaks, the program finds the dispersion points automatically at each frequency until the mouse is released at the end point. The points that are picked on the dispersion spectrum form the dispersion curve. Because the energy peaks on the dispersion spectrum are usually clear and continuous at high frequencies (> 15 Hz), there are more dispersion points at those frequencies than at low frequencies (< 15 Hz).

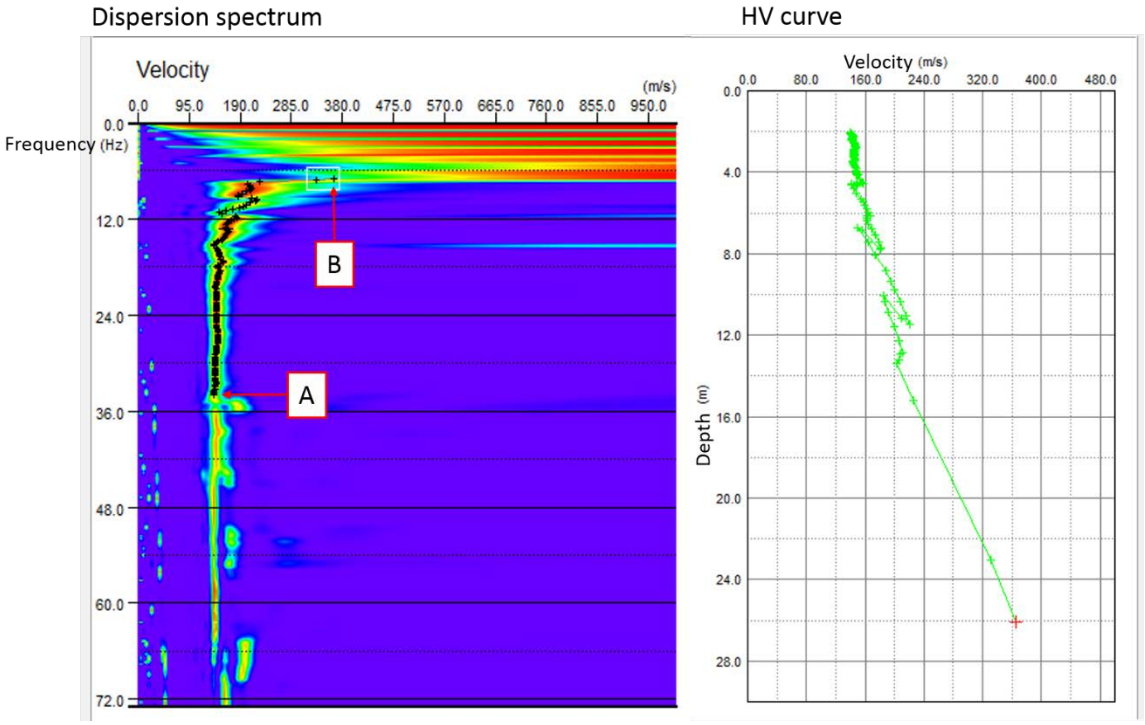

Figure 5: Example of the dispersion analysis. The black dots on the dispersion spectrum (left plot) are the dispersion points picked by the continuous picking option in the software. The picking starts at point A by clicking the left mouse button, and then after dragging along the peaks of the spectrum, the picking stops at point B. As the dispersion curve is picked, the observed HV curve is calculated and displayed in green on the panel on the right.

When picking the dispersion points on the dispersion spectra, if low-velocity trends are in the same velocity-frequency window on the dispersion spectra of multiple shot records, a low-velocity layer is assumed to cause this low velocity trend, and a low-velocity zone is included when building the forward models. An example of a low-velocity trend on a dispersion spectrum with its corresponding HV curve compared with a typical dispersion curve is shown in **Figure 6**. If the low-velocity trends do not appear in the same velocity-frequency windows on multiple dispersion spectra, the low-velocity trends are regarded as the interference of higher mode Rayleigh waves, and thus no low-velocity layer is included in the forward models.

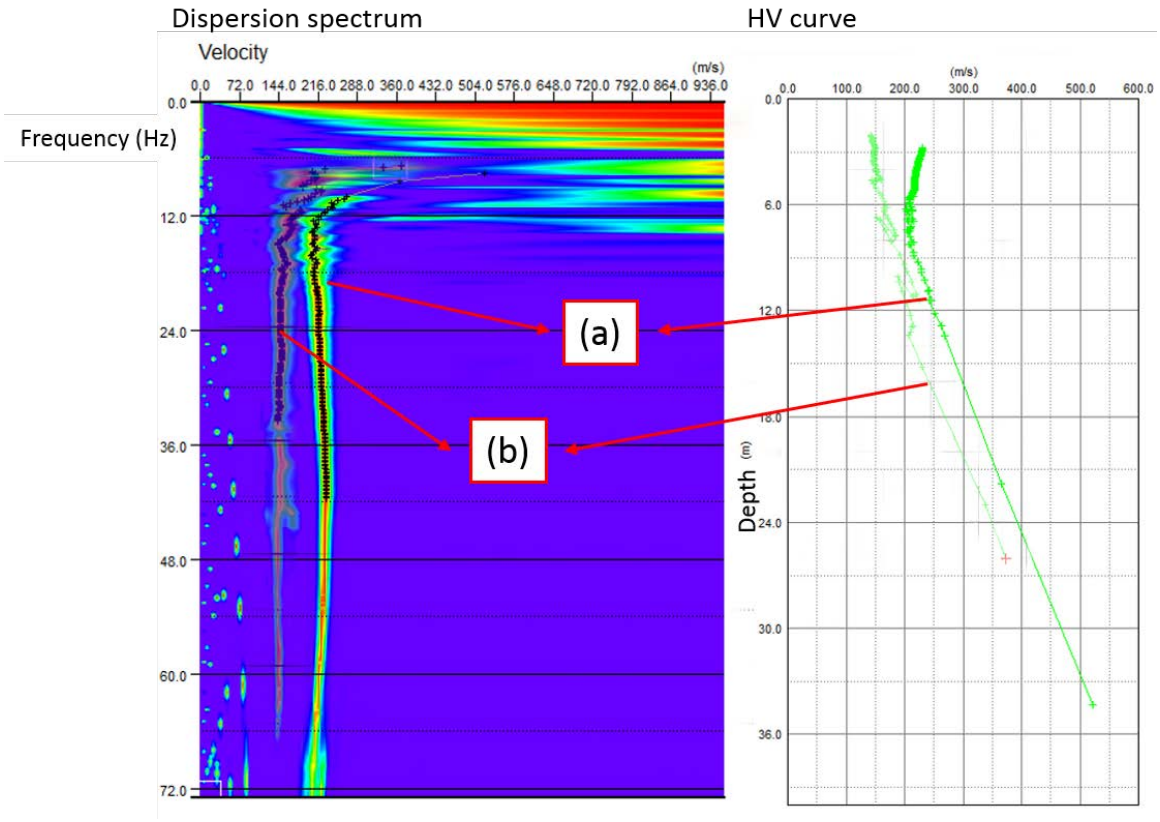

Figure 6: The two curves labeled by box (a) on the dispersion spectrum and the HV curve show an example of a low-velocity trend on the dispersion spectrum. By recognizing this low-velocity trend as a sign of low-velocity layer, the dispersion points were picked along the low-velocity trend. Correspondingly, it shows a low-velocity layer

on the HV curve. In comparison, the two curves labeled by box (b) are an example of a normal dispersion curve and its corresponding HV curve.

The Rayleigh-wave phase velocity for the kinds of surficial materials typically found in the Boston area is usually ranges from several tens of m/s to 400 - 500 m/s. If the dispersion points picked have higher velocities than this range, for example 800 - 900 m/s, these points may need to be adjusted or deleted. An example of deleting dispersion points is shown in **Figure 7**.

The modeling process is shown in **Figures 8** and **9**. The inversion is carried out in the program using genetic algorithm (GA), which imitates the principles of genetics and evolution to find the optimum model from a set of models.

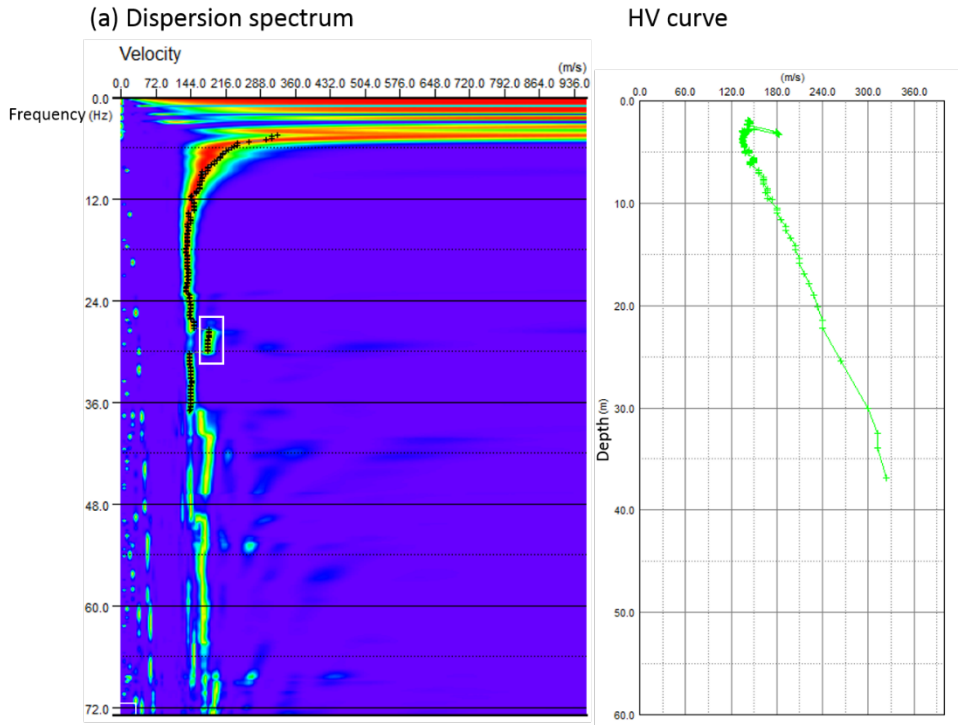

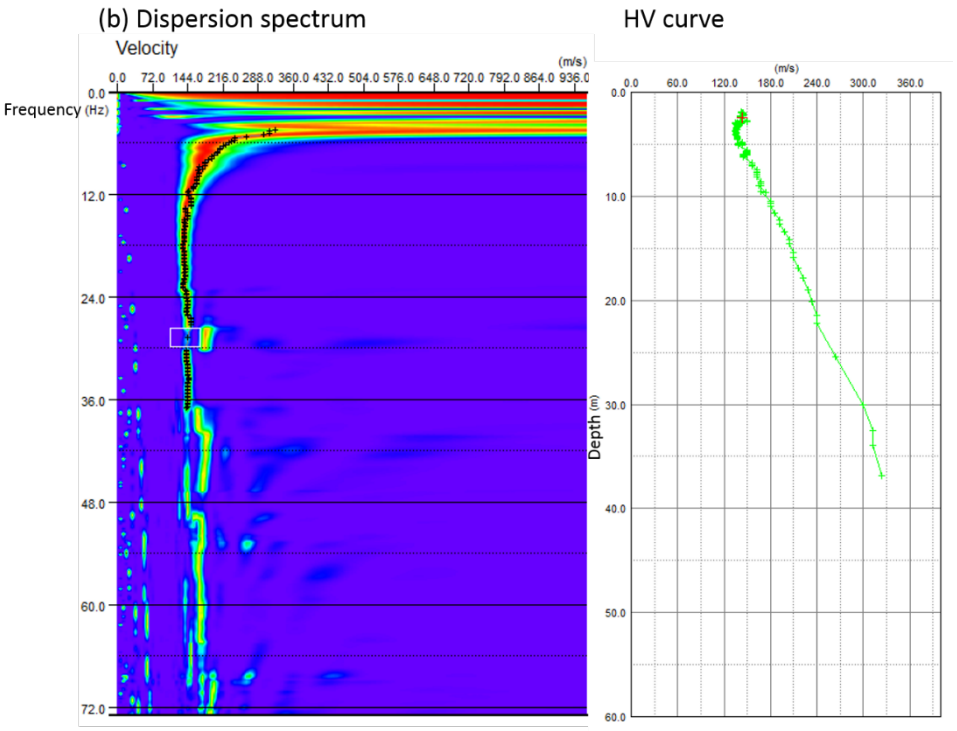

Figure 7: Example of deleting dispersion points on a dispersion curve. (a) On the dispersion spectrum is a dispersion curve of MASW data picked by continuous picking. The dispersion points in the white box are caused by the energy of some strong higher-mode Rayleigh waves and thus need to be deleted from the dispersion curve for the fundamental-mode waves. (b) The dispersion points that are boxed in (a) are deleted. A new point is put in the middle of the gap of the energy peaks to represent the phase velocity at the center frequency in the box where the points were deleted. This new point together with the other dispersion points that remain unchanged constitute an edited dispersion curve. The HV curve is revised to represent the curve from the edited dispersion curve.

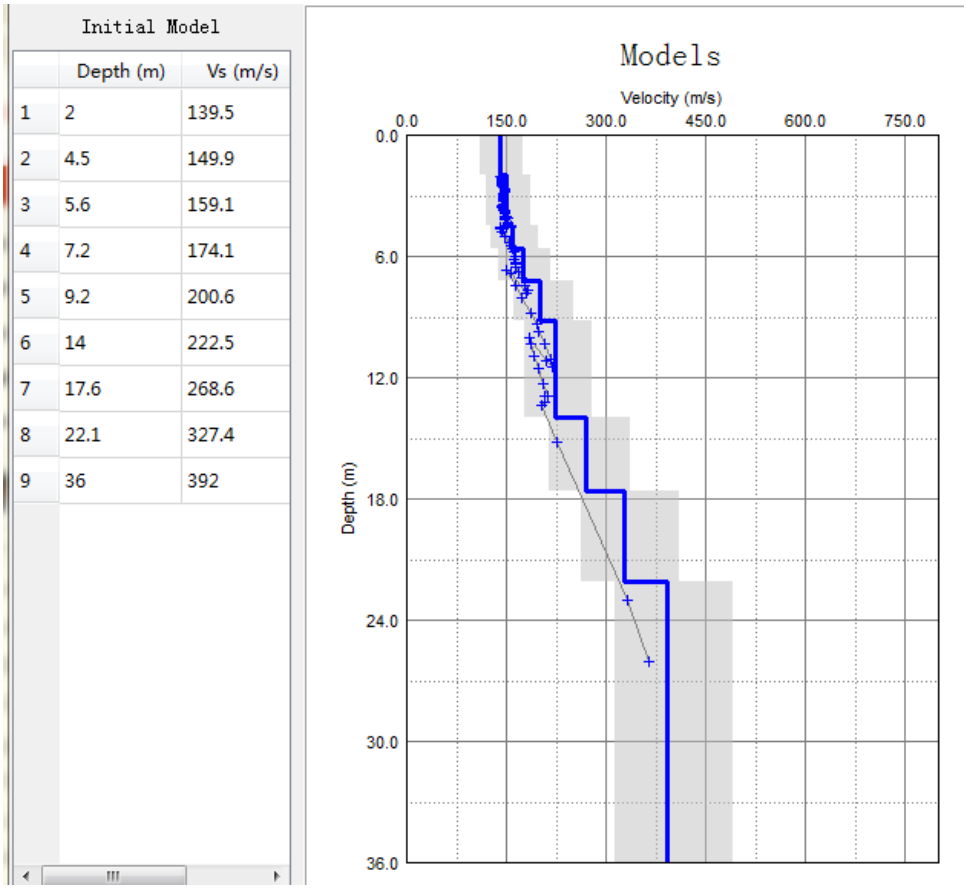

Figure 8: Example of building the forward model. The left panel contains the parameters of the initial model. The right panel shows the profile of the initial model (blue thick curve) with the HV curve (thin blue line with blue crosshairs) imported from the earlier dispersion analysis of the data.

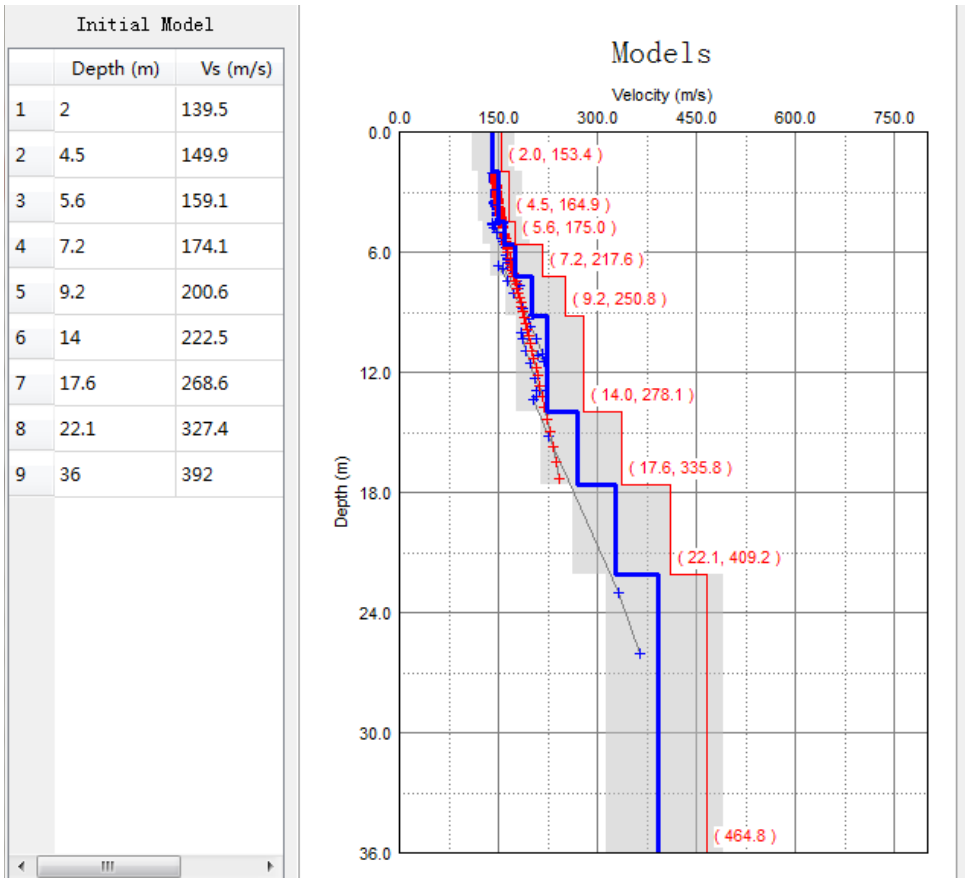

Figure 9: Inversion to determine the best estimate of the S-wave velocity model. The Models sub window shows the initial model (blue line), the optimum model (red line), the observed HV curve (gray line with blue crosshairs), and the calculated HV curve from the optimum model (gray line with red crosshairs) that was determined by an inversion of the HV data.

1.4.2 SeisOpt

The SeisOpt software uses refraction microtremor recordings to estimate shear-wave velocities as a function of depth. There are two programs in SeisOpt: ReMiVspect for dispersion analysis and ReMiDisper for modeling.

In the ReMiVspect program, the field records in the time-distance domain are first transformed into a section of slowness (p) and intercept time (tau) by a p-tau transform. The next analysis step computes the Fourier transform of the p-tau section

and the power spectrum of the Fourier transform to create a record section in the slowness (p)-frequency (f) domain. Then spectral ratios are calculated by taking the power at each slowness-frequency combination against the average power over all the slownesses at that frequency in the power spectra. On the resulting slowness-frequency image (**Figure 10**), the surface wave dispersion curves always trend along the maxima of the spectral ratios from the upper left corner to the lower right corner (Louie, 2001).

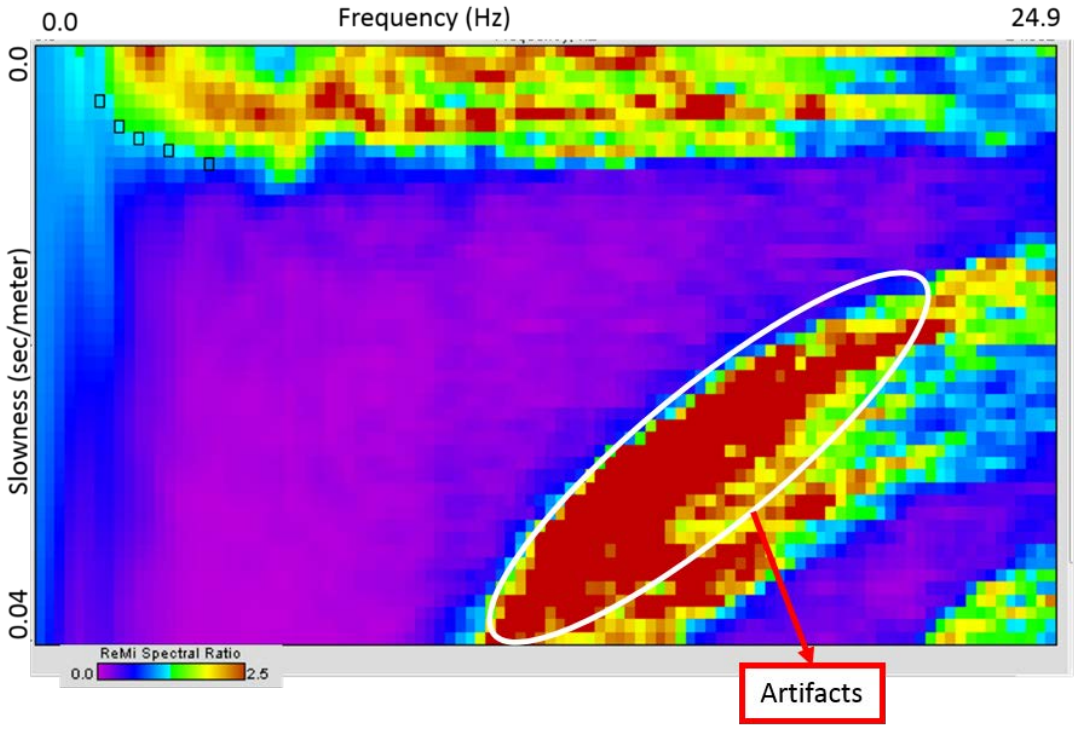

Figure 10: Example of a slowness-frequency image (velocity spectrum). Red areas indicate high spectral ratios; blue areas indicate low spectral ratios. Frequency increases from left to right along the x-axis; slowness increases from top to bottom along the y-axis. The black squares are the picks that define the dispersion curve. The high spectral ratio area circled in the figure is artifacts that do not have the trend of a dispersion curve.

The ReMiDisper program uses the picked dispersion curves to build the Vs models using forward modeling. The models are built by adjusting the number of layers,

layer thicknesses, and velocity values to fit the calculated dispersion curve with the red dots (dispersion picks) in the Dispersion Curve panel as shown in **Figure 11**.

Figure 11: Example of forward modeling using ReMi. By clicking and dragging the Vs profile (vertical red shaded area in the "Model Profiles" panel) and the layer interfaces (horizontal black lines in the "Model Profiles" panel), the modeled dispersion curve (blue line in the "Dispersion Curve" panel) can be adjusted to overlay the dispersion picks (red filled circles). The RMS error (2.195 m/s) that is shown here is small enough to finish the forward modeling.

The Automatic Dispersion Inversion function is not stable and the program developer recommends that the inversion function not be used. Therefore, for this study, the ReMi models were built by forward modeling only.

1.5 Comparison methods

In order to determine which surface-wave method gives the best estimate of subsurface shear-wave velocity profile, comparisons of the three methods are made in

terms of accuracy and precision. The average relative difference between the surface-wave results and direct measurements (either SCPT - Seismic Cone Penetration Testing, or crosshole measurements) is used to assess the accuracy of the surface-wave results. Equation (1) gives the way to calculate the average relative difference between two variables *x* and *y*.

$$relative\ difference = abs\left(\frac{x-y}{\frac{x+y}{2}}\right) = 2 \times abs\left(\frac{x-y}{x+y}\right) \quad (1)$$

Before calculating the average relative difference, Vs profiles from the surface-wave methods or from the direct measurements that have nonuniform layer thicknesses were transformed to models with a uniform layer thickness to calculate the relative difference between the surface-wave Vs models and the direct measurement Vs profiles of each layer. Because layer thicknesses of surface-wave models are generally larger than 2 m, the new uniform Vs profiles, *Vs-uni(i)*, are constructed at 2 m depth intervals from the Vs profiles. Equation (2) gives the average relative difference between the surface-wave models and a direct measurement profile.

$$average\ relative\ difference = \frac{2}{N}\sum_{i=1}^{N}\frac{abs(V_{s-uni-surface}(i) - V_{s-uni-direct}(i))}{V_{s-uni-surface}(i) + V_{s-uni-direct}(i)}, \quad (2)$$

where *Vs-uni-surface(i)* is the uniform Vs model from the MASW, SASW or ReMi method; *Vs-uni-direct(i)* is the uniform Vs profiles from the direct measurement (SCPT or crosshole measurements); *i* is the index of layers; and *N* is the number of layers in the model. If the depth of the Vs models is 30 m, then *N = 15*.

Precision of the surface-wave methods is evaluated by calculating the standard deviation of a set of uniform velocity models at each layer. The standard deviation is given by equation (3).

$$standard\ deviation\ (i) = std([V_{s-uni-1}(i), V_{s-uni-2}(i), \dots, V_{s-uni-n}(i)]), \quad (3)$$

where $V_{s-uni-1}(i), V_{s-uni-2}(i), \dots, V_{s-uni-n}(i)$ are a set of Vs models from a surface-wave method of a dataset; and *i* is the index of layers. If the model depth is 30 m, *i* ranges from 1 to 15. *n* is the number of the models. In most cases in this thesis, there were 12 Vs models from a surface-wave method of a dataset, n = 12.

2.0 RESULTS

For the analyses carried out in this thesis, data were collected at three sites in the Boston area: the intersection of I-93 and I-95 in Canton, MA (42°12'N 71°08'W), at the Fore River bridge, in Weymouth, MA (42°14'N 70°57'W), and at Winchester High School, in Winchester, MA (42°27'N, 71°08'W). The sites were selected because of available Vs models from direct measurements that can be used to compare with the models from the surface-wave methods that are tested in this thesis.

2.1 Canton

The Canton site is at the intersection of I-93 and I-95 in Canton, MA (42°12'N 71°08'W) (**Figure 12**). Seismic data from two survey lines were collected at the site. Each line has two sets of geophone intervals and shot offsets, which are presented in **Table 1**. Geophones were assembled with spikes at both lines in Canton. Each dataset is labeled with a code that is comprised of a 6-digit number. The first four digits represent the date when the data were collected. The last two digits indicate either a different survey line or the type of source for the seismic data, either an active or passive source.

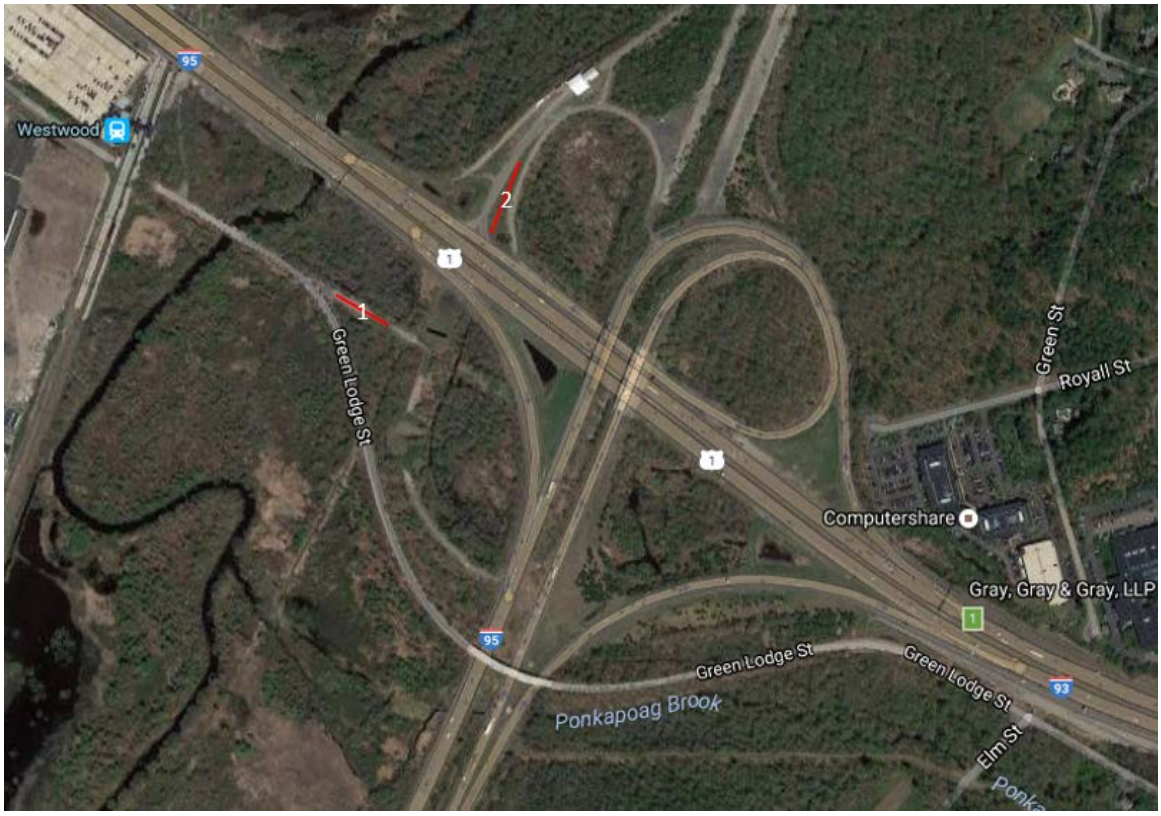

Figure 12: Canton site map. I-93 runs from the upper left to lower right, I-95 runs across I-93 from the bottom left to the top cloverleaf. The two red lines with white numbers superimposed on the image indicate the locations of the two seismic survey lines that were laid out to collect the data for this thesis at this site.

Table 1: Data Collection Geometry at the Canton site

Line	Line 1	Line 2
Geophone interval Δx (m)	1.5	2
Dataset (active)	061601	061702
Shot offset x (m)	5 to 14	5 to 15
Dataset (passive)	061602	061701

There are four sets of Vs measurements that can be considered as possible target values for the comparison with the analysis results in this thesis at Line 1 in Canton, including two crosshole measurements (crosshole1 and crosshole2), one downhole measurement and one SCPT measurement. The “downhole” measurement

was eliminated as a possible target profile because comparisons require the target profile to have velocity values at 0-30 m depth and the downhole profile only yields velocity values to a depth of 24 m. **Figure 13** shows the Vs profiles of the two crosshole profiles and of the SCPT measurements along with the average profile of the three measurements.

To find out which measurement will be used as a comparison in this thesis, "diff" in equation (4) was defined to give the average of the absolute differences between a single direct measurement profile and the average profile of the three measurements.

$$diff = \frac{1}{d+1}\sum_{i=0}^{d} abs\big(direct(i) - average(i)\big), \qquad (4)$$

where *diff* is the average of absolute difference; *direct(i)* is the vector of velocity values that contains the Vs values from the crosshole1, crosshole2, or SCPT profile at 1 m depth intervals; *average(i)* is the vector of velocity values that contains the average velocity values of the profiles from the three measurements at 1 m depth intervals; *i* is the index of layers; and *d* is the depth of the Vs profile. For these profiles, *d = 30*.

By comparing the average of the absolute differences of the three reported velocity profiles (**Figure 14**), it is seen that the crosshole1 profile has a smaller absolute difference than that from either of the other two profiles. Therefore, the crosshole1 velocity profile was selected to be the target profile for the comparisons with the results from the three methods for the data from Line 1 in Canton.

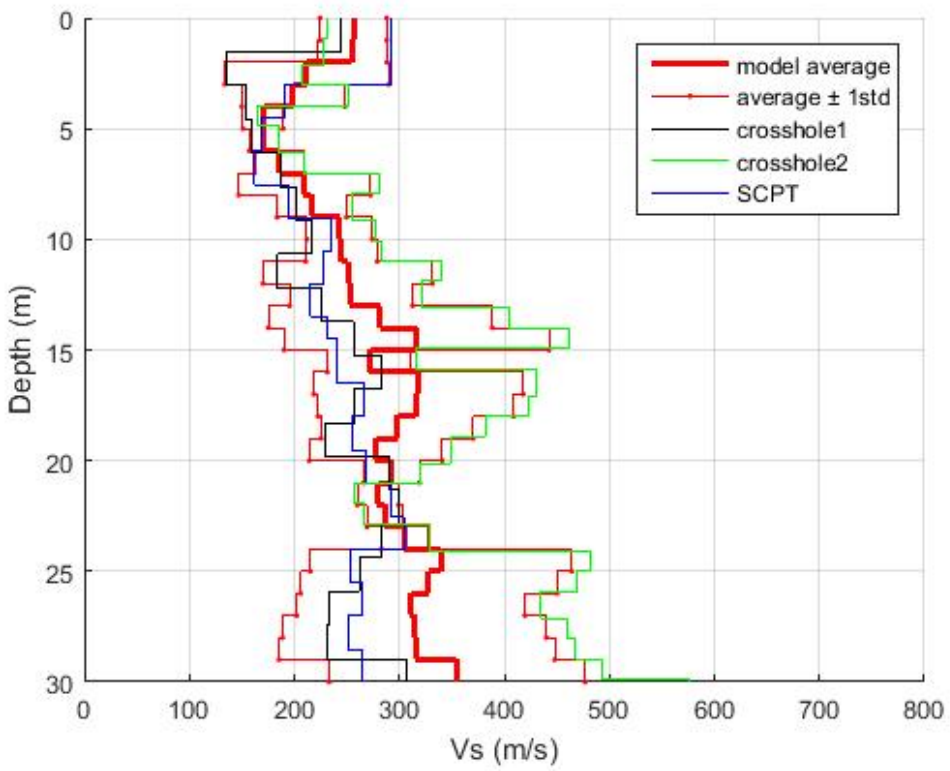

Figure 13: Three Vs measurements that can be used as target Vs values. The model average contains the average velocity of the three profiles calculated at every 1 m depth. Each line except the red lines represents one report profile.

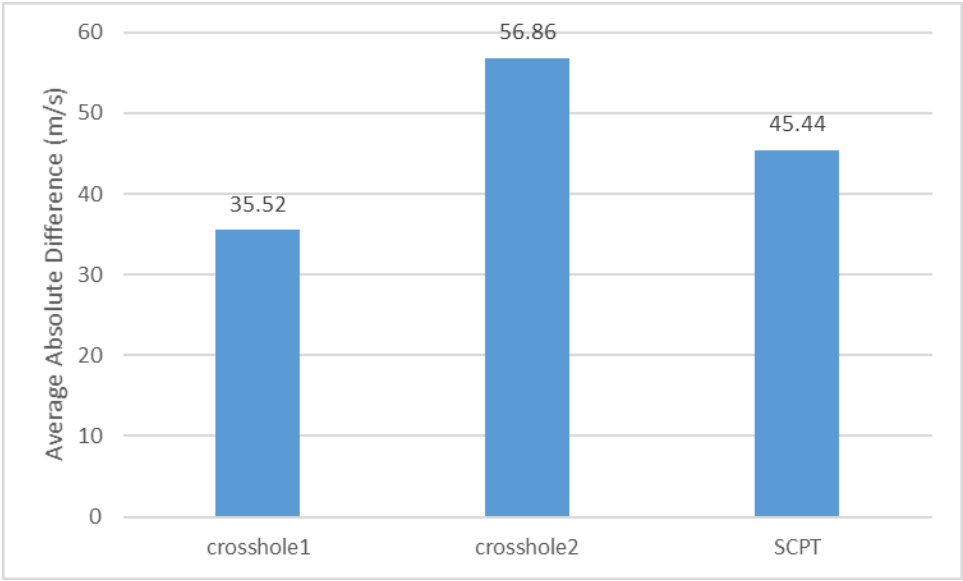

Figure 14: Average of absolute difference between each measurement profile and the average profile of the three measurement profiles calculated from 0 m to 30 m depth.

The “diff” values for crosshole1, crosshole2 and SCPT profiles are plotted in blue bars in the figure.

For Line 2 in Canton, the Vs models are compared with the SCPT profile because it is the only available measurement for comparison. This SCPT profile reaches only 24-m depth. The Vs models from every shot record, compared with the crosshole profile at Line1 and with the SCPT profile at Line 2, together with the standard deviation of the models, are presented in **Figures 15 – 18** and **20 – 23**.

2.1.1 Line 1 061601 and 061602

For Line 1, the MASW and SASW methods were processed with 12 active data records and have 12 models. **Figure 15** shows that the velocities of the Vs models determined from the MASW data range from around 150 m/s to 450 m/s. The SASW models (**Figure 16**) show a rather similar velocity range as seen in the MASW models, with SASW Vs values ranging from around 100 m/s to 580 m/s. The Canton site was the first site at which the data were collected. There were only 4 records of the passive data at each line in Canton, each 10 s in length. The data collection of 10 s length range of passive data was not sufficient to calculate the standard deviation of the ReMi models. Therefore, the passive data at Canton were analyzed in terms of how well they matched the crosshole1 model but the uncertainty in the model from the passive data was not determined (**Figure 17**).

The crosshole profile shows low-velocity layers at 12 m, 19 m, and 24 - 29 m, which are not seen in the Vs models computed from the MASW, SASW, and ReMi data. This is because when picking the dispersion points on the dispersion spectrum, the low-

velocity trends of the different shot records are in different velocity-frequency windows. Therefore, as a possible signal of a low-velocity layer, the low-velocity trend on the dispersion spectrum is regarded as the interference of higher modes Rayleigh waves, and thus is not treated as a low-velocity layer in the dispersion analysis for the data collected from Line 1 in Canton.

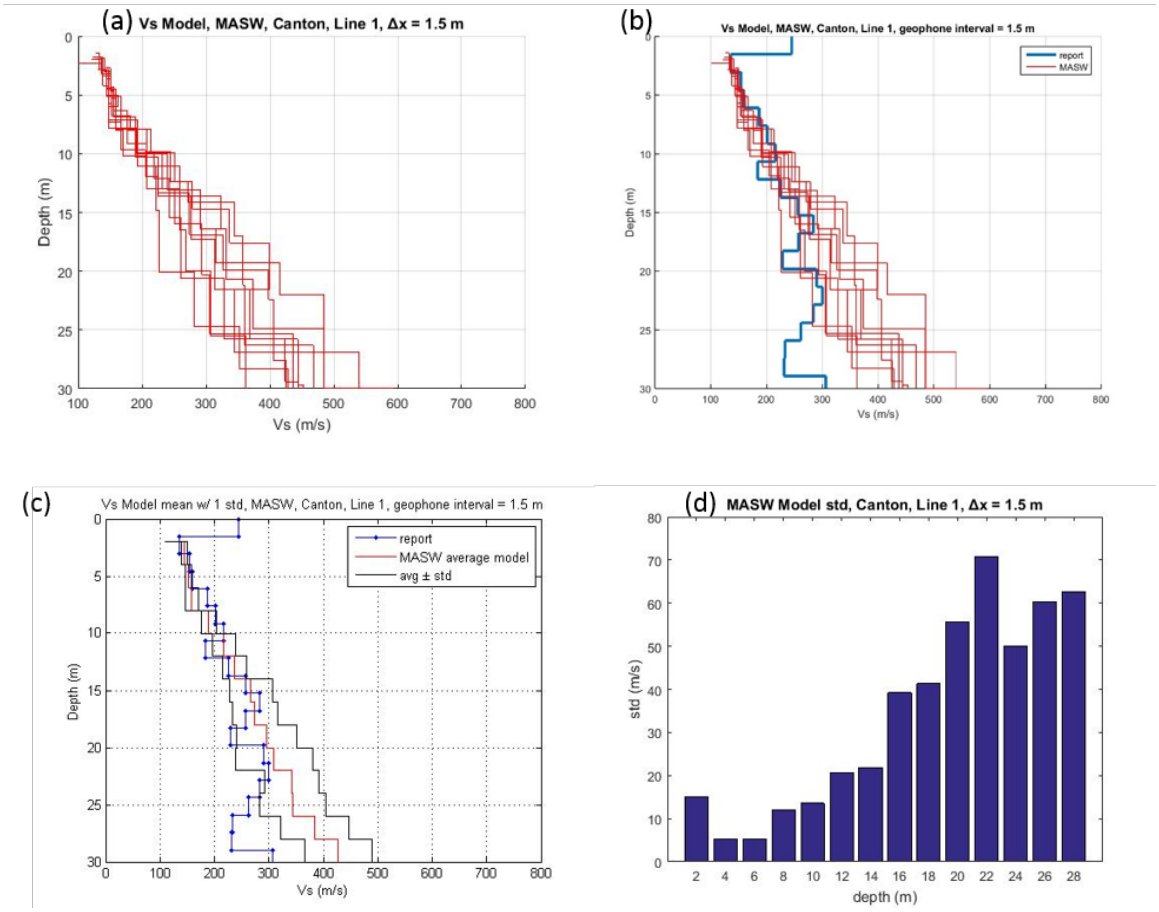

Figure 15: MASW Vs models, 061601, Line 1, Canton, Δx = 1.5m. (a) Plots of the MASW Vs models. Each red line represents one Vs model processed from one shot record. There were 12 MASW records collected with a geophone interval = 1.5 m and with varying shot offsets. (b) The 12 MASW Vs models (red lines) and the crosshole profile (thick blue line). (c) Average model of the 12 models in (a) (red line), average +/- standard deviation (two black lines), and the crosshole profile (blue dotted line) (d) Standard deviations of the 12 models in (a).

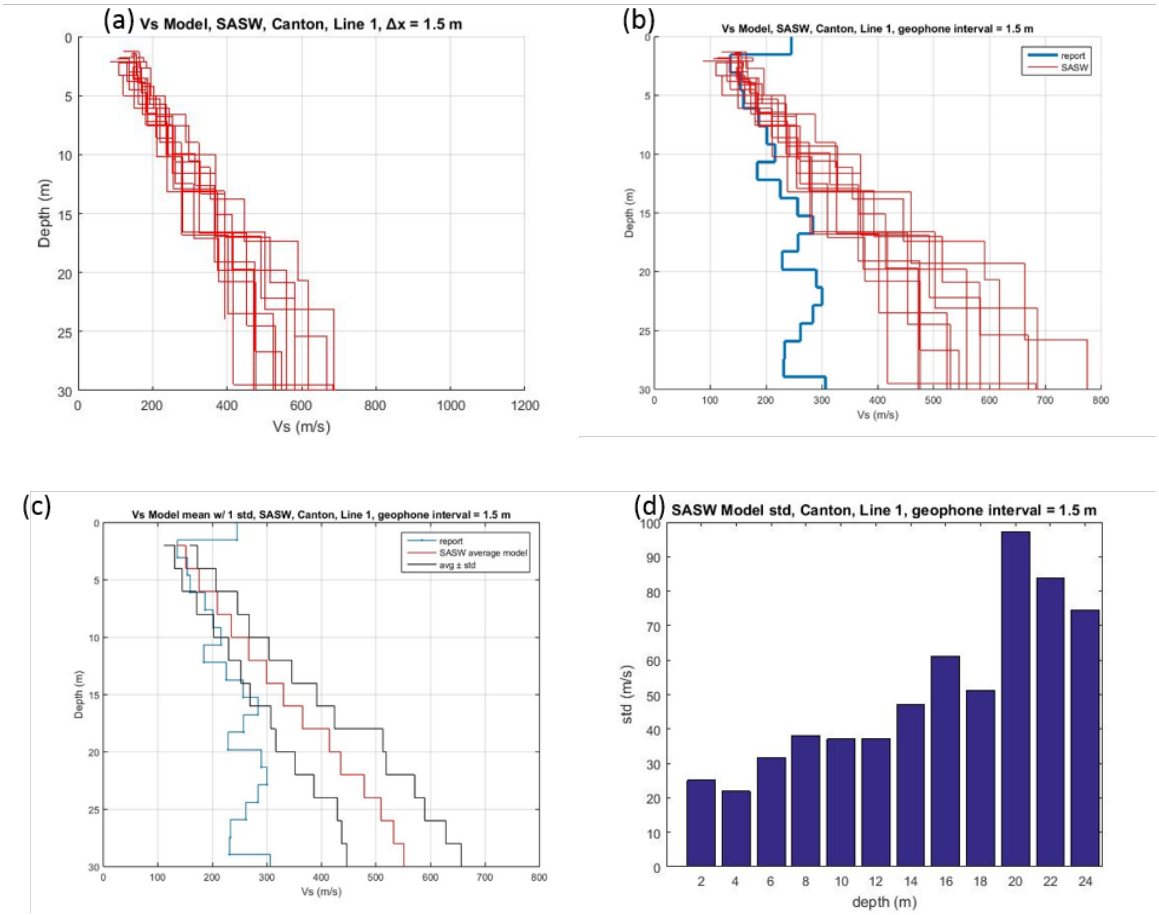

Figure 16: SASW Vs models, 061601, Line 1, Canton, Δx = 1.5m. (a) Plots of the SASW Vs models. Each red line represents one Vs model processed from one shot record. (b) The SASW Vs models (red lines) and the crosshole profile (thick blue line). (c) Average model of the SASW models in (a), average +/- standard deviation (two black lines), and the crosshole profile (blue dotted line) (d) Standard deviations of the SASW models in (a).

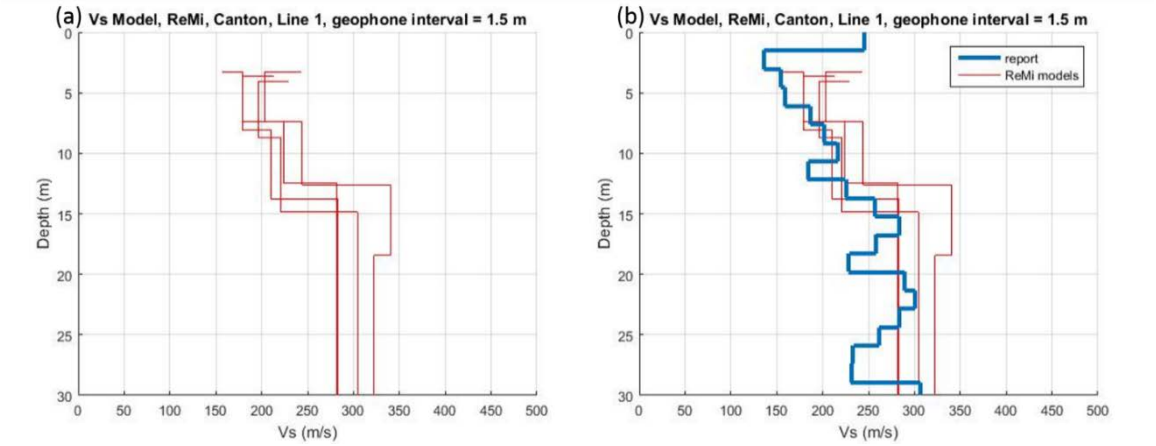

Figure 17: ReMi Vs models, 061602, Line 1, Canton, Δx = 1.5m. (a) Plots of the ReMi Vs models. Each red line represents one Vs model processed from one record. There are 4 passive records collected with geophone interval = 1.5 m. (b) The 4 ReMi Vs models (red lines) and the crosshole profile (thick blue line)

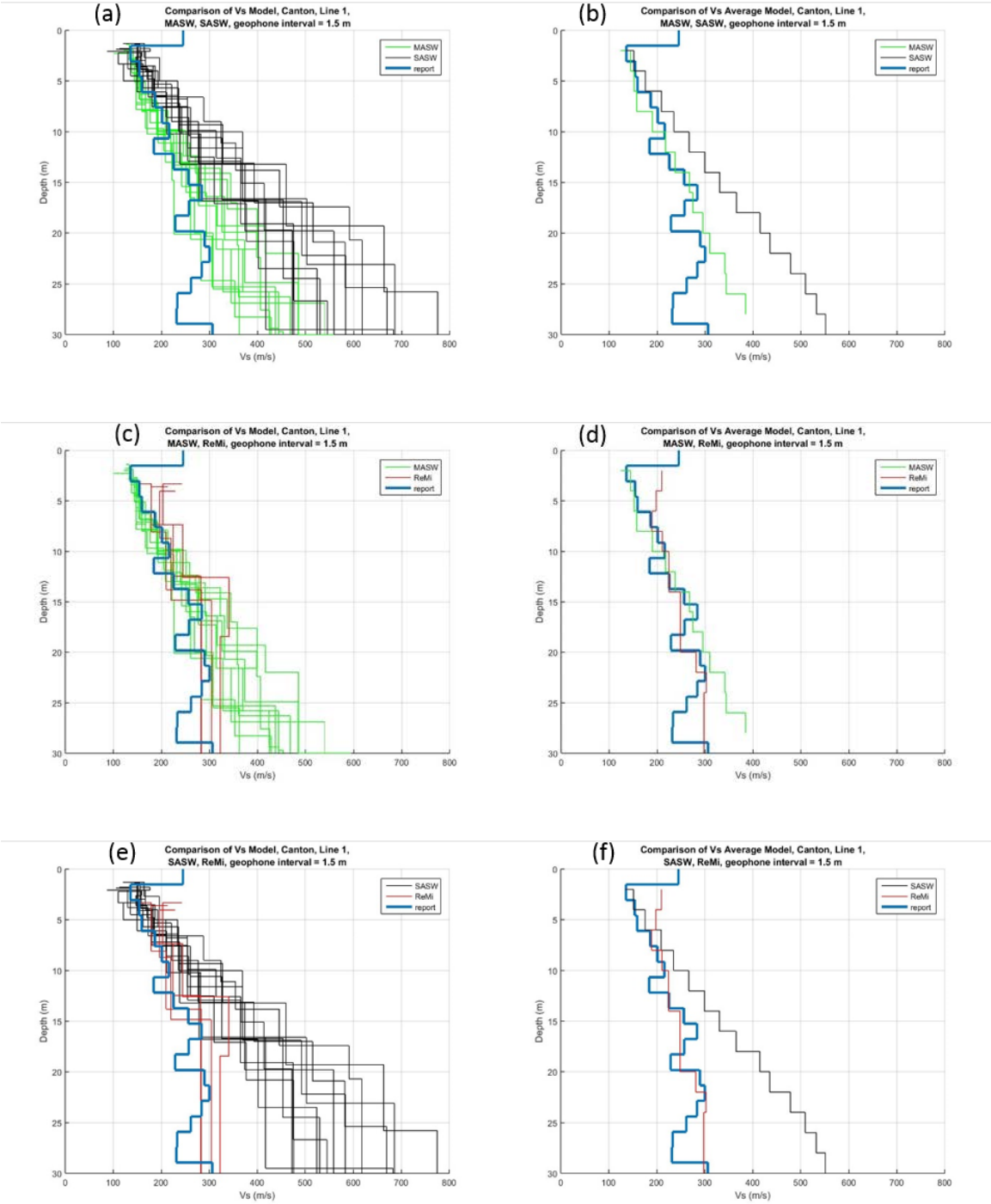

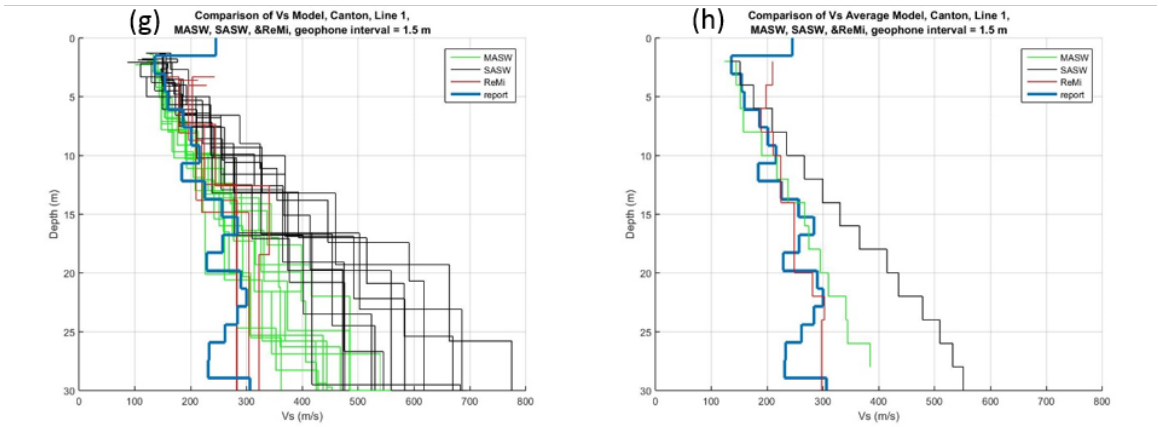

Figure 18: Comparison of the Vs models from the MASW, SASW and ReMi analyses for 061601 and 061602, Line 1, Canton, Δx = 1.5 m. (a), (c), (e) are plots of the Vs models from each of the three methods, plotted in pairs for comparisons of the results. (g) is the comparison of the three methods together. The average models in (b), (d), (f), (h) are calculated from the corresponding Vs series in (a), (c), (e) and (g).

2.1.2 Line 2 061701 and 061702

For Line 2 in Canton, there were 12 models for the MASW and the SASW method and 4 models for the ReMi method. The Vs models using the MASW method range from around 200 m/s to 500 m/s (**Figure 20**).

There was a low-velocity trend in the same velocity-frequency window on every dispersion spectrum of the MASW data. Four examples of the spectra are shown in **Figure 19**. As discussed in section 2.4.1, it was determined from the low-velocity trends on the dispersion spectra that there is a low-velocity layer at a depth of 5-10 m. This is consistent with the SCPT profile. Shown in **Figure 21**, the Vs values from the SASW models at Line 2 in Canton range from 150 to 600 m/s and do not show the low-velocity layer seen in the other profiles. **Figure 22** shows the Vs models from the ReMi method, which also does not have the 5-10 m deep low-velocity layer.

(a) Dispersion spectrum

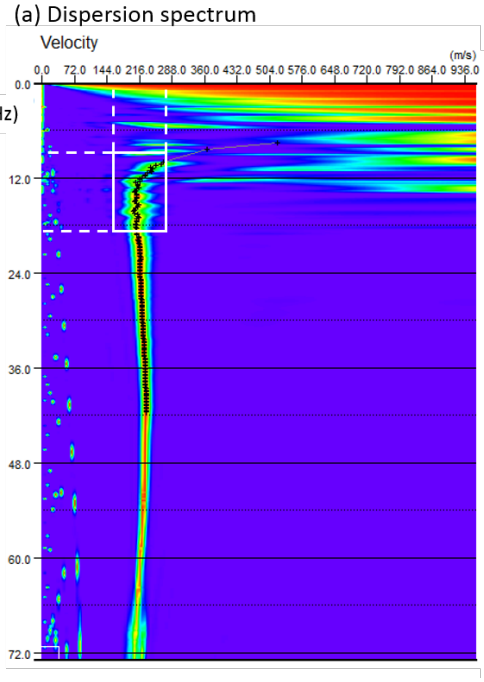

HV curve

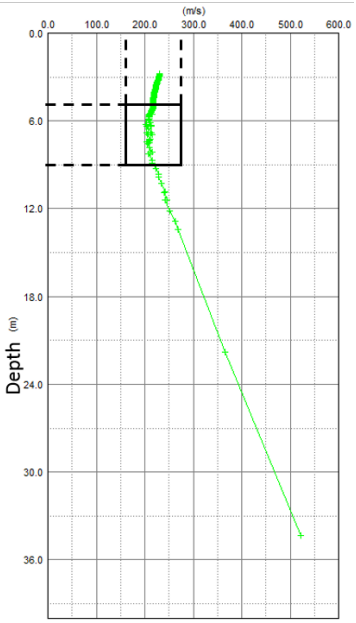

(b) Dispersion spectrum

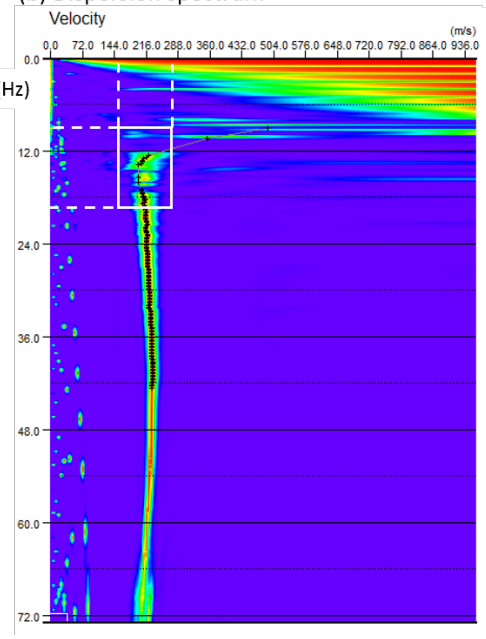

HV curve

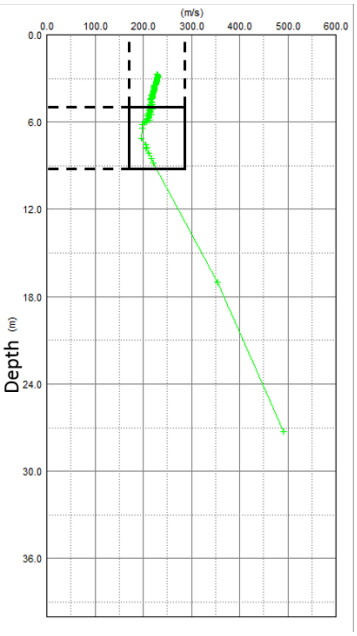

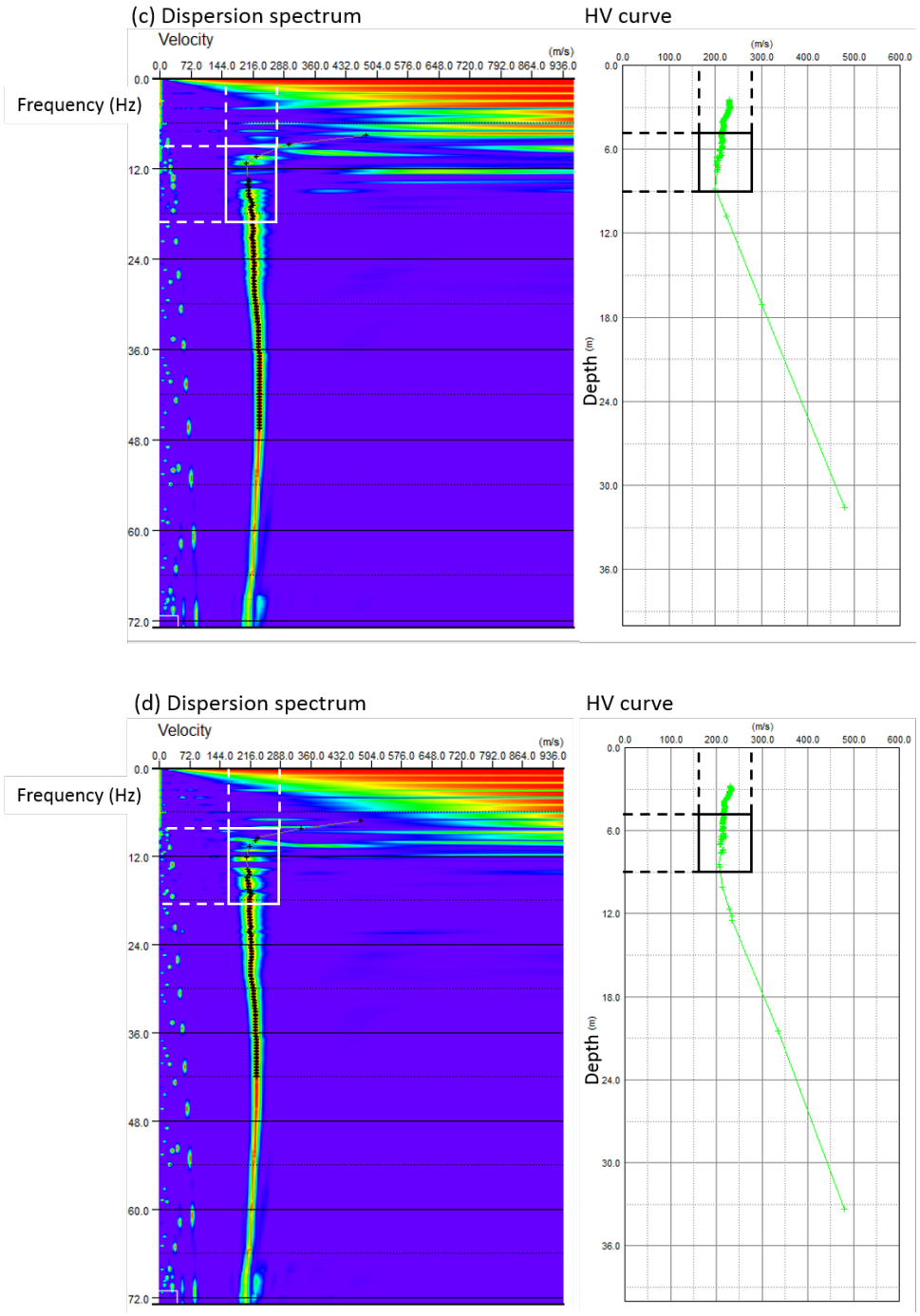

Figure 19: (a) - (d) gives four dispersion spectra with the corresponding HV curves from the MASW dataset 061702. The white box with the white dashed lines on the dispersion spectrum indicates the velocity-frequency window where the low-velocity trend is seen; the black box with the black dashed lines on the HV curves indicates the low-velocity layer that was determined.

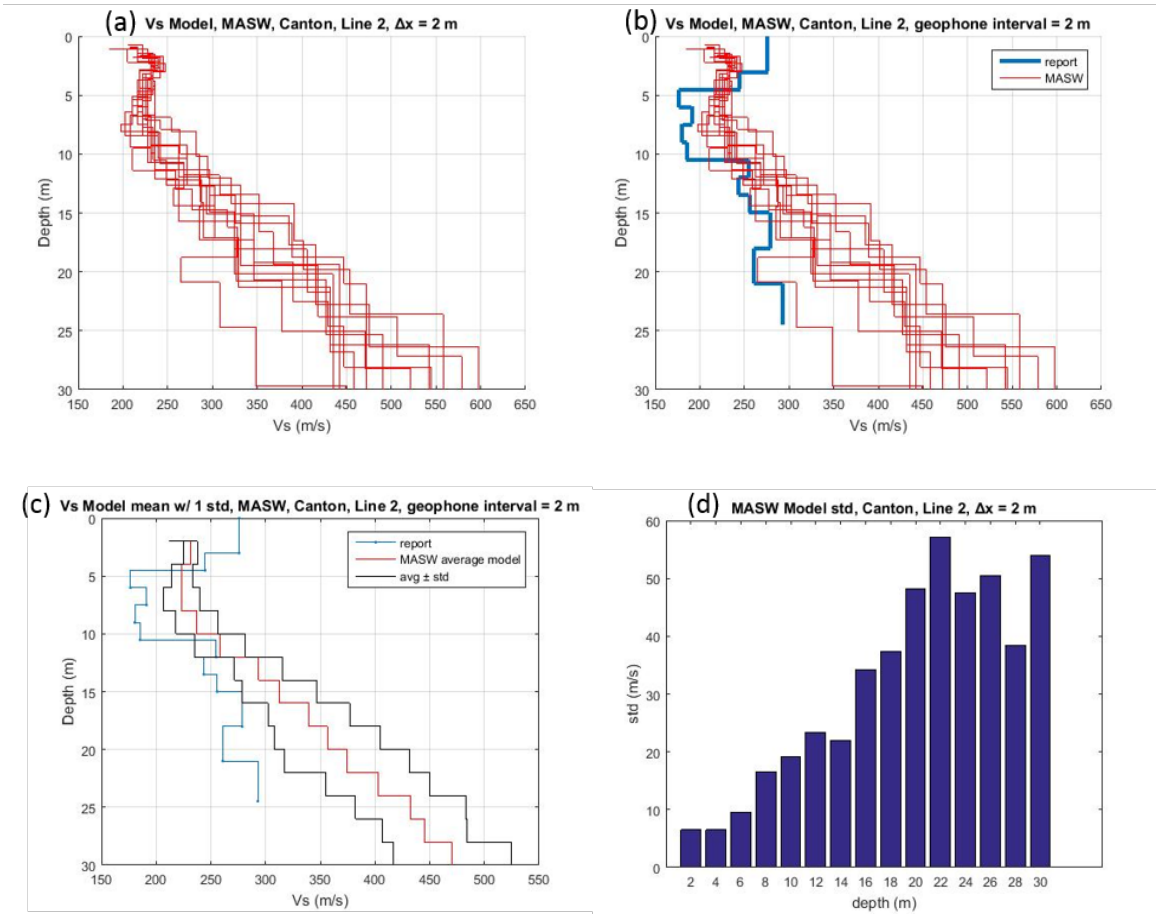

Figure 20: MASW Vs models, 061702, Line 2, Canton, Δx = 2m. (a) Plots of the MASW Vs models. Each red line represents one Vs model processed from one shot record. (b) The MASW Vs models (red lines) and the SCPT profile (thick blue line). (c) Average model of the MASW models in (a) (red line), average +/- standard deviation (two black lines), and the SCPT profile (blue dotted line) (d) Standard deviations of the MASW models in (a).

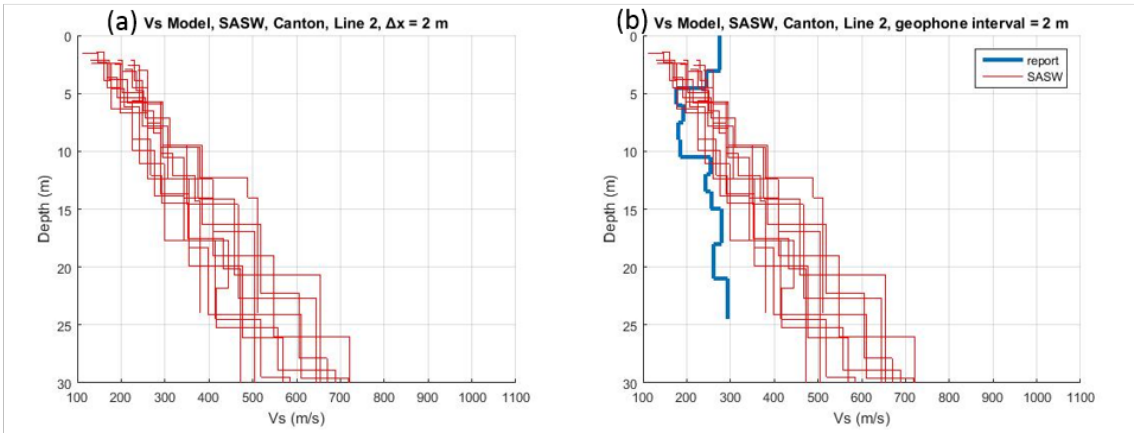

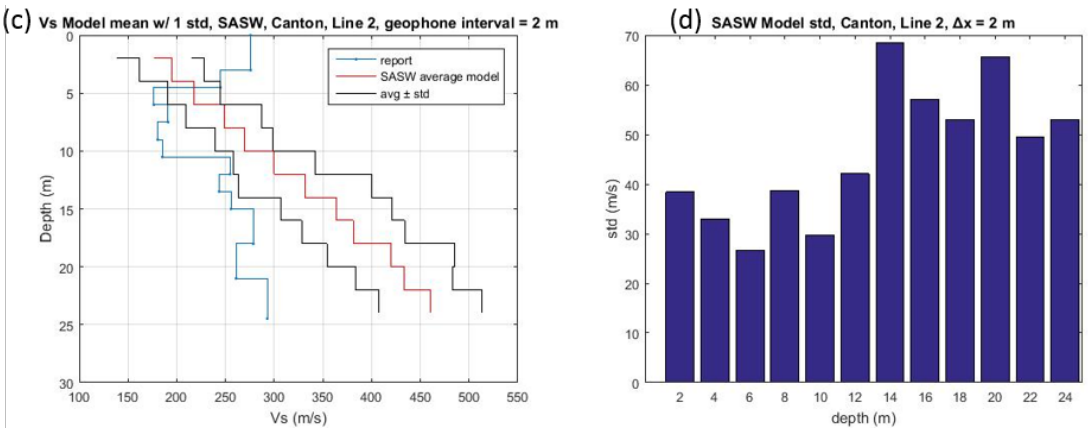

Figure 21: SASW Vs models, 061702, Line 2, Canton, Δx = 2m. (a) Plots of the SASW Vs models. Each red line represents one Vs model processed from one shot record. (b) The SASW Vs models (red lines) and the SCPT profile (thick blue line). (c) Average model of the SASW models in (a) (red line), average +/- standard deviation (two black lines), and the SCPT profile (blue dotted line) (d) Standard deviations of the SASW models in (a).

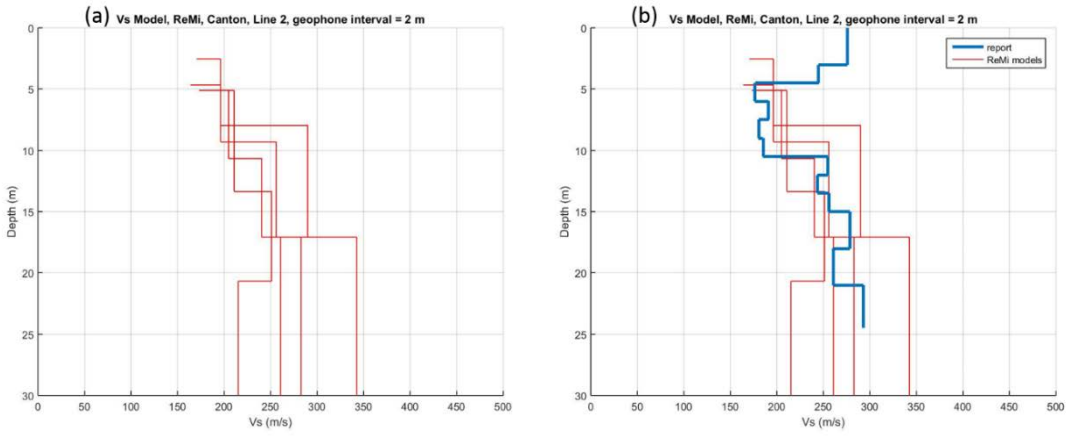

Figure 22: ReMi Vs models, 061701, Line 2, Canton, Δx = 2m. (a) Plots of the ReMi Vs models. Each red line represents one Vs model processed from one record. There are 4 passive records collected with geophone interval = 1.5 m. (b) The 4 ReMi Vs models (red lines) and the SCPT profile (thick blue line)

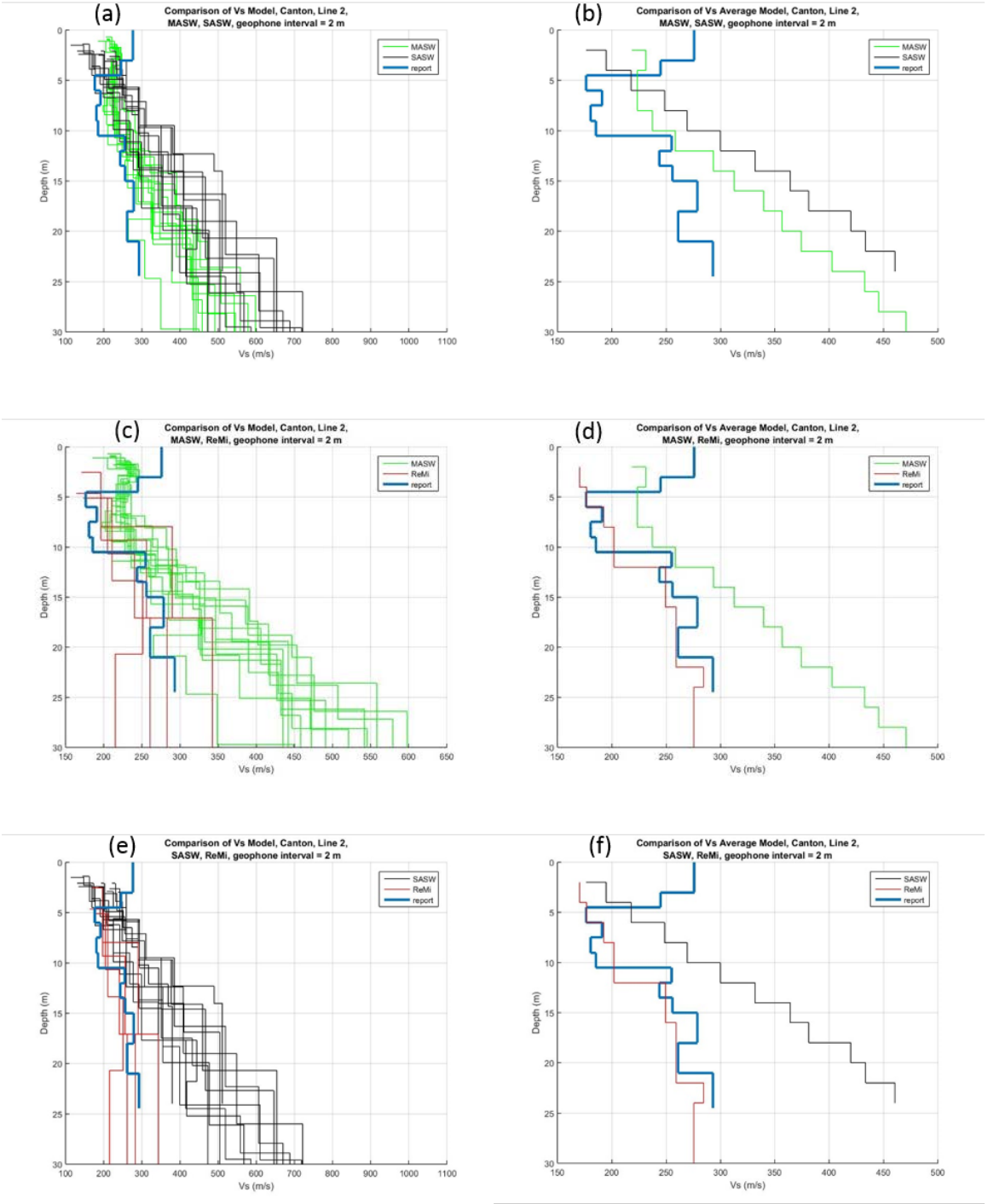
(a)
Comparison of Vs Model, Canton, Line 2,
MASW, SASW, geophone interval = 2 m
MASW
SASW
report
Depth (m)
Vs (m/s)
(b)
Comparison of Vs Average Model, Canton, Line 2,
MASW, SASW, geophone interval = 2 m
MASW
SASW
report
Depth (m)
Vs (m/s)
(c)
Comparison of Vs Model, Canton, Line 2,
MASW, ReMi, geophone interval = 2 m
MASW
ReMi
report
Depth (m)
Vs (m/s)
(d)
Comparison of Vs Average Model, Canton, Line 2,
MASW, ReMi, geophone interval = 2 m
MASW
ReMi
report
Depth (m)
Vs (m/s)
(e)
Comparison of Vs Model, Canton, Line 2,
SASW, ReMi, geophone interval = 2 m
SASW
ReMi
report
Depth (m)
Vs (m/s)
(f)
Comparison of Vs Average Model, Canton, Line 2,
SASW, ReMi, geophone interval = 2 m
SASW
ReMi
report
Depth (m)
Vs (m/s)

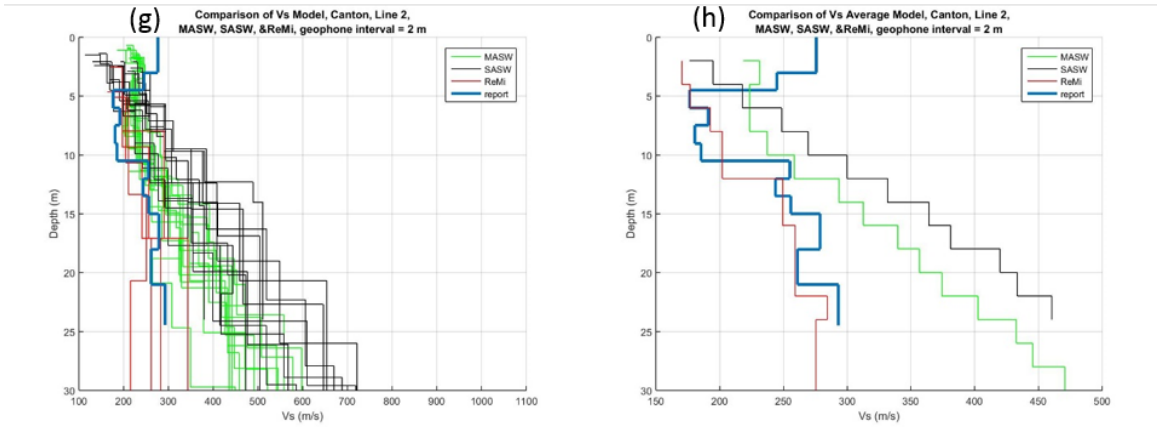

Figure 23: Comparison of the Vs models from the MASW, SASW and ReMi analyses for 061701 and 061702, Line 2, Canton, Δx = 2 m. The caption for Figure 18 also applies here.

The average relative difference between the Vs models of the MASW, SASW or ReMi methods and the Vs profile from the crosshole measurement calculated by Equation (2) is shown in **Figure 24**. According to the data collected in Canton, the ReMi method yields the smallest average relative differences, followed by the MASW and SASW methods. Therefore, based on the Canton part of this study, the ReMi method has the smallest uncertainty and is the most accurate method compared to the MASW and SASW methods.

Figure 25 shows the standard deviation of the MASW and SASW models calculated using Equation (3). The MASW data at both lines in Canton have the smaller standard deviation than the SASW method. Because there were only 4 passive records collected at each survey line in Canton, the standard deviation of the ReMi models were not analyzed because of lack of sufficient length of the data windows. To conclude, from data at both lines in Canton, the MASW method is more precise than the SASW method.

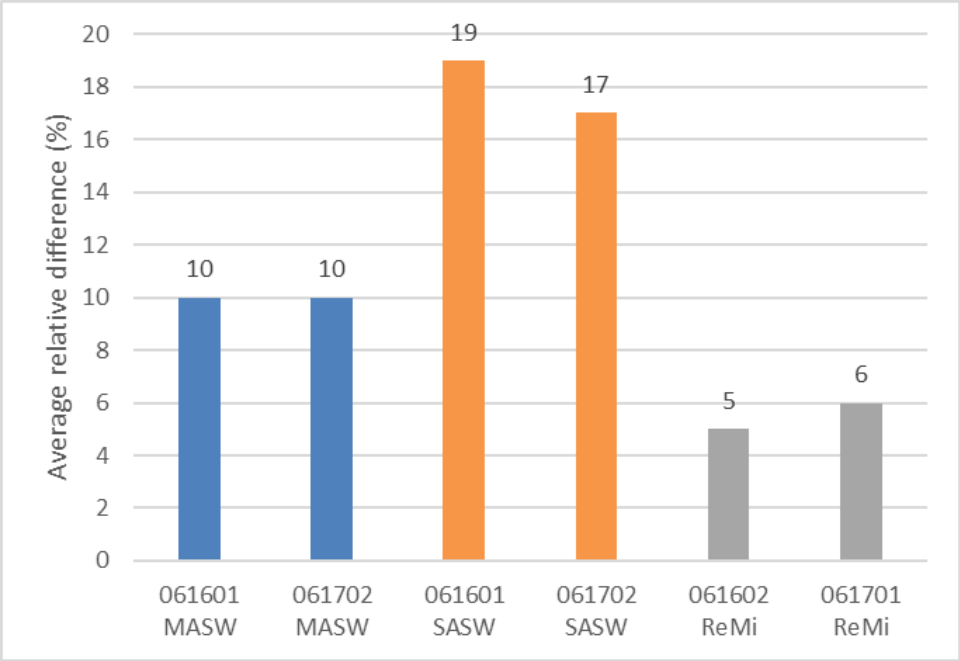

Figure 24: Average relative difference between the crosshole Vs profile or the SCPT Vs profile and the Vs models from the MASW, SASW and ReMi methods, Canton

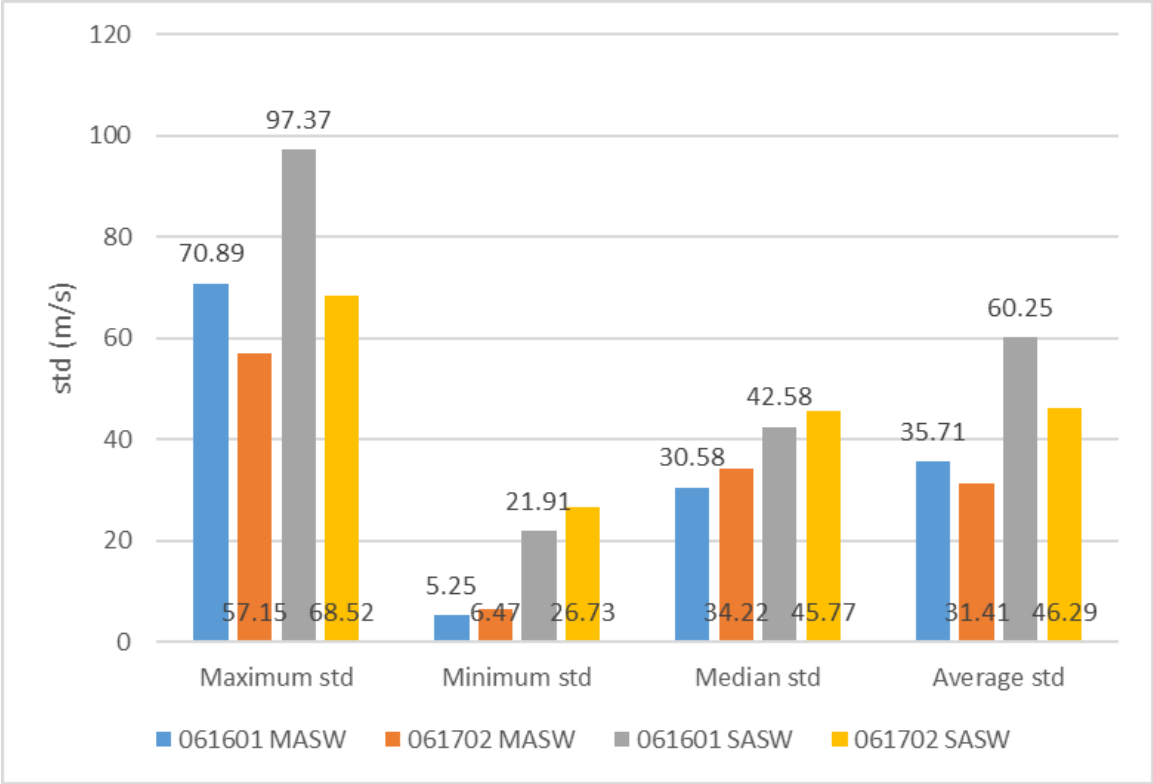

Figure 25: Model standard deviations, Canton

2.2 Fore River

The Fore River site is near the Fore River bridge in Weymouth, MA (42°14'N 70°57'W) (**Figure 26**). Three lines were set up at the Fore River site (**Table 2**). Line 1 was set up on the grass area to the south of the old bridge. The grass area was soft, so the geophones were installed into the soil with spikes. Line 2 is on the gravel-covered land along the road to the north of the bridge and to the east of a construction area. The soil here is made up of compressed gravels and is too hard to insert spikes into it. Therefore, at Line 2, the data were collected with geophones assembled with tripods. Line 3 was located beneath the old bridge. It was also in an area of compressed gravels and thus required geophones with tripods. The passive data were collected in windows 32 s in length (the maximum recording time in SEISTRONIX) and 12 records for each passive dataset at Fore River.

Table 2: Data Collection Geometry at the Fore River site

Line	Line 1		Line 2	Line 3
Geophone interval Δx (m)	1.5	1.5	1.5	1
Dataset (active)	080901	091801	092503	092501
Shot offset x (m)	2.5 to 10	3 to 12	5 to 15	5 to 15
Dataset (passive)	080902	091802	092504	092502

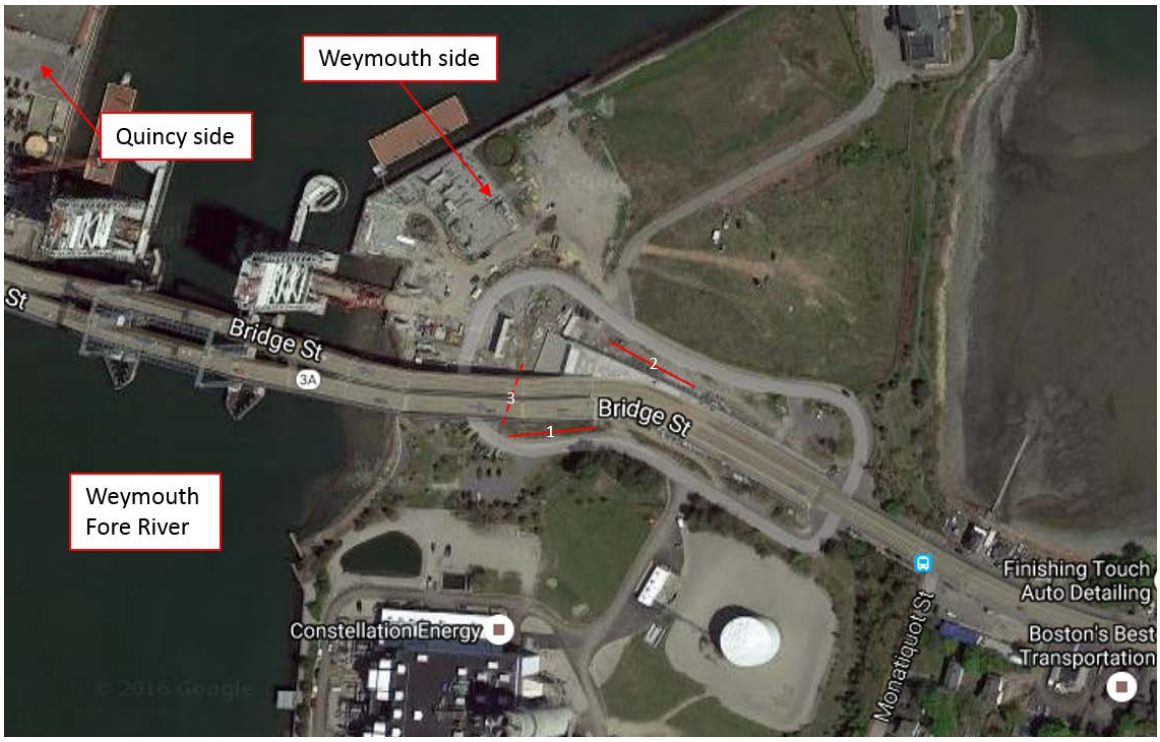

Figure 26: Site map in the vicinity of the Fore River bridge. The data were collected around the piers of the old bridge on the Weymouth side of the river. The red lines with white numbers are the locations where the survey lines were laid out.

With a new bridge under construction at the time the data were collected and busy traffic running by all the time on the old bridge, the data generally look noisy. As boxed in white in panels (b) and (d) in **Figure 27**, the energy peaks at low frequencies (6-18 Hz) on Line 1 and Line 2 at Fore River are not clear enough to identify the dispersion curve of the fundamental mode Rayleigh wave. Therefore, there is rather large uncertainty in picking the dispersion points at these low frequencies, which results in a relatively large uncertainty of the velocities of the deeper layers. Data from Line 3 are too noisy to isolate the energy of the fundamental mode Rayleigh wave from the energy of the higher modes and other noise sources (**Figure 27**-e, f), and thus they were not processed for a Vs profile. In comparison, the dispersion spectrum for the data from

Line 1 in Canton (**Figure 27**-h) has clear and continuous energy peaks, which indicates that the data from Canton were more useful for surface-wave analysis methods than the data from Fore River.

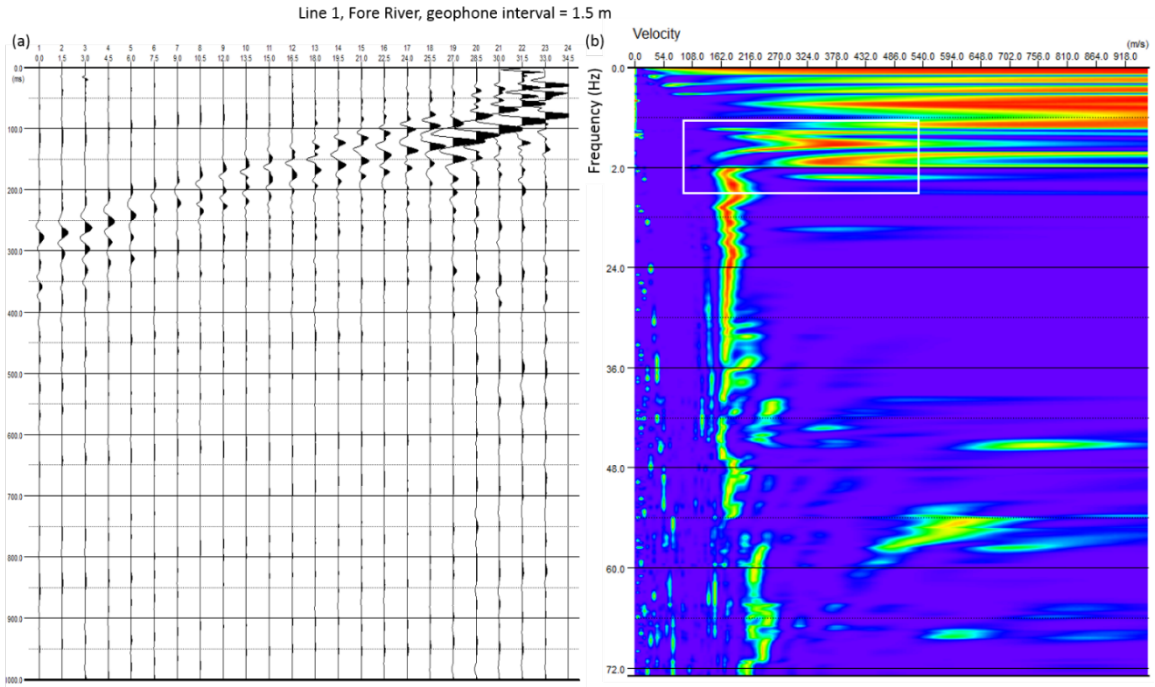

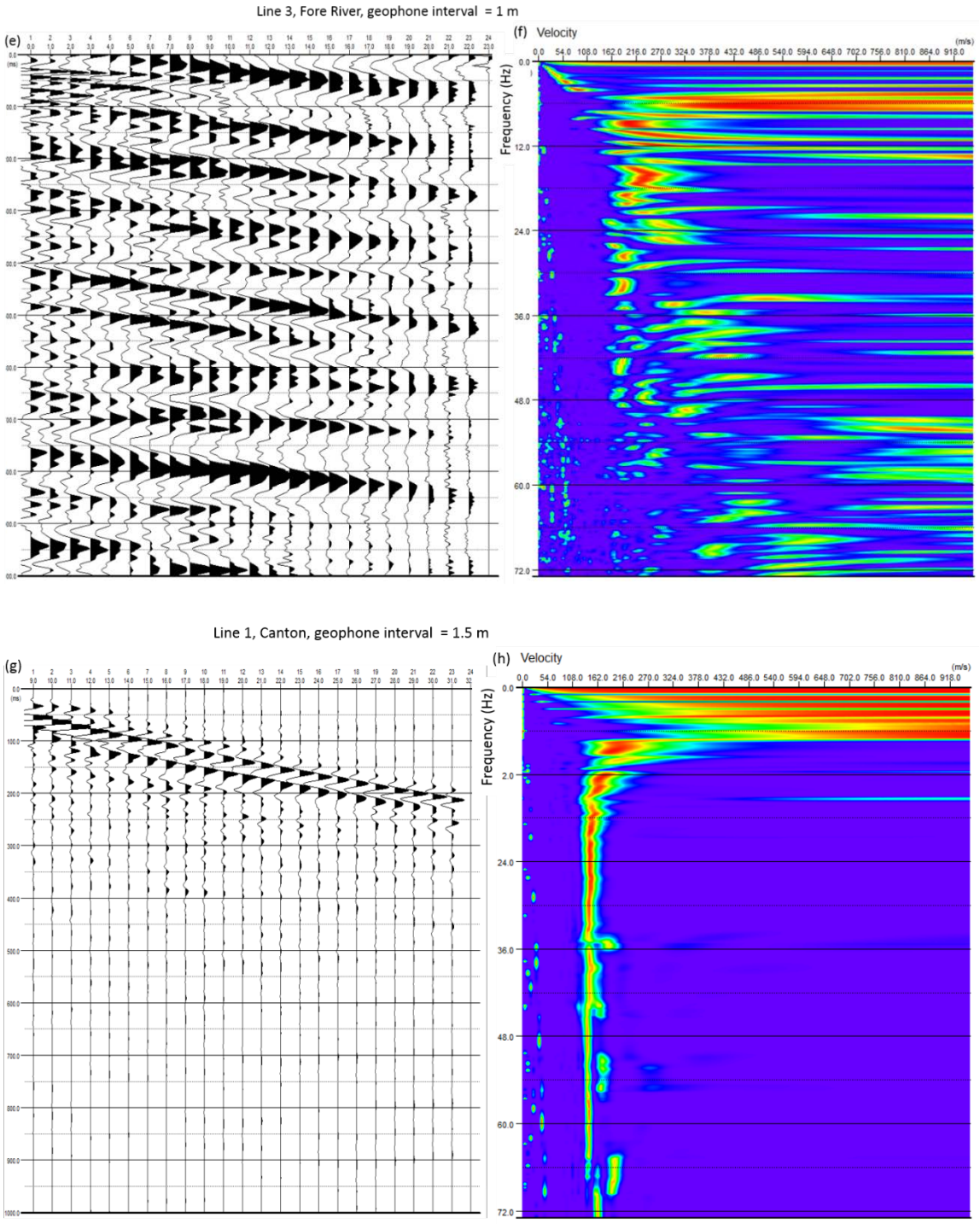

Figure 27: A comparison of the data from Canton and the data from Fore Rive. Panels (a), (c), (e), (g) give examples of the seismic profile of one shot record for the survey line indicated in the title of the panel. Panels (b), (d), (f), (h) are the corresponding dispersion spectra of the records in the corresponding plot panel to the left. The white boxes in (b) and (d) shows where the energy peaks were not clear and continuous enough to determine the dispersion curve of the fundamental mode Rayleigh wave.

An SCPT profile and a crosshole profile are available at Fore River that can be considered as the target profile for comparison. Based on the discussion of the determination of the target profile for Line 1 in Canton, the crosshole profile is considered more accurate than the SCPT profile. Therefore, the crosshole profile from Fore River is considered as the target values of the Vs profile. **Figures 28 - 39** show the Vs models processed from data collected at Fore River using the MASW, SASW, and ReMi methods.

The two MASW datasets (080901, 091801) show that the shear-wave velocity at Line 1 starts at 70 m/s near the surface and steadily increases to 425 m/s - 450 m/s at 30 m depth. For Line 2 at Fore River, the Vs values from the MASW data increase with depth from 100 m/s to 435 m/s. Each dataset was processed for 12 models for the corresponding surface-wave method at Fore River (080901 for MASW and SASW, 080902 for ReMi; 091801 for MASW and SASW, 091802 for ReMi; and 092503 for MASW and SASW, 092504 for ReMi).

2.2.1 Line 1 080901, 080902 and 091801, 091802

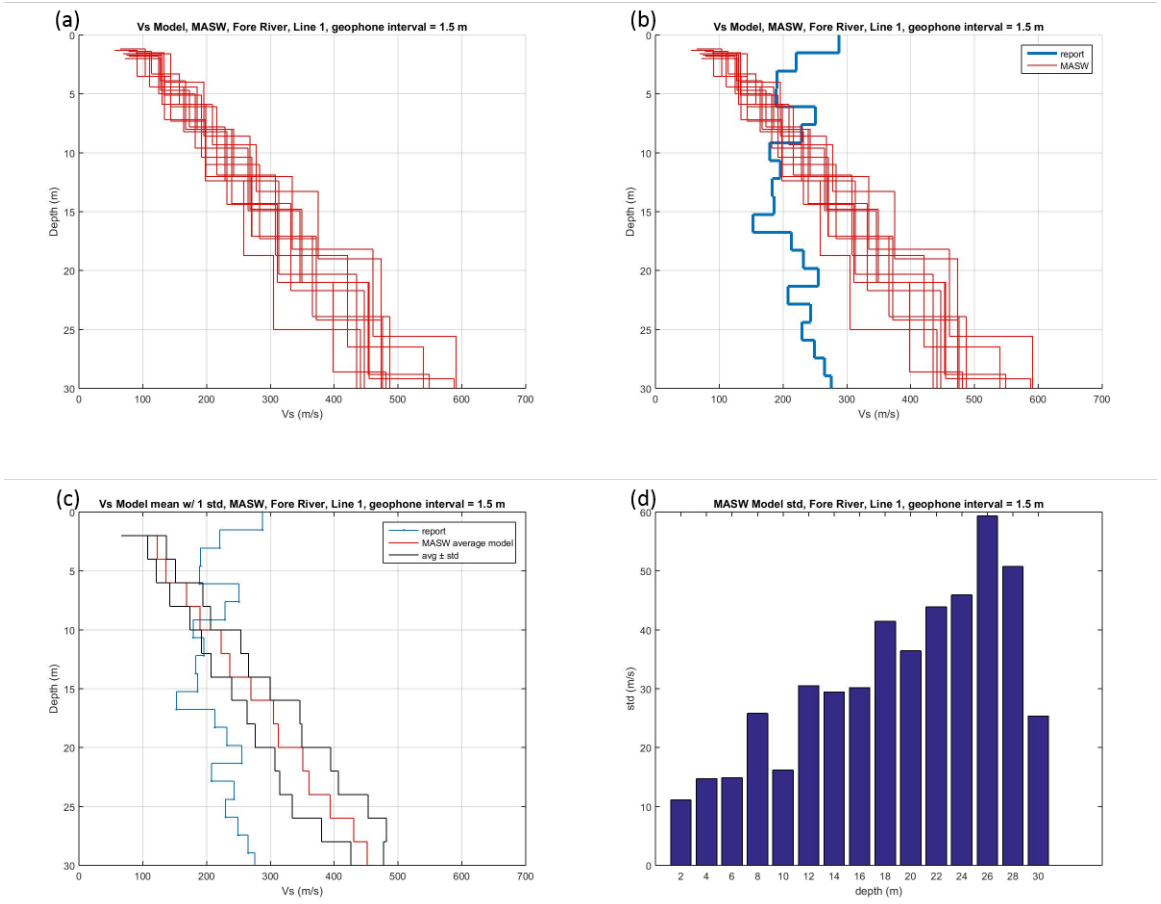

Figure 28: MASW Vs models, 080901, Line 1, Fore River, Δx = 1.5m. The caption for Figure 15 also applies here.

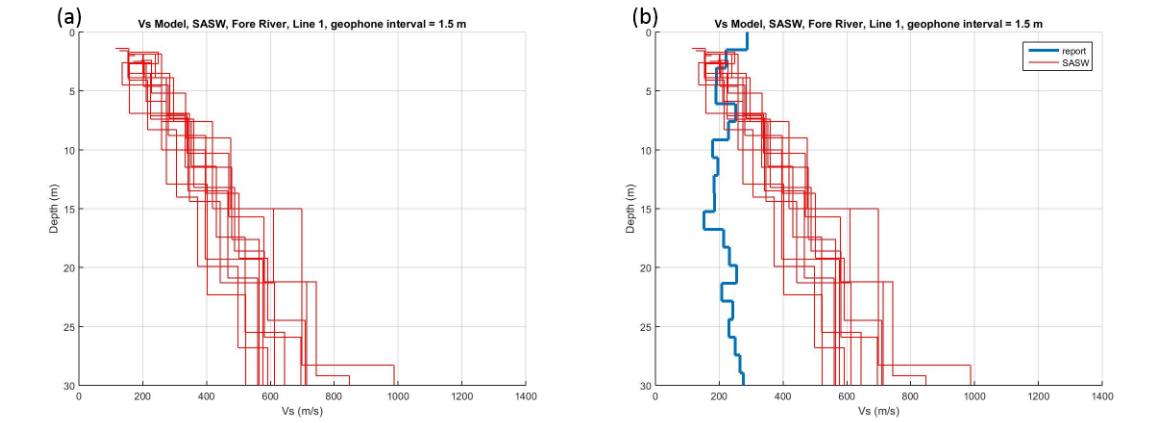

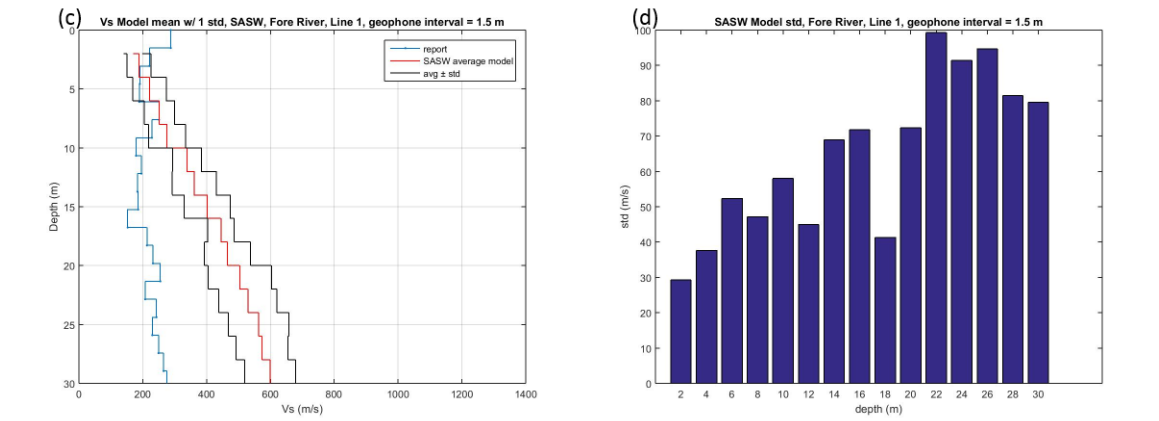

Figure 29: SASW Vs models, 080901, Line 1, Fore River, Δx = 1.5m. The caption for Figure 16 also applies here.

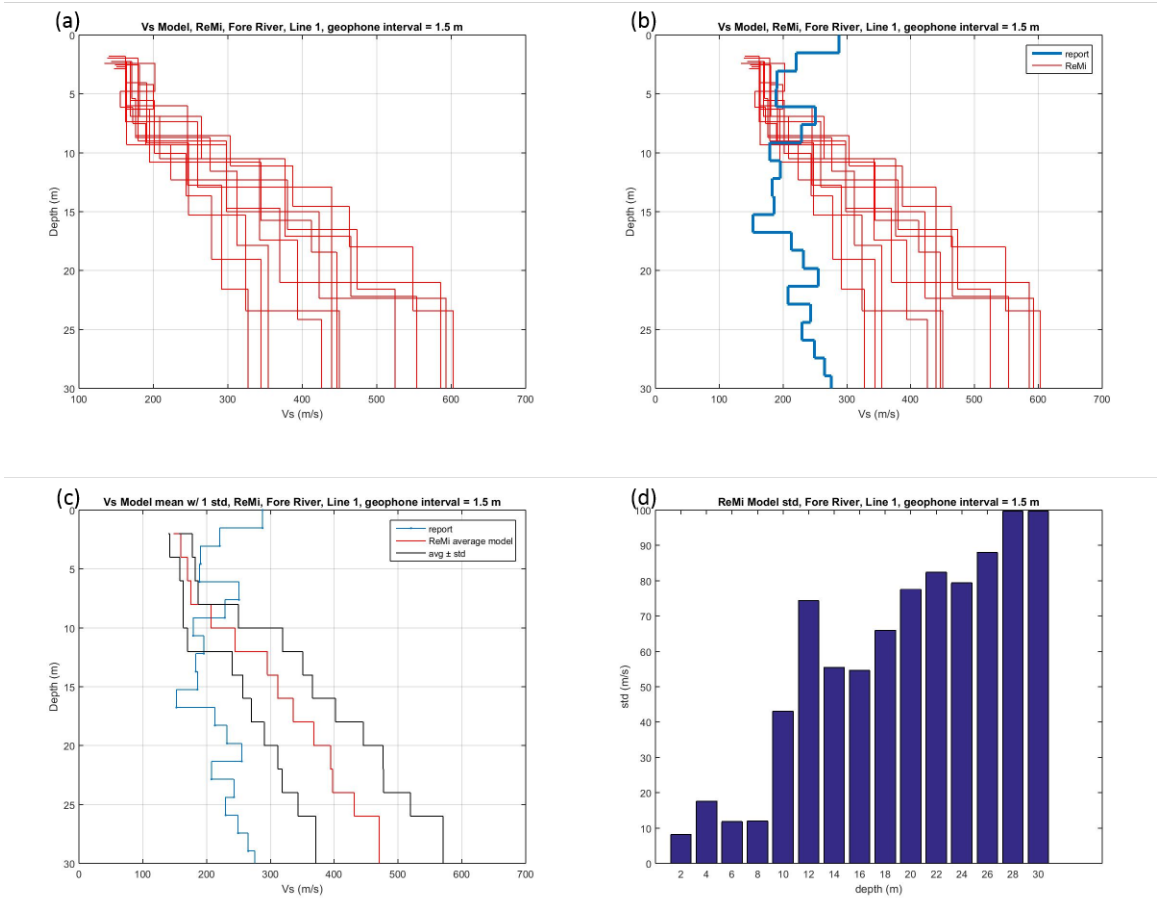

Figure 30: ReMi Vs models, 080902, Line 1, Fore River, Δx = 1.5m. (a) Plots of the ReMi Vs models. Each red line represents one Vs model processed from one record. (b) The ReMi Vs models (red lines) and the crosshole profile (thick blue line). (c) Average model

of the ReMi models in (a) (red line), average +/- standard deviation (two black lines), and the crosshole profile (blue dotted line) (d) Standard deviations of the ReMi models in (a).

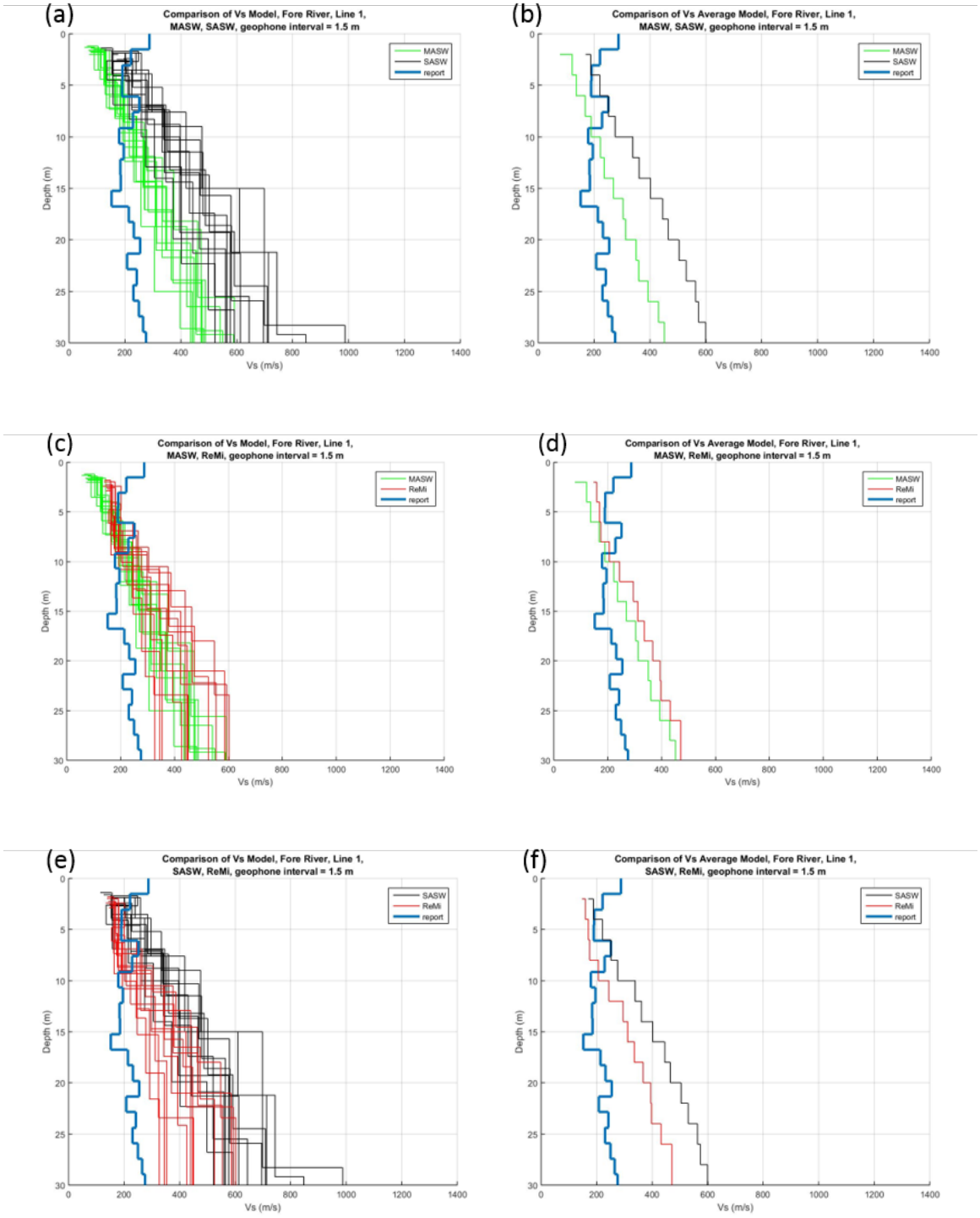

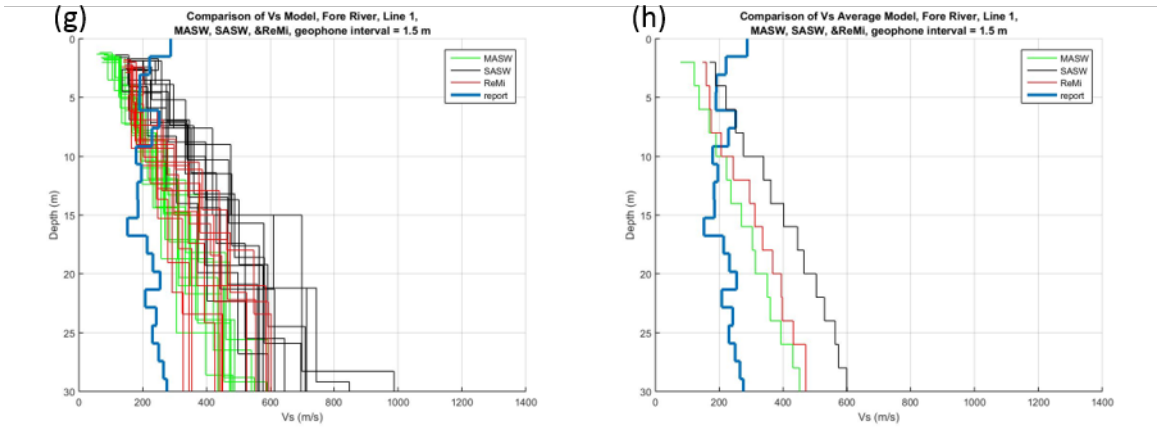

Figure 31: Comparison of the Vs models from the MASW, SASW and ReMi analyses for 080901 and 080902, Line 1, Fore River, Δx = 1.5 m. The caption for Figure 18 also applies here.

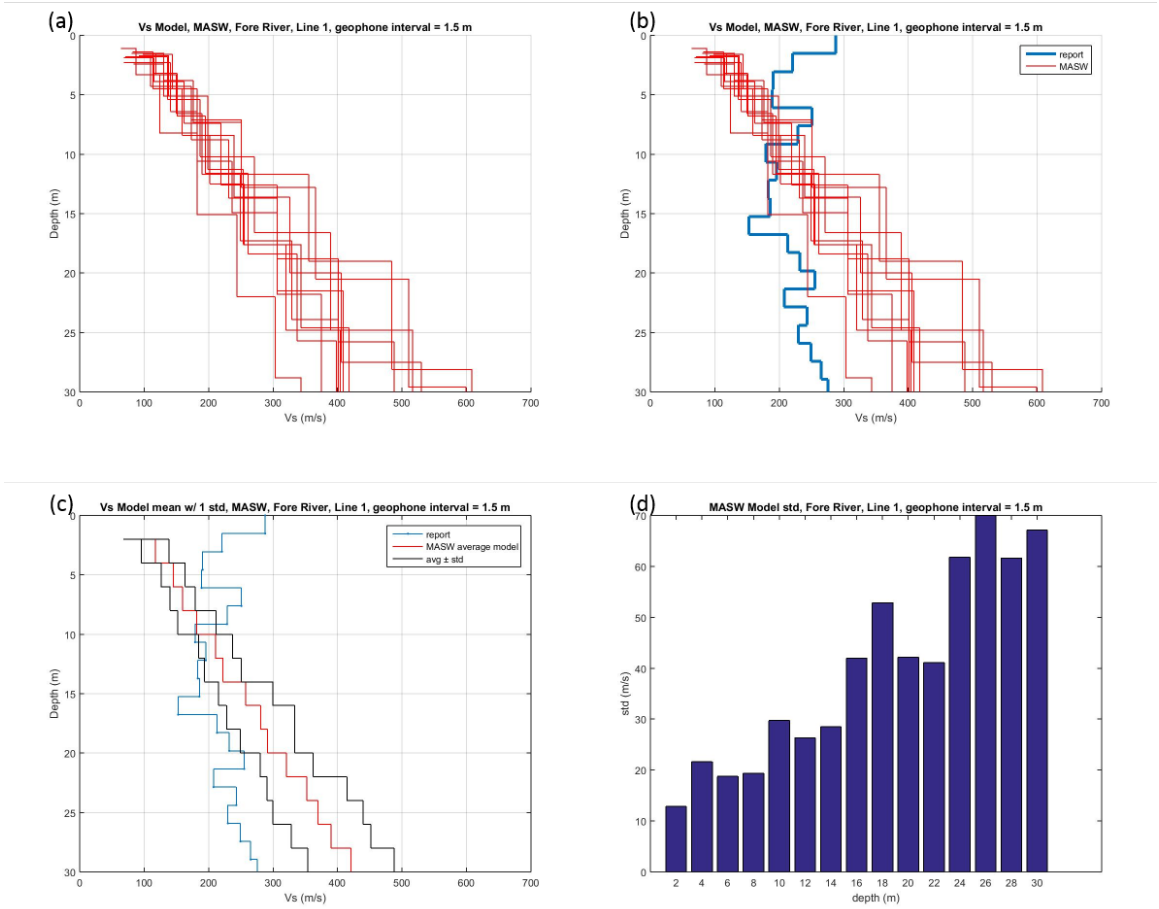

Figure 32: MASW Vs models, 091801, Line 1, Fore River, Δx = 1.5m. The caption for Figure 15 also applies here.

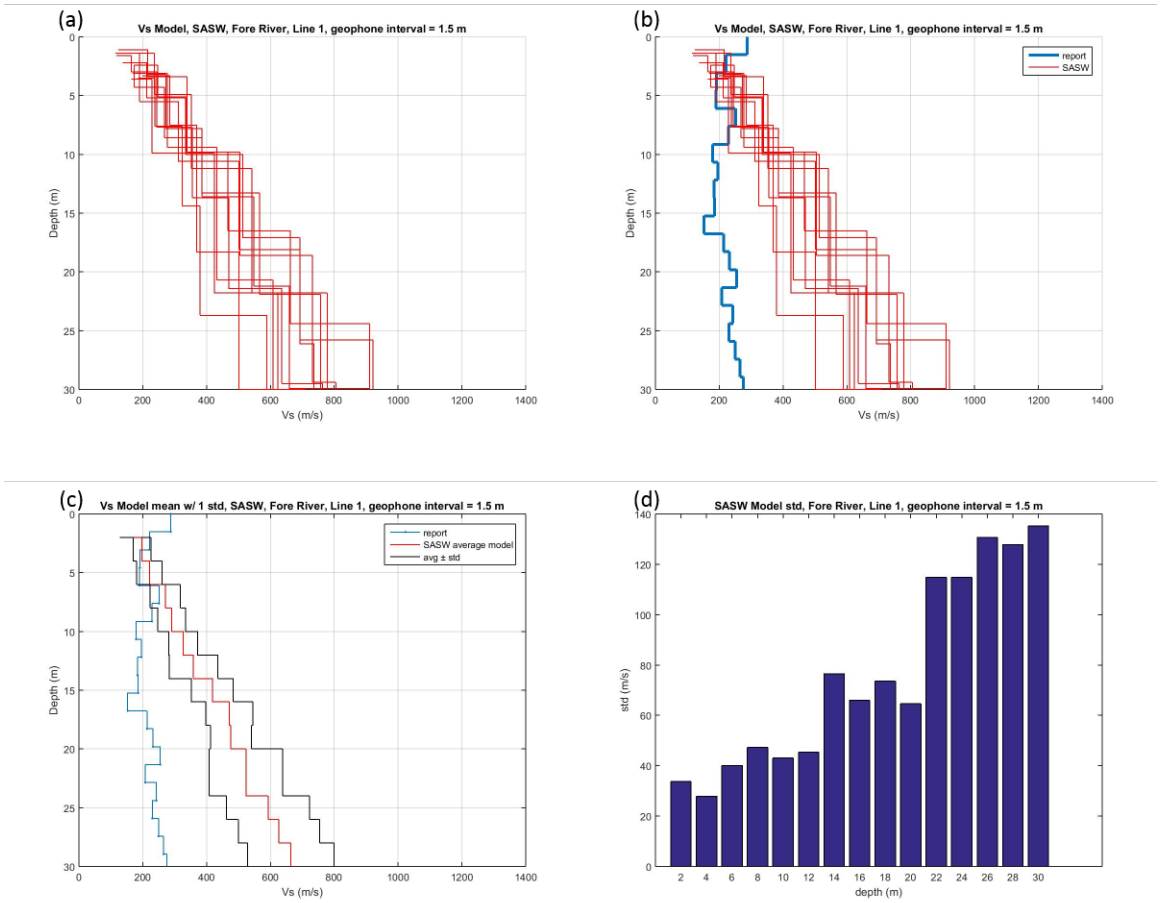

Figure 33: SASW Vs models, 091801, Line 1, Fore River, Δx = 1.5m. The caption for Figure 16 also applies here.

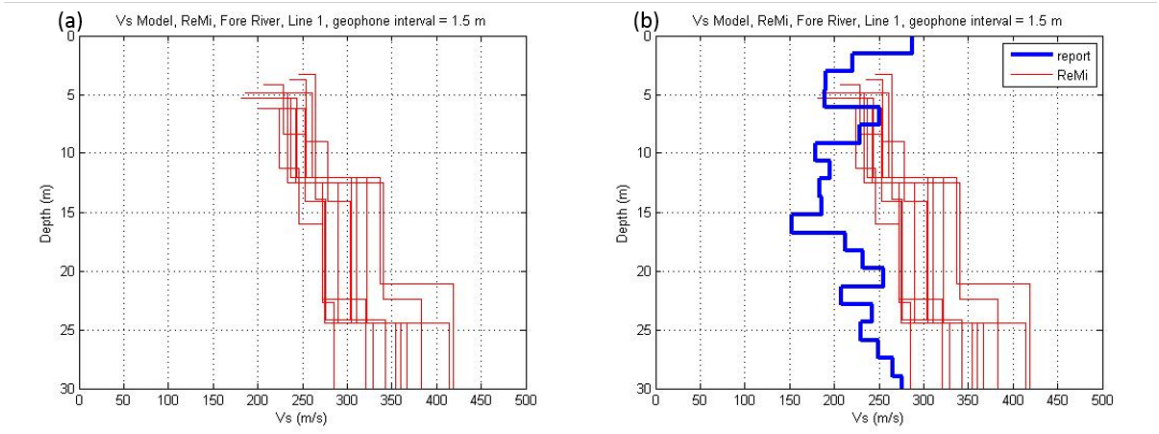

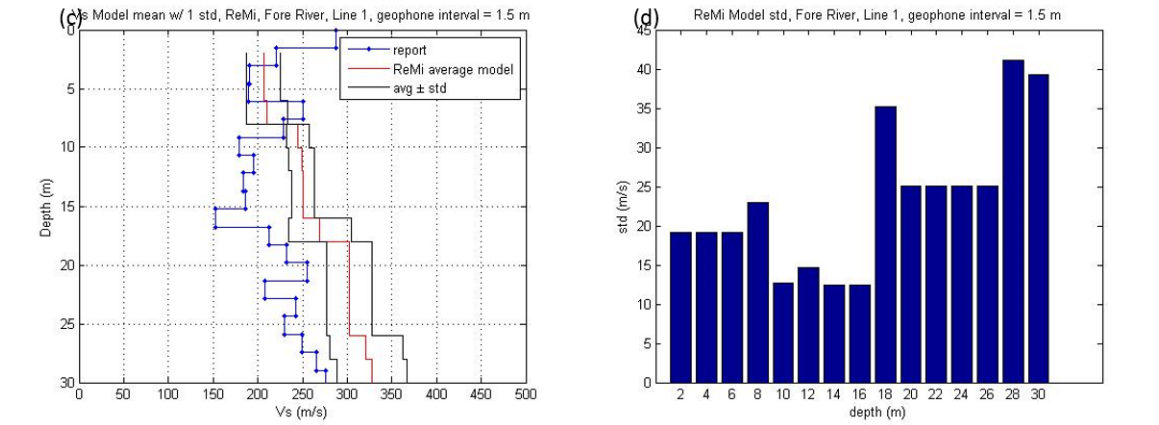

Figure 34: ReMi Vs models, 091802, Line 1, Fore River, Δx = 1.5m. The caption for Figure 30 also applies here.

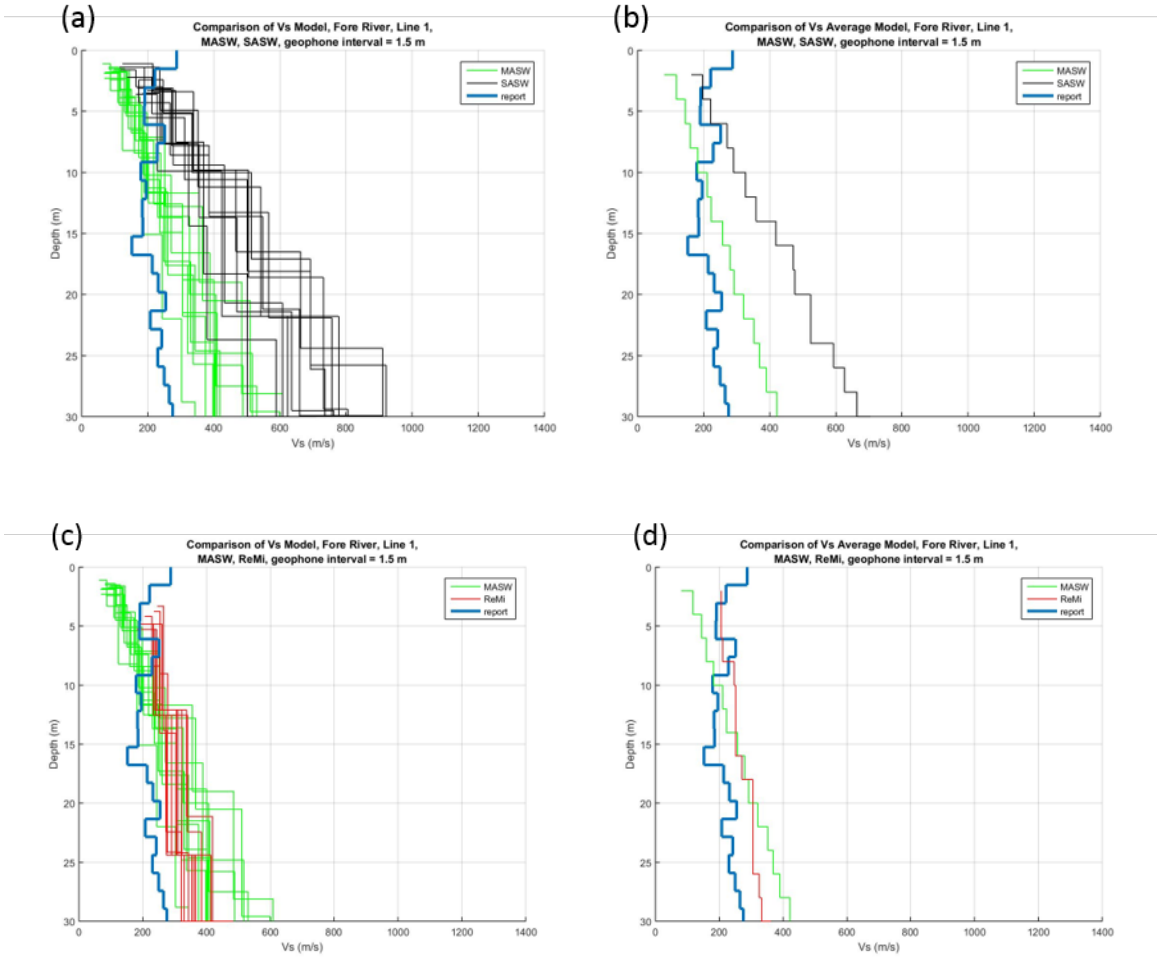

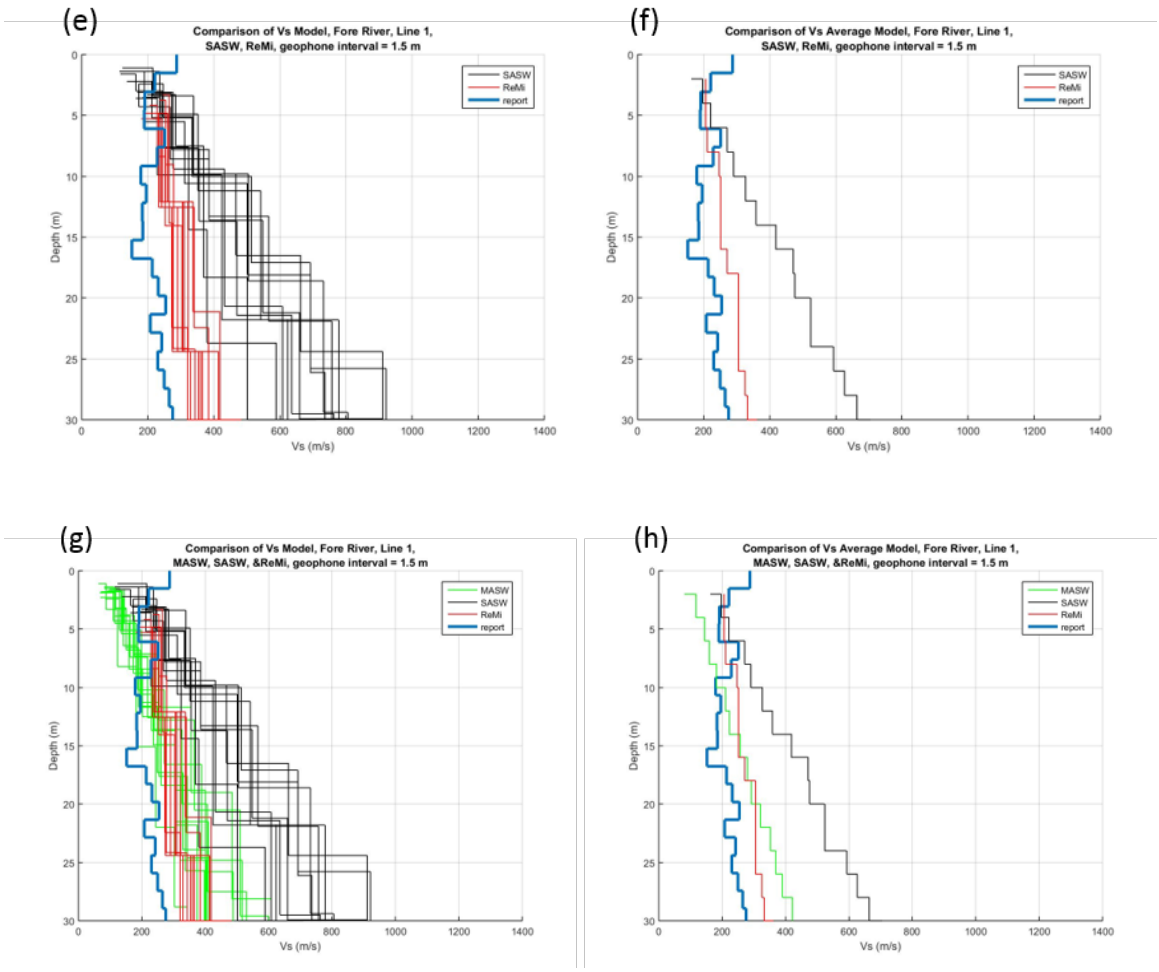

Figure 35: Comparison of the Vs models from the MASW, SASW and ReMi analyses for 091801 and 091802, Line 1, Fore River, Δx = 1.5 m. The caption for Figure 18 also applies here.

2.2.2 Line 2 092503 and 092504

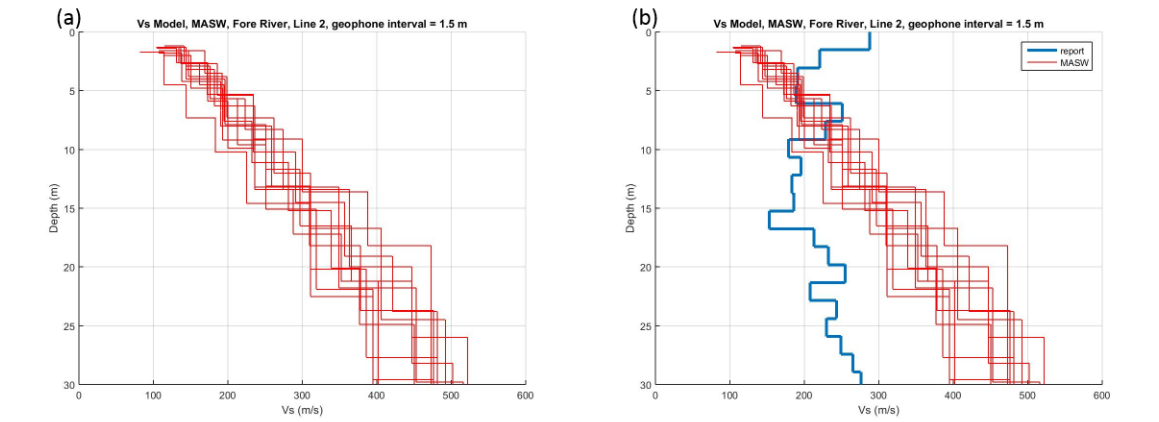

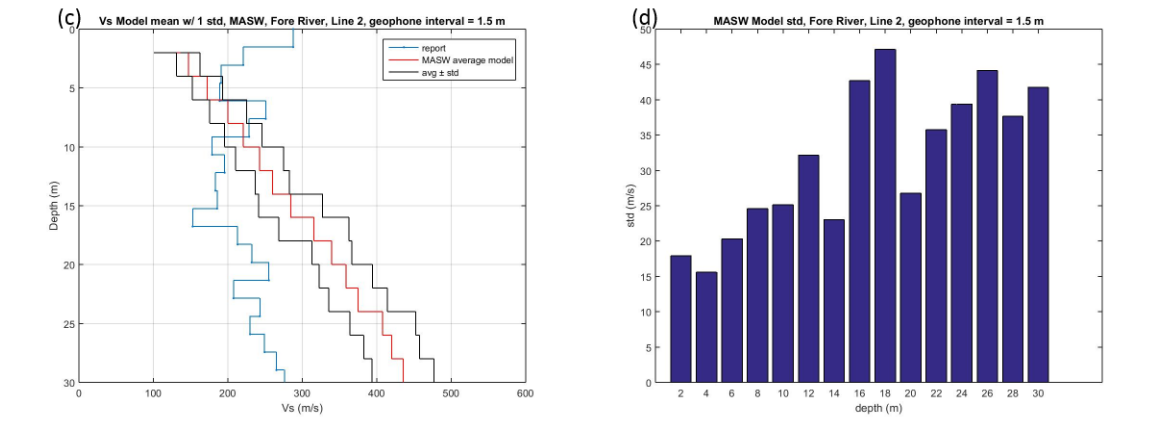

Figure 36: MASW Vs models, 092503 Line 2, Fore River, Δx = 1.5m. The caption for Figure 15 also applies here.

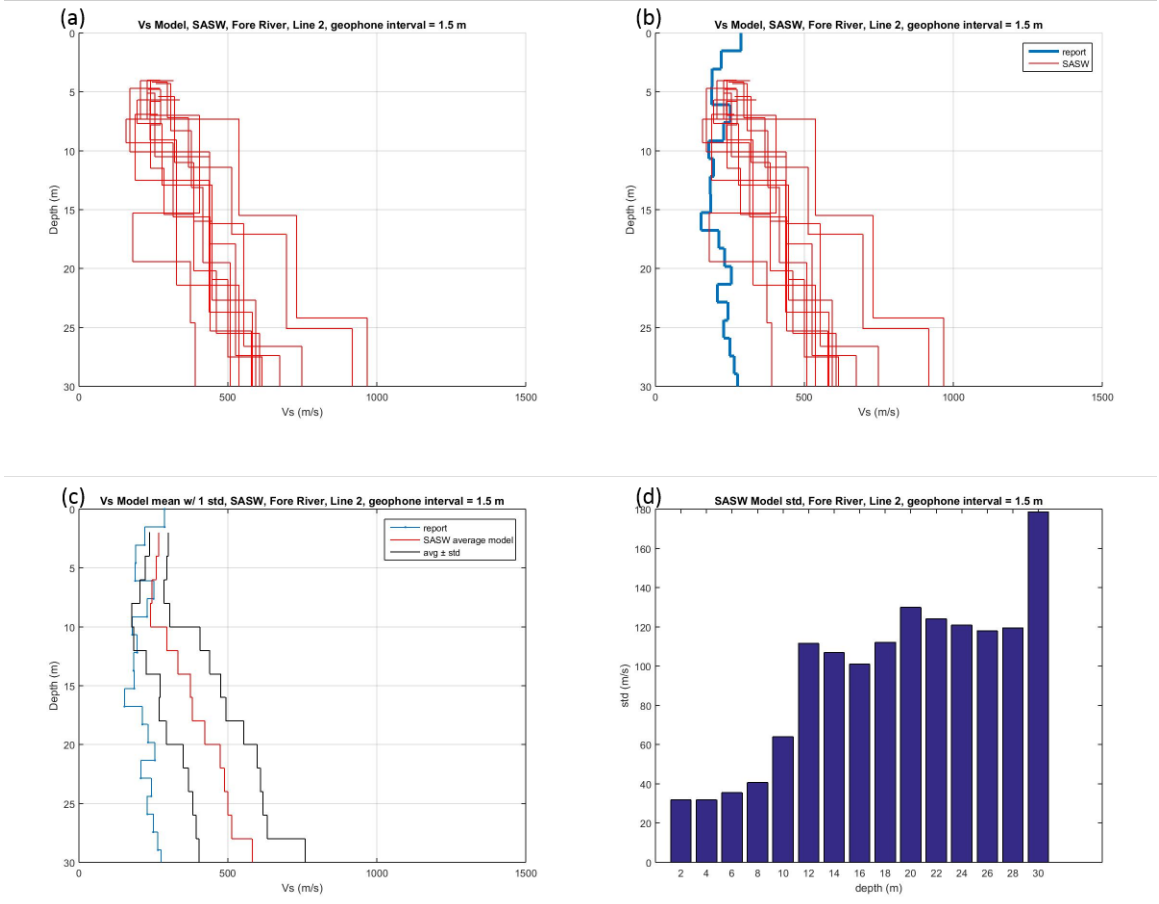

Figure 37: SASW Vs models, 092503, Line 2, Fore River, Δx = 1.5m. The caption for Figure 16 also applies here.

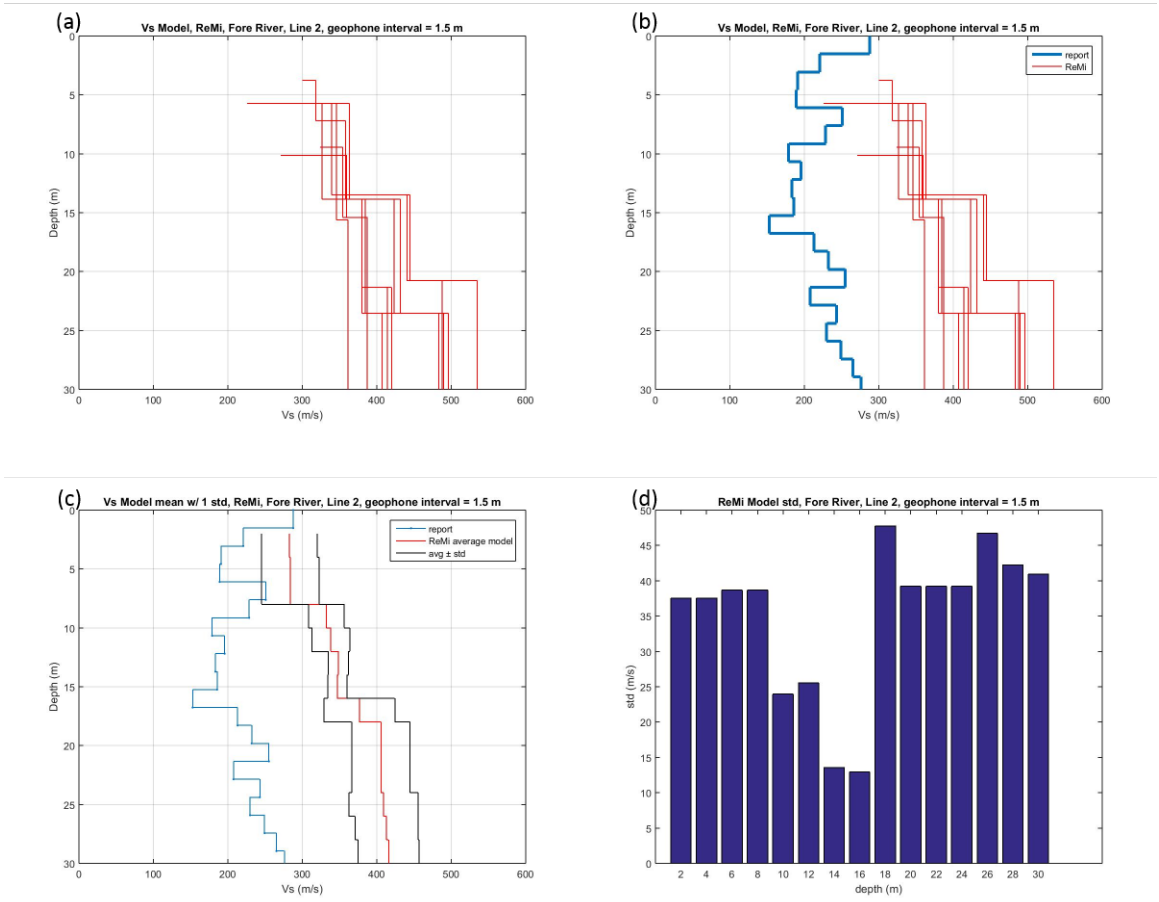

Figure 38: ReMi Vs models, 092504, Line 2, Fore River, Δx = 1.5m. The caption for Figure 30 also applies here.

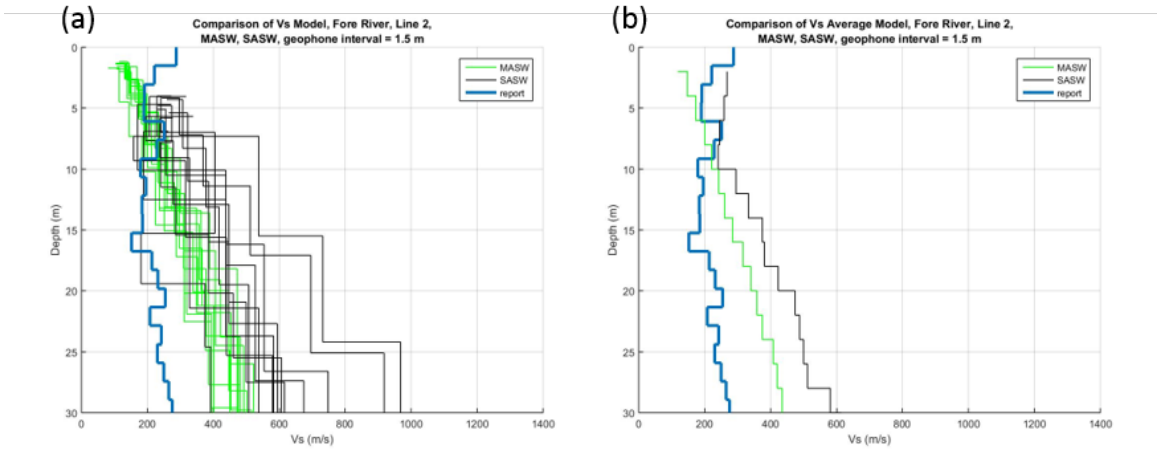

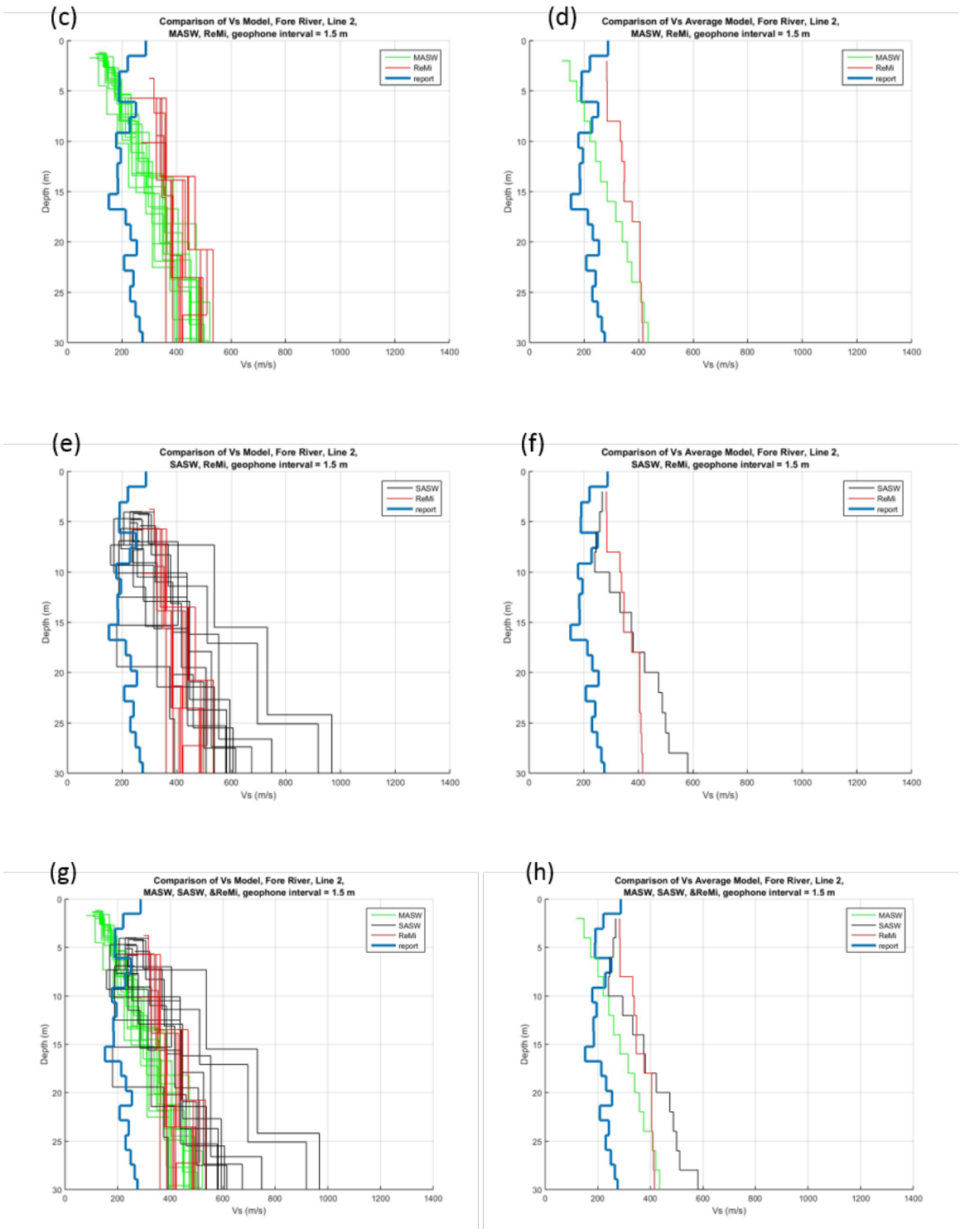

Figure 39: Comparison of the Vs models from the MASW, SASW and ReMi analyses for 092503 and 092504, Line 2, Fore River, Δx = 1.5 m. The caption for Figure 18 also applies here.

Figure 40 shows the average relative difference between the Vs models of the MASW, SASW or ReMi methods and the crosshole Vs profile. The MASW and ReMi methods show similar average relative difference values, while the MASW models show a more consistent accuracy than the ReMi models. The ReMi models have a lower minimum and a higher maximum of average relative differences than the MASW models. Except for the ReMi dataset 092504 (that has a percentage difference of 23%), all of the MASW and ReMi models yield accuracy within 20%. The MASW and the ReMi methods have lower average relative differences than the SASW method, and thus they have better precision than the SASW method.

The standard deviation of the models computed from the three surface-wave methods in **Figure 41** indicates that the MASW method and the ReMi method have lower model standard deviations than the SASW method. The ReMi method has a larger range of standard deviation values than the MASW method, with a higher maximum and a lower minimum. Overall, it is concluded from Fore River data that the MASW method yields the most precise results of the three methods.

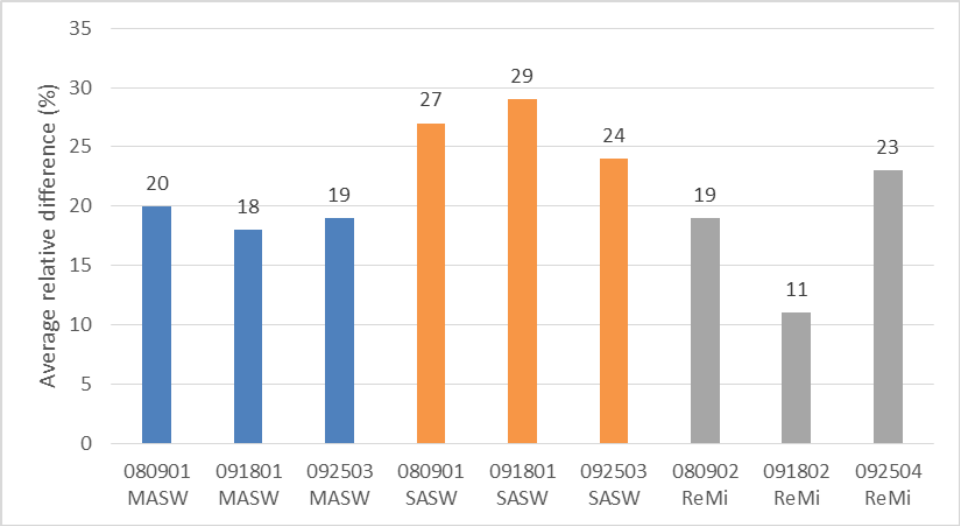

Figure 40: Average relative difference, Fore River. The caption for Figure 24 also applies here.

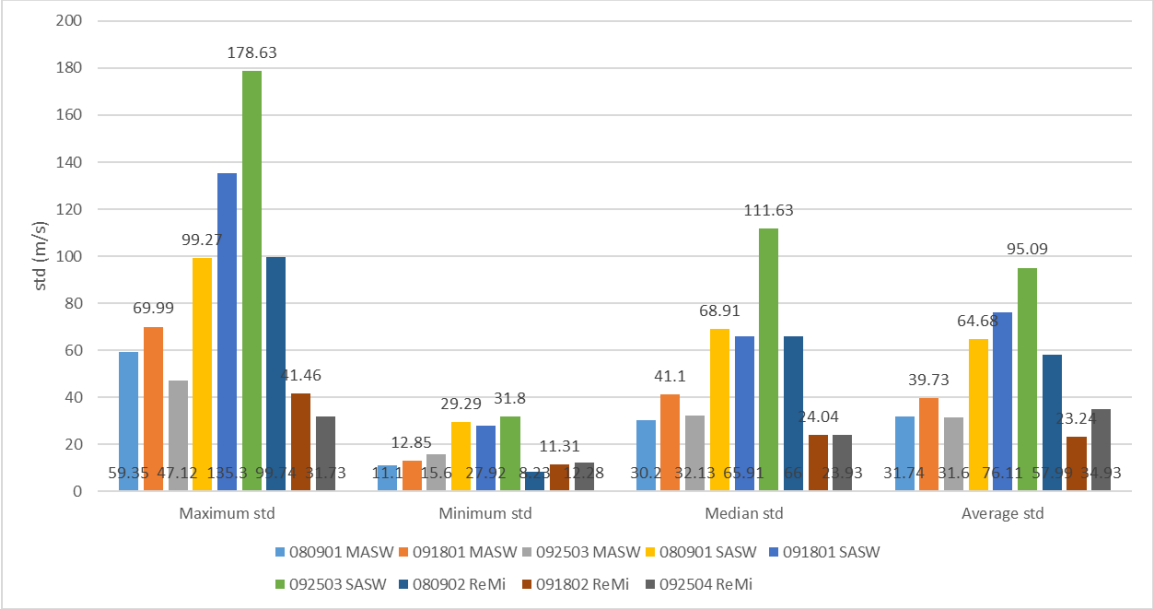

Figure 41: Model standard deviations, Fore River

2.3 Winchester

At Winchester, MA, we laid out two survey lines around Winchester High School (42°27'N, 71°08'W), as shown in **Figure 42**. Line 1 was laid out to the west of the high school along the parking lot. The area is paved, so geophones with tripods were used for Line 1. A shorter line was instrumented to the north of the high school on the soft dirt

area beside Spruce St. The geophones for this line used the spikes. The data collection geometry is given in **Table 3**. At Winchester, the passive data were collected with 32 s windows and with 12 records for each geometry.

The MASW and the SASW models from datasets 092505 and 092509 all have 12 models. Dataset 092506 was processed using the ReMi method, which also yielded 12 models. Because one or two records of each of datasets 092510, 111301 and 111302 were not good enough to yield a surface-wave model, for dataset 092510, only 11 records were processed for the ReMi models; for dataset 111301, there were 12 models for the MASW method, and 11 models for the SASW method; and for dataset 111302, there were 10 models for the ReMi method.

There were no Vs profiles available that could be used as target models at Winchester. Therefore, the surface-wave results at Winchester are not assessed in terms of accuracy. However, the standard deviations of the surface-wave models are compared to assess the precision of the surface-wave methods. The model results are shown in **Figures 43 – 54**.

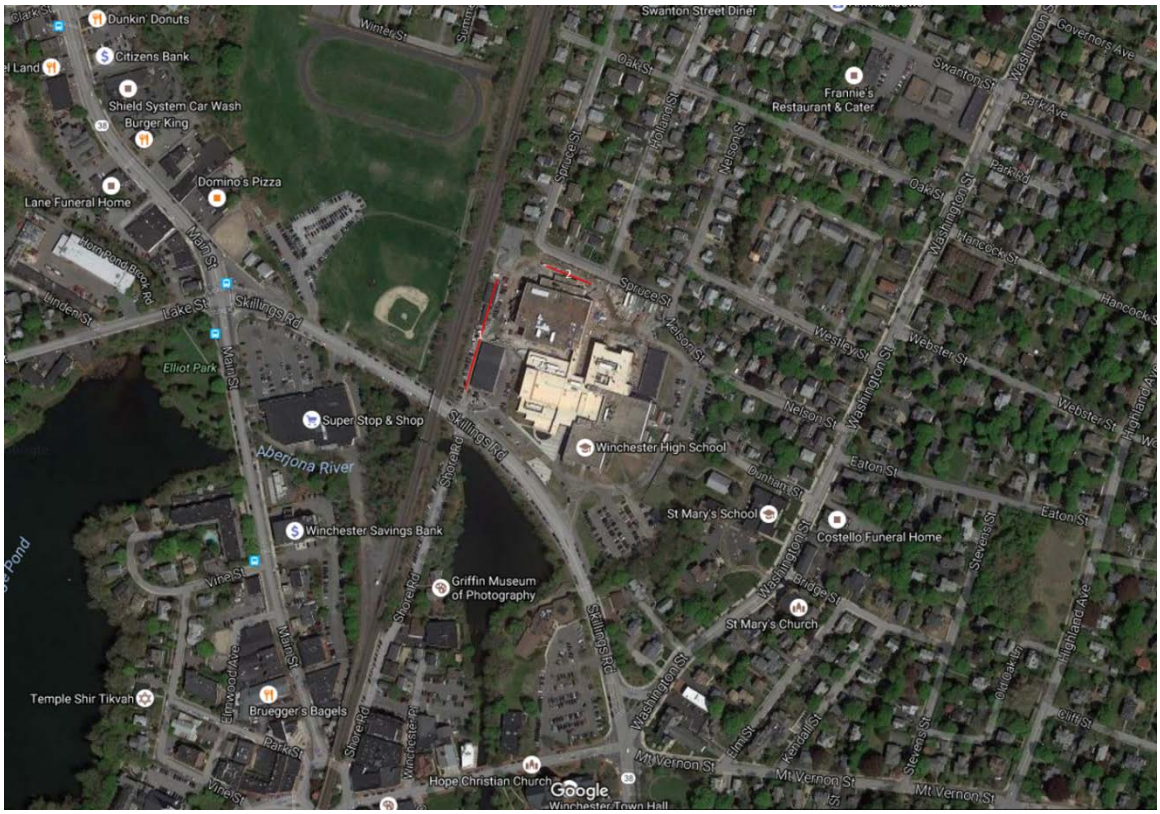

Figure 42: Site map, Winchester

Table 3: Data Collection Geometry at the Winchester site

Line	Line 1		Line 2
Geophone interval Δx (m)	2	1.5	1.5
Dataset (active)	092505	092509	111301
Shot offset x (m)	5 to 20	5 to 20	5 to 25
Dataset (passive)	092506	092510	111302

The MASW models for Line 1 at Winchester show that the Vs values increase with depth from 75 m/s to 250 m/s (**Figures 43, 47**). For the MASW models from Line 2, the shear-wave velocities vary from 100 m/s to 360 m/s (**Figure 51**).

2.3.1 Line 1 092505, 092506 and 092509, 092510

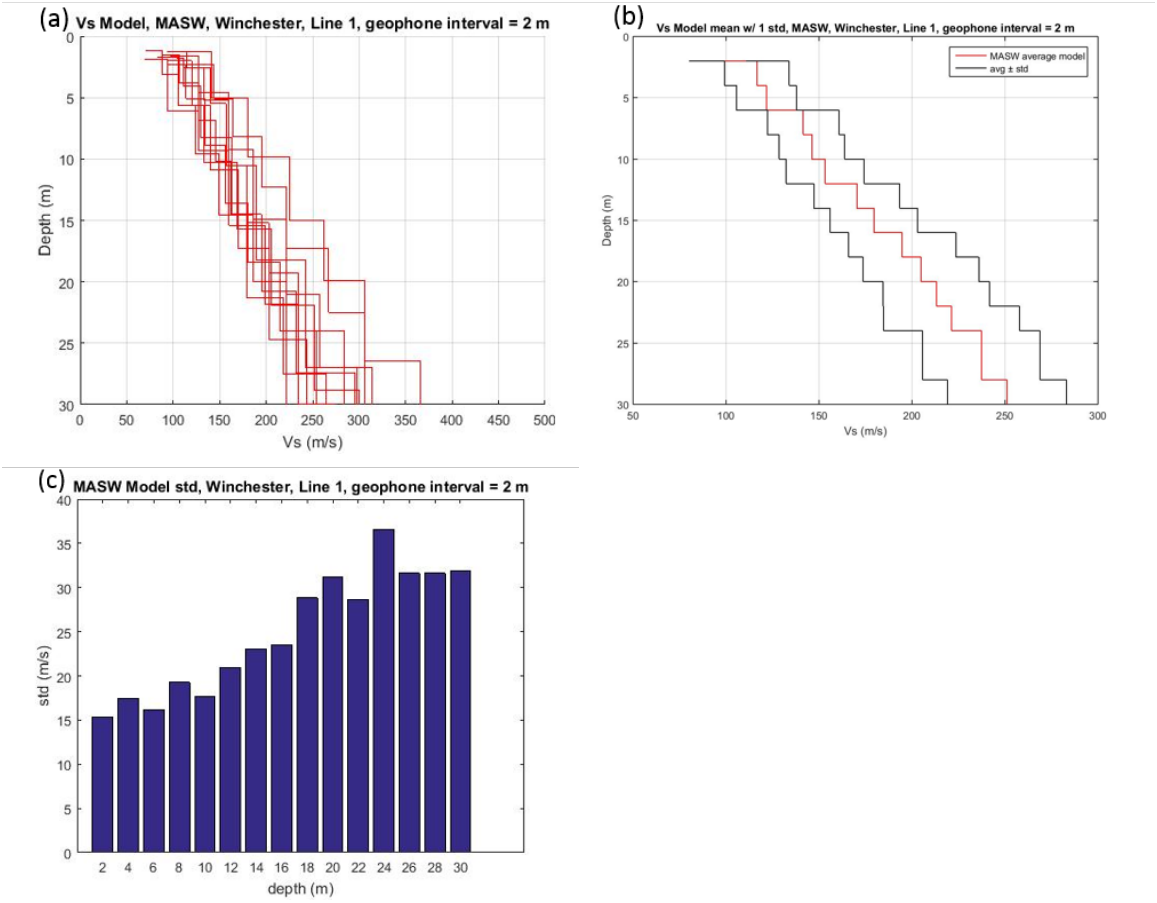

Figure 43: MASW Vs models, 092505, Line 1, Winchester, Δx = 2m. (a) Plots of the MASW Vs models. Each red line represents one Vs model processed from one shot record. (b) Average model of the MASW models in (a) calculated at 2-m depth intervals (red line), average +/- standard deviation (two black lines) (c) Standard deviations of the MASW models in (a) calculated at 2-m depth intervals.

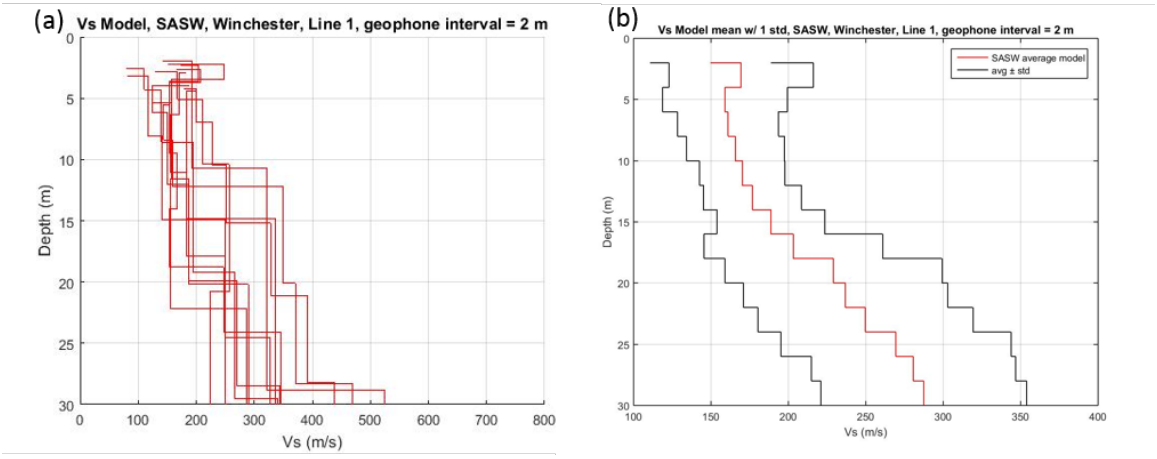

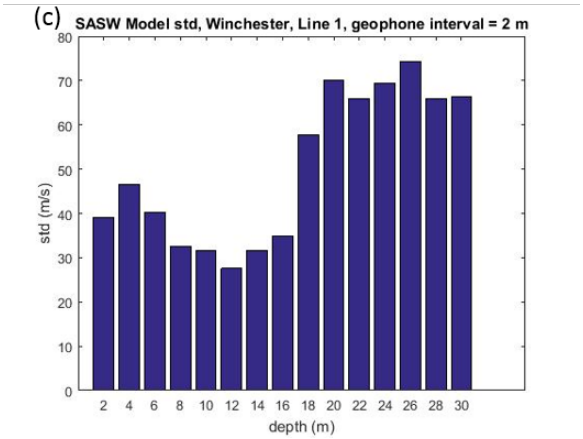

Figure 44: SASW Vs models, 092505, Line 1, Winchester, Δx = 2m. (a) Plots of the SASW Vs models. Each red line represents one Vs model processed from one shot record. (b) Average model of the SASW models in (a) calculated at 2-m depth intervals (red line), average +/- standard deviation (two black lines) (c) Standard deviations of the SASW models in (a) calculated at 2-m depth intervals.

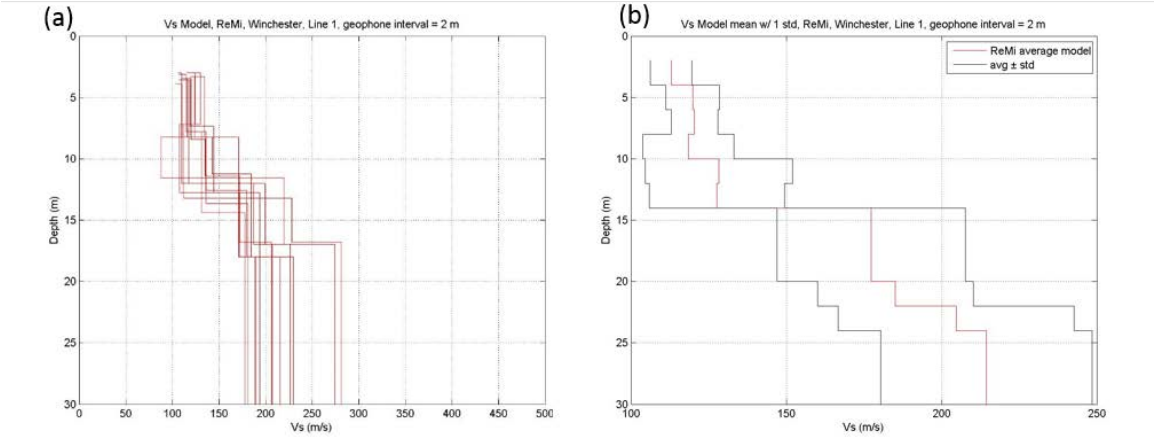

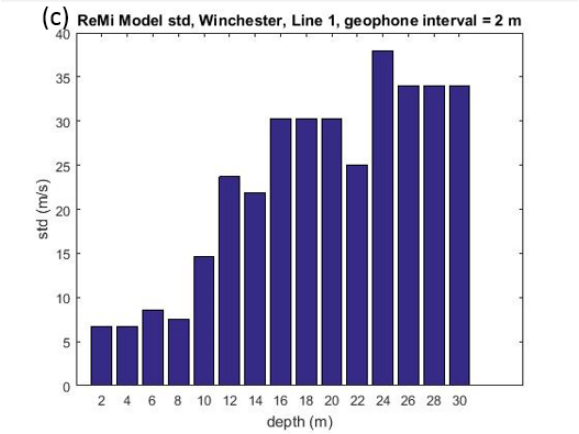

Figure 45: ReMi Vs models, 092506, Line 1, Winchester, Δx = 2m. (a) Plots of the ReMi Vs models. Each red line represents one Vs model processed from one shot record. (b) Average model of the ReMi models in (a) calculated at 2-m depth intervals (red line), average +/- standard deviation (two black lines) (c) Standard deviations of the ReMi models in (a) calculated at 2-m depth intervals.

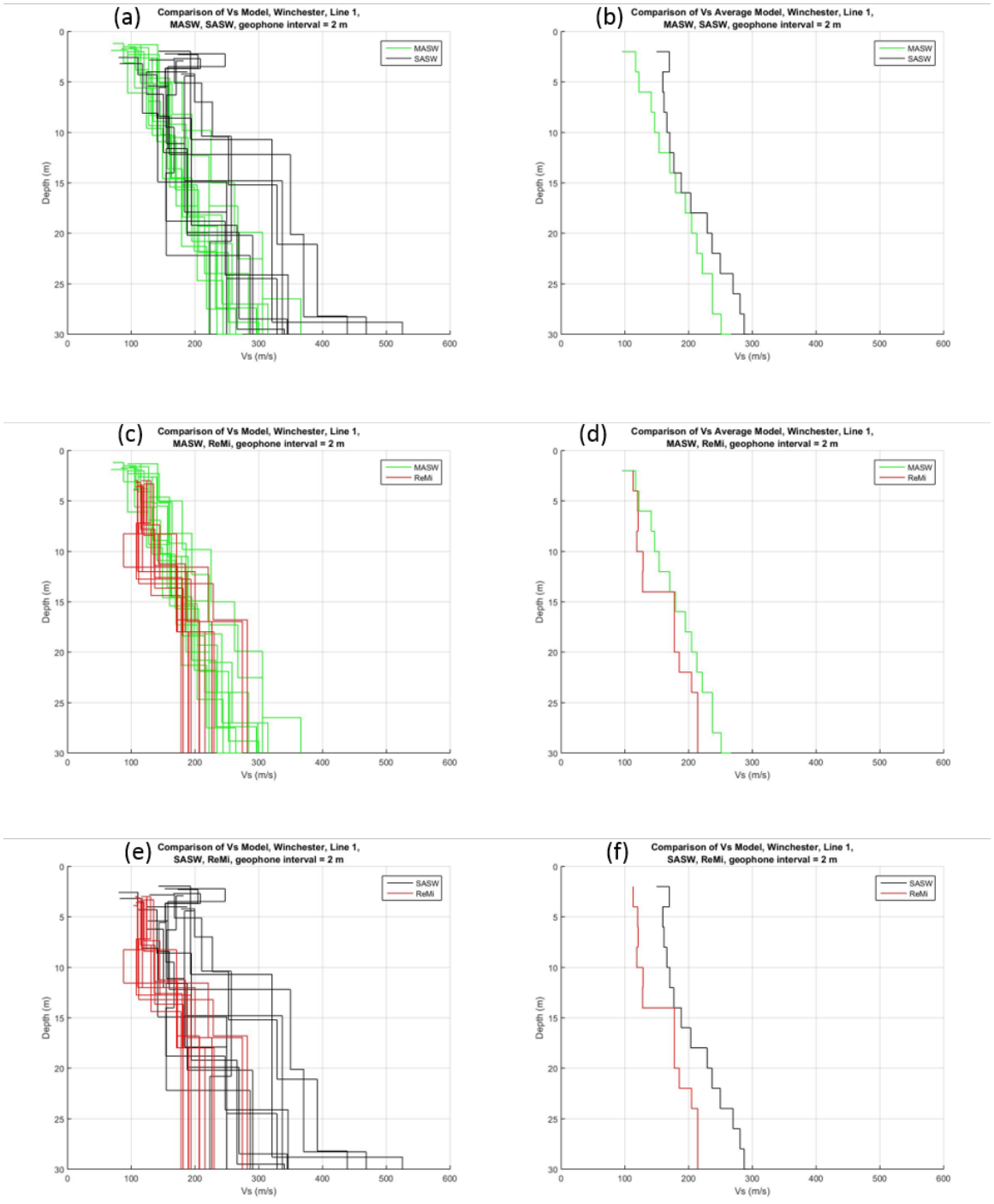

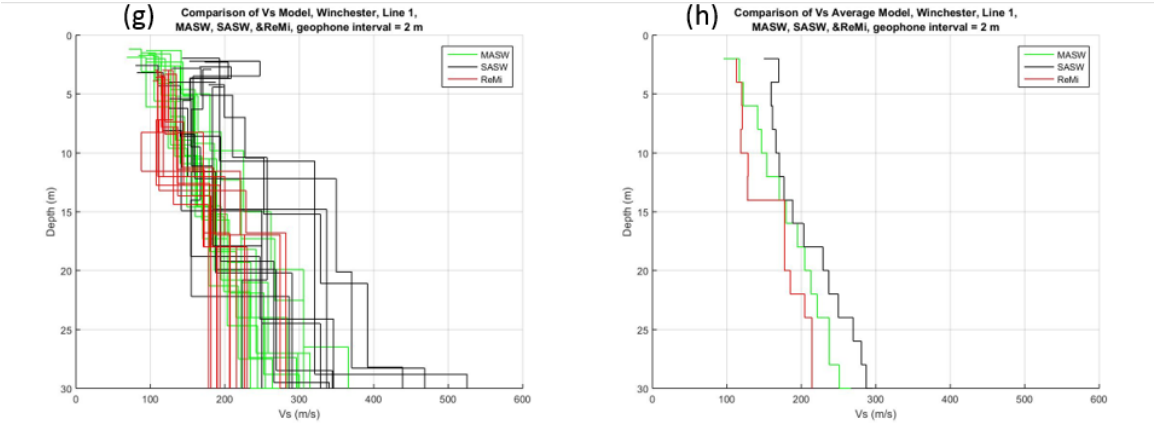

Figure 46: Comparison of the Vs models from the MASW, SASW and ReMi analyses for 092505 and 092506, Line 1, Winchester, Δx = 2 m. The caption for Figure 18 also applies here.

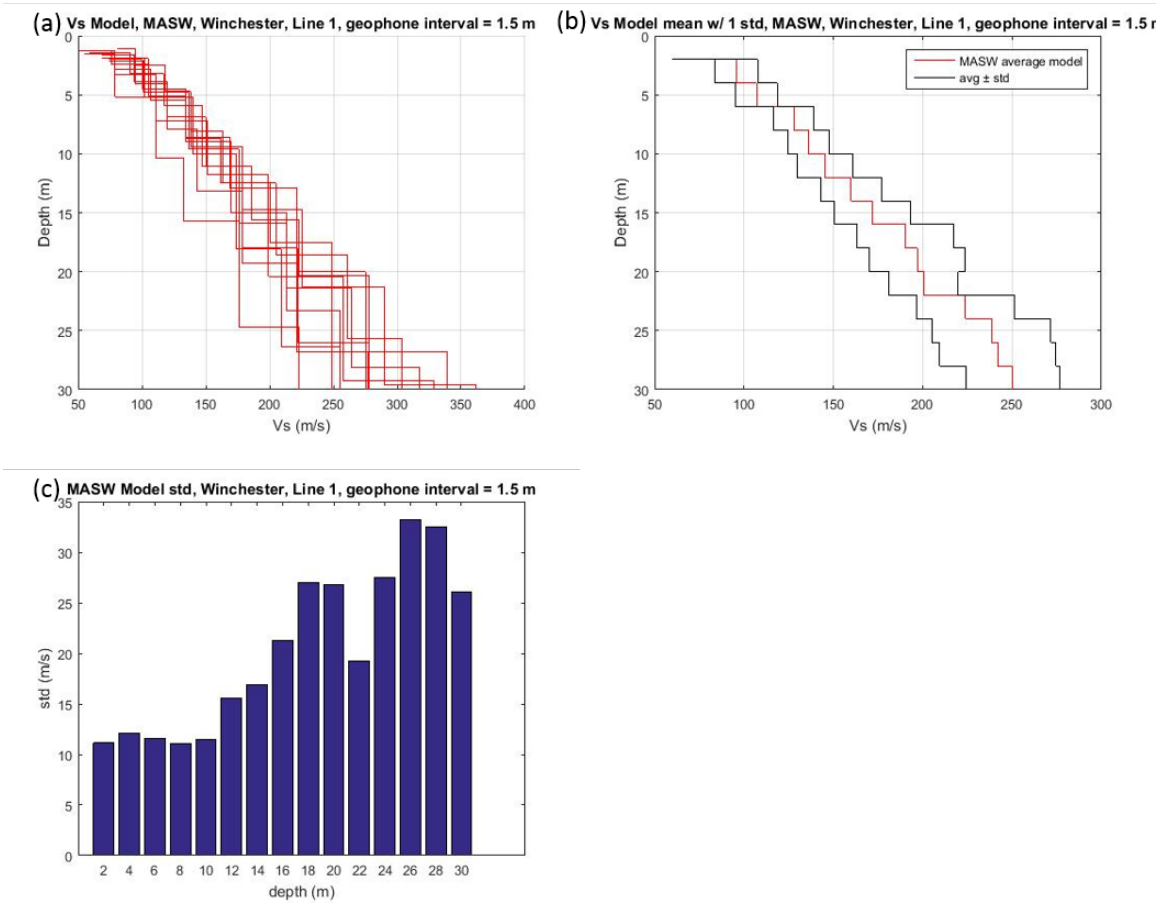

Figure 47: MASW Vs models, 092509 Line 1, Winchester, Δx = 1.5m. The caption for Figure 43 also applies here.

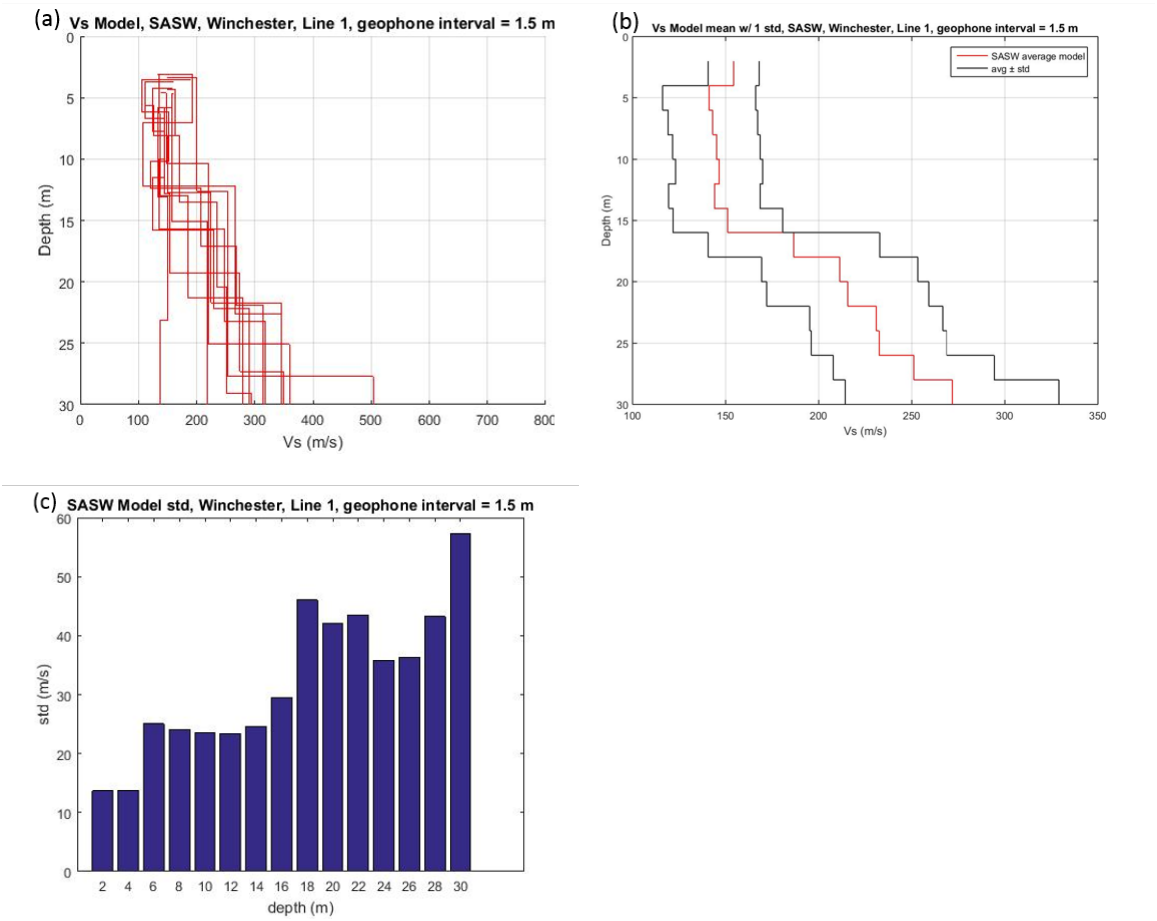

Figure 48: SASW Vs models, 092509 Line 1, Winchester, Δx = 1.5m. The caption for Figure 44 also applies here.

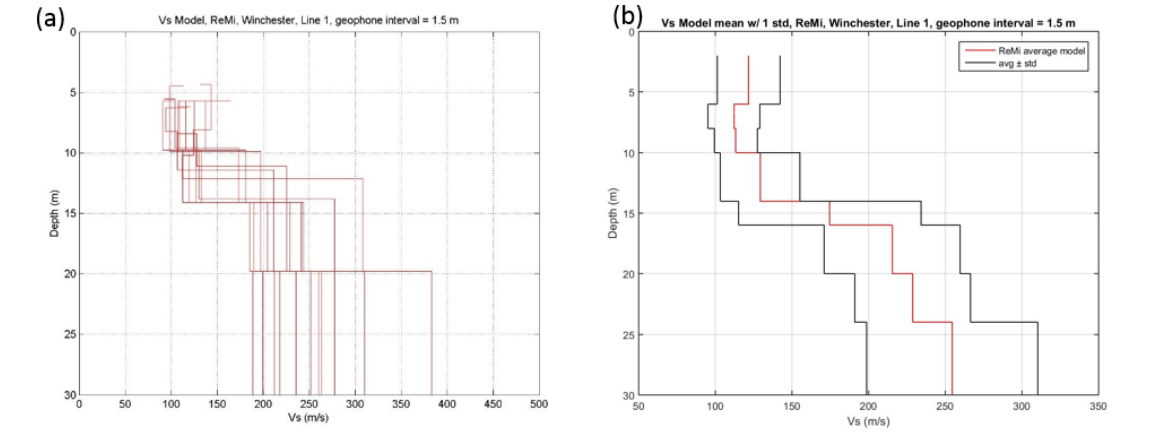

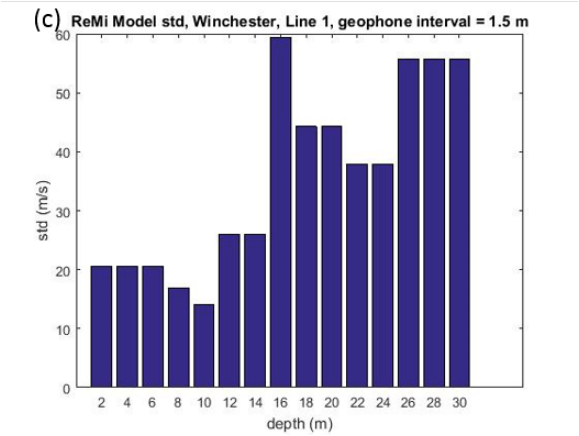

Figure 49: ReMi Vs models, 092510 Line 1, Winchester, Δx = 1.5m. The caption for Figure 45 also applies here.

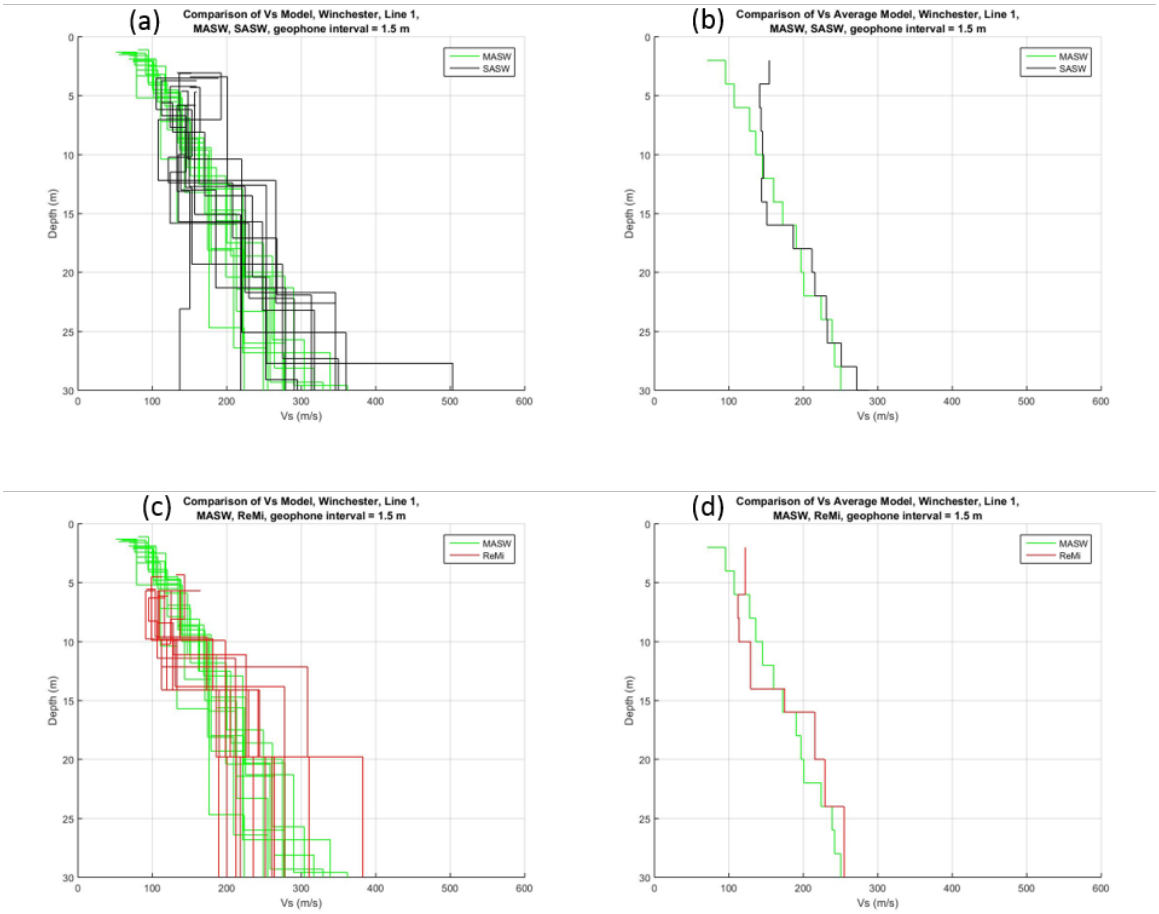

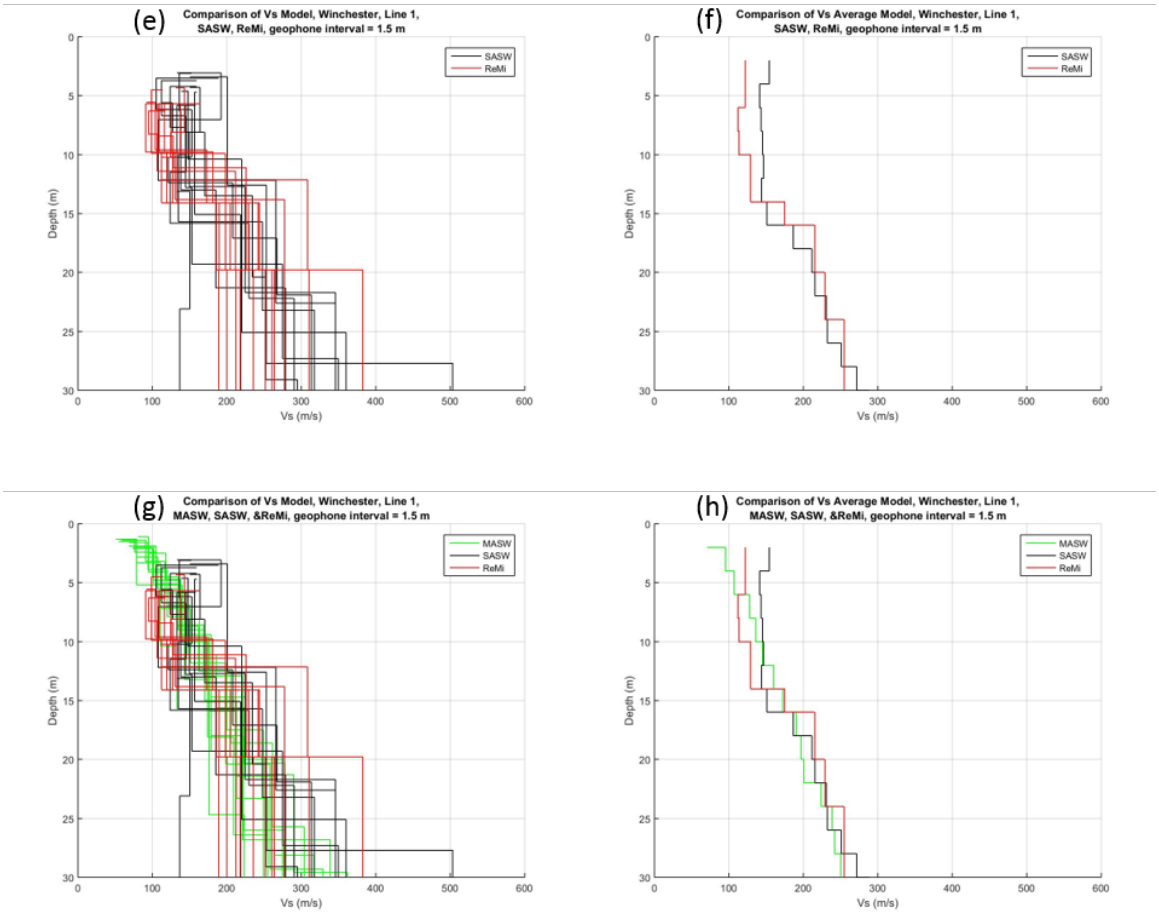

Figure 50: Comparison of the Vs models from the MASW, SASW and ReMi analyses for 092509 and 092510, Line 1, Winchester, Δx = 1.5 m. The caption for Figure 18 also applies here.

2.3.2 Line 2 111301 and 111302

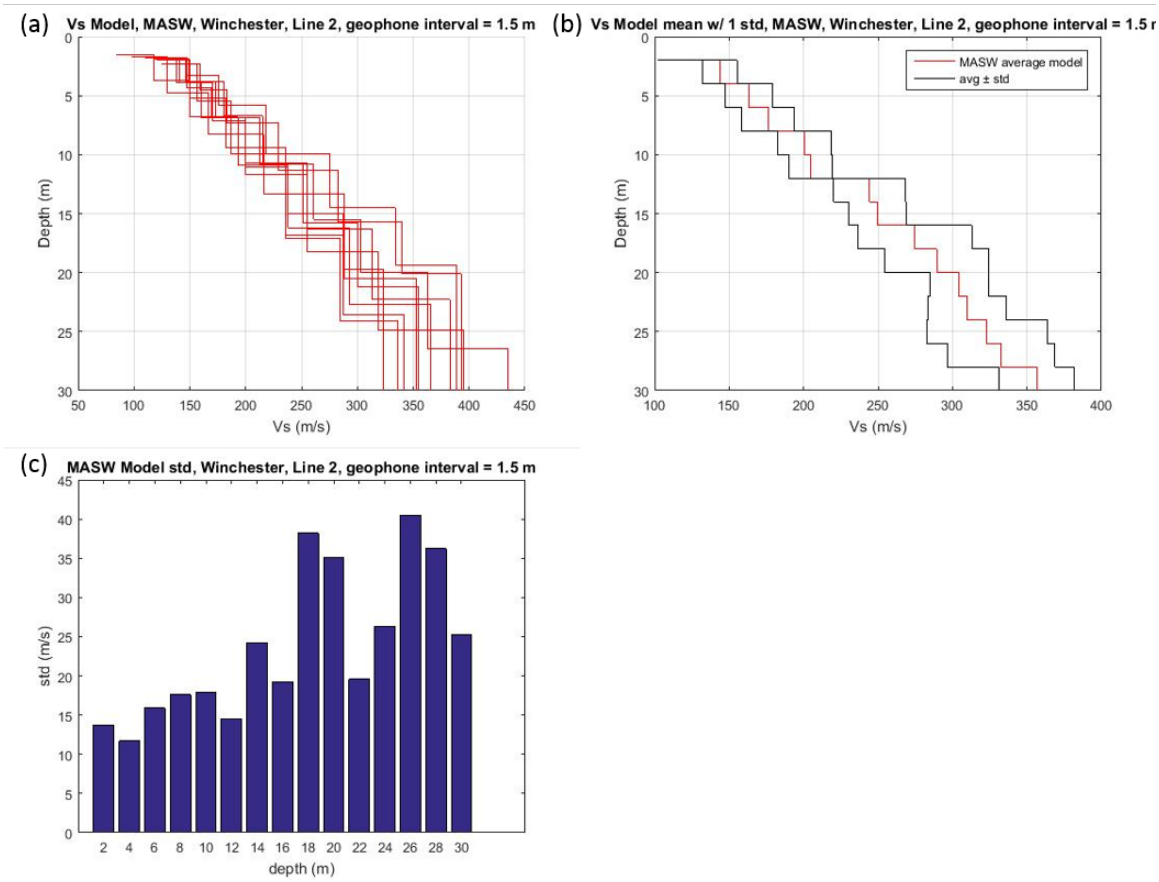

Figure 51: MASW Vs models, 111301 Line 2, Winchester, Δx = 1.5m. The caption for Figure 43 also applies here.

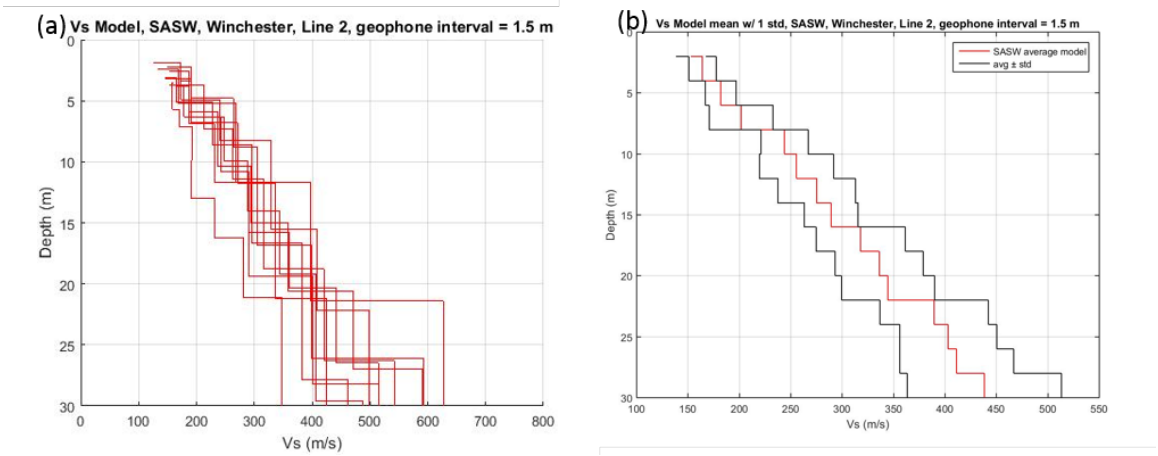

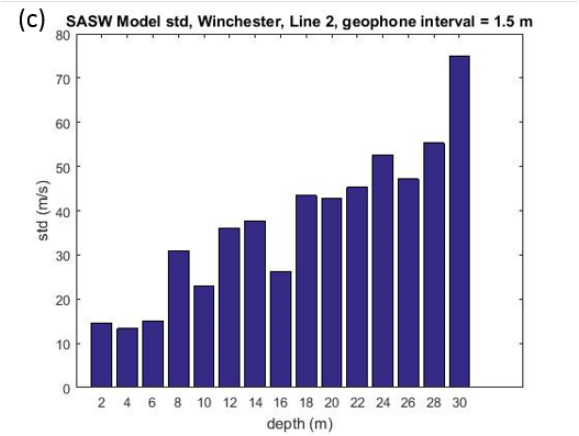

Figure 52: SASW Vs models, 111301 Line 2, Winchester, Δx = 1.5m. The caption for Figure 44 also applies here.

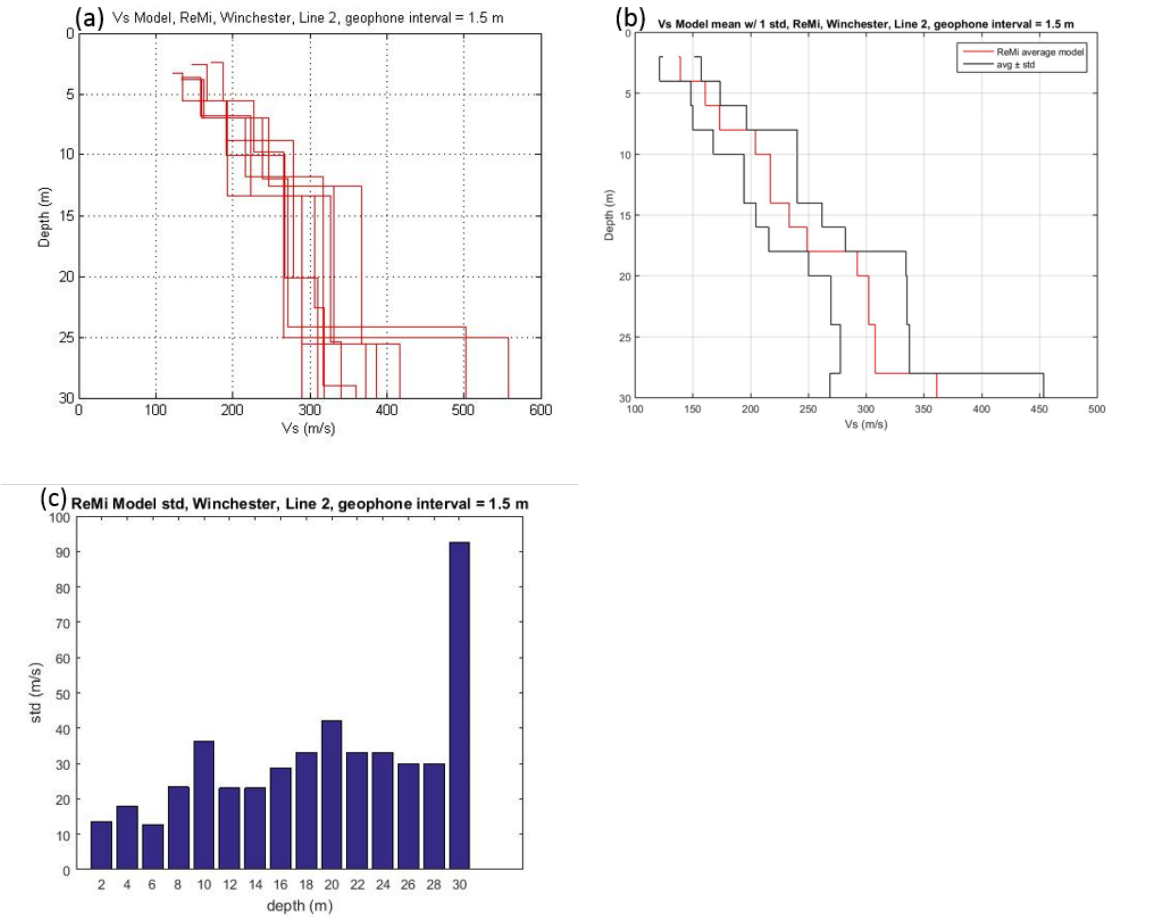

Figure 53: ReMi Vs models, 111302 Line 2, Winchester, Δx = 1.5m. The caption for Figure 45 also applies here.

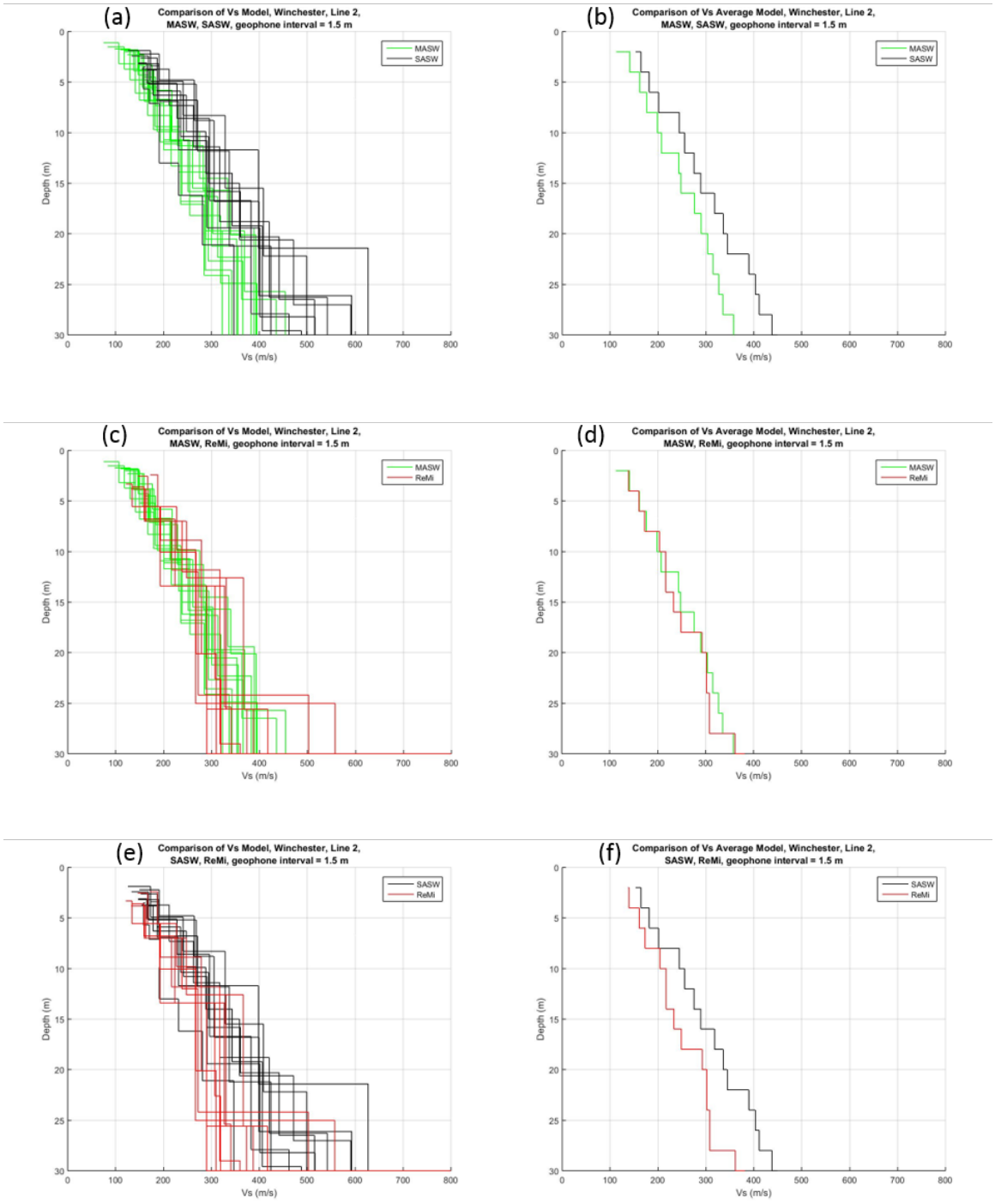
(a)
Comparison of Vs Model, Winchester, Line 2,
MASW, SASW, geophone interval = 1.5 m
MASW
SASW
Depth (m)
Vs (m/s)
(b)
Comparison of Vs Average Model, Winchester, Line 2,
MASW, SASW, geophone interval = 1.5 m
MASW
SASW
Depth (m)
Vs (m/s)
(c)
Comparison of Vs Model, Winchester, Line 2,
MASW, ReMi, geophone interval = 1.5 m
MASW
ReMi
Depth (m)
Vs (m/s)
(d)
Comparison of Vs Average Model, Winchester, Line 2,
MASW, ReMi, geophone interval = 1.5 m
MASW
ReMi
Depth (m)
Vs (m/s)
(e)
Comparison of Vs Model, Winchester, Line 2,
SASW, ReMi, geophone interval = 1.5 m
SASW
ReMi
Depth (m)
Vs (m/s)
(f)
Comparison of Vs Average Model, Winchester, Line 2,
SASW, ReMi, geophone interval = 1.5 m
SASW
ReMi
Depth (m)
Vs (m/s)

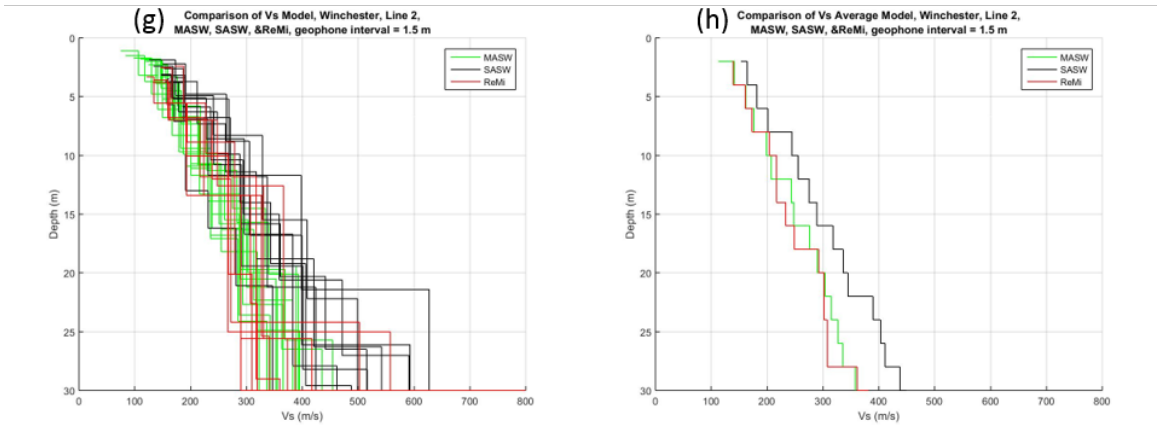

Figure 54: Comparison of the Vs models from the MASW, SASW and ReMi analyses for 111301 and 111302, Line 2, Winchester, Δx = 1.5 m. The caption for Figure 18 also applies here.

Figure 55 shows the standard deviation of the MASW, SASW and ReMi models. From data at Winchester, the MASW method has the smallest standard deviation, followed by the ReMi method. In conclusion, the MASW method is the most precise among the three methods. The SASW method has the highest standard deviation, and thus is the least precise of the three methods.

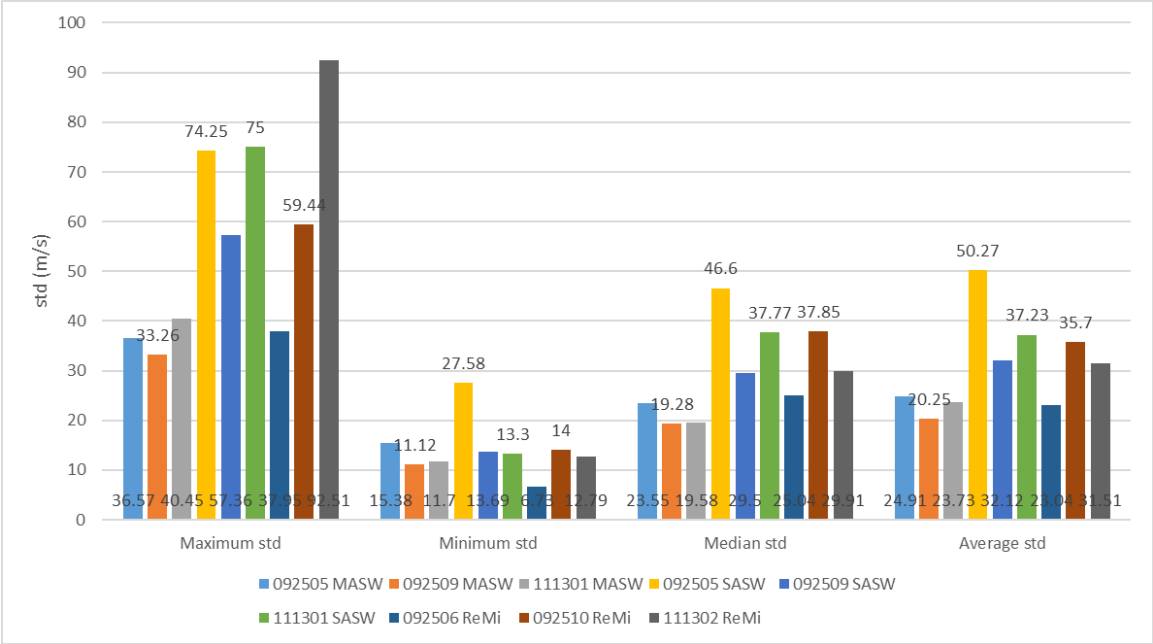

Figure 55: Model standard deviations, Winchester

3.0 DISCUSSION

There are many published comparisons of surface-wave methods. For example, Xia et al. (2002) used the MASW method and compared their results with borehole measurements at sites in Kansas, British Columbia, and Wyoming. Yilmaz et al. (2008) compared Vs profiles estimated by the MASW method with the results of a downhole survey and the SASW method in Turkey. Stephenson et al. (2005) analyzed the Vs profiles acquired by the MASW and ReMi methods in comparison with borehole surveys in Santa Clara Valley in California. Brown et al. (2002) compared the shear-wave slownesses from the SASW method and borehole measurements in the Los Angeles region. However, not many of these studies include comparisons with crosshole surveys, and still fewer are in New England.

From the comparison conducted at Lawrence, Kansas by Xia et al. (2002), the average relative difference between the results from the MASW method and the downhole survey was 18%. The difference dropped to 9% by excluding the first layer. At the site along the Fraser River in Vancouver, Canada, the average relative difference was less than 15% (Xia et al., 2002). Stephenson et al. (2005) showed that the percentage differences of $V_{s,30}$ from the MASW method and borehole measurement were 7 – 10% in

the Santa Clara Valley in California. Yilmaz et al. (2008) evaluated depth average of percentage differences and the percentage differences of $V_{s,avg}$ calculated using the NEHRP velocity (Building Seismic Safety Council, B.S.S.C., 2003) between the MASW method and the borehole seismic data. They found that at 6 of their 10 sites in Turkey, the percentage differences were within 15%, while at the other 4 sites, the percentage differences were above 15% with a maximum of 55%.

In general, the Vs models from the MASW method in my study yield percentage differences within 20%. The average relative differences between the Vs models from the MASW method and the Vs profiles from borehole measurements were 10% at Canton, which is consistent with the 15% threshold found by others, and within 20% at Fore River. The higher percentage difference seen at Fore River compared to Canton may be attributed to the poor recording conditions at Fore River (with the nearby construction and the busy traffic running by all the time).

The ReMi datasets that were compared with crosshole or SCPT profiles at Canton and at Fore River yield 5 – 23% average relative differences, comparable to the quality of MASW data (10 – 20%). From the results found by Louie (2001) and Heath et al. (2006), the difference of $V_{s,30}$ from ReMi and borehole measurement is less than 20%. Stephenson et al. (2005) also concluded that both the MASW method (percentage difference of 7 – 10%) and the ReMi method (percentage difference of 1 – 15%) could provide appropriate Vs profiles of comparable accuracy. The MASW method yields a smaller range of percentage differences than the ReMi method.

According to the analyses of the surface-wave data collected at three sites in this thesis, the MASW method has the smallest standard deviations and is concluded to be the most precise of the three methods. At Canton, the MASW models have smaller standard deviations than the SASW models. At Fore River, the ReMi method has a larger range of standard deviation values than the MASW method, with a higher maximum and a lower minimum. At Winchester, the MASW method has the smallest standard deviation, followed by the ReMi method (**Figures 25, 41** and **55**).

Overall, the MASW models (percentage difference of 10 - 20%) and ReMi models (percentage difference of 5 - 23%) may have higher or lower velocity values than the reference profiles at different sites or survey lines. For the MASW data, Xia et al. (2002) and Yilmaz et al. (2008) have also drawn the same conclusion that the borehole measurement and MASW velocities do not exhibit a systematic difference. Based on their results, the MASW method generally has a percentage difference of accuracy within 15%. The SASW method gives larger Vs values than the borehole measurements as well as the other two surface-wave methods. It has the highest average relative differences (17 - 29%, **Figure 24** and **Figure 40**) and the highest standard deviations (**Figures 25, 41** and **55**), and thus it is concluded to be the least accurate and the least precise method among the three surface-wave methods that were tested in this thesis.

4.0 CONCLUSION

Comparisons of the three surface-wave methods are made in terms of accuracy and precision in this thesis. Based on the data analyzed for Canton and Fore River, the average relative differences of the MASW Vs models are between 10% and 20%. The ReMi models have comparable accuracy with the MASW models, but with a larger range of percentage differences (5 - 23%). The MASW method has the best precision with the smallest standard deviations compared to the ReMi and the SASW methods. Overall, the MASW method is the best method to determine the shear-wave velocity profile of the subsurface soil layers in the greater Boston area. Among the methods tested here, the SASW method is concluded to be the least accurate and least precise method with the highest average relative differences and the highest standard deviations.

REFERENCES

Brown, L.T., Boore, D.M. and Stokoe, K.H., 2002. Comparison of shear-wave slowness profiles at 10 strong-motion sites from noninvasive SASW measurements and measurements made in boreholes. *Bulletin of the Seismological Society of America*, *92*(8), pp.3116-3133.

Building Seismic Safety Council, B.S.S.C., 2003. NEHRP recommended provisions for seismic regulations for new buildings and other structures. *Report FEMA-450 (Provisions), Federal Emergency Management Agency (FEMA), Washington*.

Castellaro, S., Mulargia, F. and Rossi, P.L., 2008. VS30: Proxy for seismic amplification?. *Seismological Research Letters*, *79*(4), pp.540-543.

Foti, S., Lai, C.G., Rix, G.J. and Strobbia, C., 2014. *Surface wave methods for near-surface site characterization*. CRC Press.

Gucunski, N. and Woods, R.D., 1991. INSTRUMENTATION FOR SASW TESTING. RECENT ADVANCES IN INSTRUMENTATION, DATA ACQUISITION AND TESTING IN SOIL DYNAMICS. PROCEEDINGS OF SESSIONS SPONSORED BY THE GEOTECHNICAL ENGINEERING DIVISION OF THE AMERICAN SOCIETY OF CIVIL ENGINEERS IN CONJUNCTION WITH THE ASCE CONVENTION ORLANDO, FLORIDA. OCTOBER 21, 1991. *Publication of: American Society of Civil Engineers*.

Heath, K., Louie, J.N., Biasi, G., Pancha, A. and Pullammanappallil, S.K., 2006. Blind tests of refraction microtremor analysis against synthetics and borehole data. In *Proceedings of the 100th Anniversary Earthquake Conference, CD-ROM*.

Louie, J.N., 2001. Faster, better: shear-wave velocity to 100 meters depth from refraction microtremor arrays. *Bulletin of the Seismological Society of America*, *91*(2), pp.347-364.

Malhotra, V.M. and Carino, N.J., 1991. *CRC handbook on nondestructive testing of concrete*. CRC press.

Nazarian, S., Stokoe, I.I., Kenneth, H. and Hudson, W.R., 1983. *Use of spectral analysis of surface waves method for determination of moduli and thicknesses of pavement systems* (No. 930).

Nazarian, S. and Desai, M.R., 1993. Automated surface wave method: field testing. *Journal of Geotechnical Engineering*, *119*(7), pp.1094-1111.

Park, C.B., Miller, R.D. and Xia, J., 1998. Imaging dispersion curves of surface waves on multi-channel record. In *SEG Technical Program Expanded Abstracts 1998* (pp. 1377-1380). Society of Exploration Geophysicists.

Park, C.B., Miller, R.D. and Xia, J., 1999. Multichannel analysis of surface waves. *Geophysics*, *64*(3), pp.800-808.

Sheriff, R.E. and Geldart, L.P., 1995. *Exploration seismology*. Cambridge university press.

Stephenson, W.J., Louie, J.N., Pullammanappallil, S., Williams, R.A. and Odum, J.K., 2005. Blind shear-wave velocity comparison of ReMi and MASW results with boreholes to 200 m in Santa Clara Valley: Implications for earthquake ground-motion assessment. *Bulletin of the Seismological Society of America*, *95*(6), pp.2506-2516.

Stokoe, K.H., Wright, S.G., Bay, J.A. and Roesset, J.M., 1994. Characterization of geotechnical sites by SASW method. *Geophysical characterization of sites*, pp.15-25.

Strobbia, C. and Cassiani, G., 2011. Refraction microtremors: Data analysis and diagnostics of key hypotheses. *Geophysics*, *76*(3), pp.MA11-MA20.

Wair, B.R., DeJong, J.T. and Shantz, T., 2012. Guidelines for estimation of shear wave velocity profiles. *PEER report*, *8*, p.95.

Xia, J., Miller, R.D., Park, C.B., Hunter, J.A., Harris, J.B. and Ivanov, J., 2002. Comparing shear-wave velocity profiles inverted from multichannel surface wave with borehole measurements. *Soil dynamics and earthquake engineering*, *22*(3), pp.181-190.

Yilmaz, O., Eser, M., Sandikkaya, A., Akkar, S., Bakir, S. and Yilmaz, T., 2008. Comparison of shear-wave velocity–depth profiles from downhole and surface seismic experiments. In *14th world conference on earthquake engineering, Beijing*.

APPENDIX SURFACE WAVE MODELS

MASW 061601, Line 1, Canton

061601-01		061601-02		061601-03	
Thickness (m)	Vs (m/s)	Thickness (m)	Vs (m/s)	Thickness (m)	Vs (m/s)
2.8	130	1.8	124	2	121
1.7	148	1.4	136	1.2	138
3.4	159	1.5	150	1.8	147
2	191	1.6	156	1.8	153
3.1	231	1.7	176	1.1	182
3.5	259	2.3	190	1.9	208
3.5	268	3	225	2.6	245
5.5	307	3.6	274	2.3	279
5.9	362	3	326	2.9	337
6.2	423	2.5	398	4	399
5.6	503	5.2	406	5.3	345
22.8	602	3.6	425	5	540
		10.8	623	10.1	619
061601-04		061601-05		061601-06	
Thickness (m)	Vs (m/s)	Thickness (m)	Vs (m/s)	Thickness (m)	Vs (m/s)
1.4	127	2	130	1.8	133
1.4	133	0.9	138	1	138
1.7	144	2.2	144	1.6	144
0.8	153	2.8	167	1.3	153
1.8	159	2	213	1.6	147
2.9	193	2.5	251	2.4	167
3.1	239	1.7	271	2.2	205
3.3	291	2.9	344	1.7	225
4.3	331	4.2	358	3.7	277
4.2	373	5.1	360	4.3	314
5.1	484	6.3	468	4.2	369
12	594	21.4	507	3.9	444
				7.3	453
				17	605
061601-07		061601-08		061601-09	
Thickness (m)	Vs (m/s)	Thickness (m)	Vs (m/s)	Thickness (m)	Vs (m/s)
2.7	144	3.4	138	2.3	101
1.9	150	0.9	150	1.9	138
1.4	156	2.6	156	3.6	147

2	159	3.1	190	3.3	193
2.2	170	2.1	219	3.7	222
2.8	208	3.3	242	5.3	226
3	251	5.2	261	4.6	282
4.3	293	5.2	328	3.6	353
5	305	3.6	424	7	428
5.5	437	4.6	444	7.7	515
5.2	455	5.5	515	5.5	584
3.9	597	14.5	442	4.7	543
14.1	677			18.8	703
061601-10		061601-11		061601-12	
Thickness (m)	Vs (m/s)	Thickness (m)	Vs (m/s)	Thickness (m)	Vs (m/s)
2.3	101	2.3	101	1.9	136
1.9	138	1.9	138	1.1	141
3.6	147	3.6	147	0.6	150
3.3	193	3.3	193	1.4	144
3.7	222	3.7	222	1	162
5.3	226	5.3	226	1.1	147
4.6	282	4.6	282	2	176
3.6	353	3.6	353	2	208
7	428	7	428	2.5	259
7.7	515	7.7	515	2.8	323
5.5	584	5.5	584	2.9	316
4.7	543	4.7	543	2.7	416
18.8	703	18.8	703	8	485

SASW 061601, Line 1, Canton

061601-01		061601-02		061601-03	
Thickness (m)	Vs (m/s)	Thickness (m)	Vs (m/s)	Thickness (m)	Vs (m/s)
1.4	144	1.3	121	1.6	143
0.4	156	0.9	150	1.7	156
0.3	176	1.1	110	1.7	121
0.5	159	2.4	162	2.6	186
1	147	4.3	236	2.6	242
1.2	170	6.6	369	6.6	279
1.7	185	6.5	502	6.7	402
2.1	210	7.5	686	10.1	524
1.8	257	7.2	845	13.1	580
2.1	261	22.2	991	16.4	814
4.6	310			38.9	1128

3.7	377				
9.2	476				
061601-04		061601-05		061601-06	
Thickness (m)	Vs (m/s)	Thickness (m)	Vs (m/s)	Thickness (m)	Vs (m/s)
2.2	145	1.8	132	1.9	106
1.7	158	4.3	150	2.6	136
3.3	180	4.1	211	3	180
6	238	6.4	282	5.4	255
6.6	374	12.9	417	6.2	365
10.2	559	15.7	683	7.6	475
20	695	22	906	11.2	545
15.9	817	34.8	999	17.1	776
36.1	1095			29	1003
061601-07		061601-08		061601-09	
Thickness (m)	Vs (m/s)	Thickness (m)	Vs (m/s)	Thickness (m)	Vs (m/s)
2.1	87	1.8	113	2.1	127
1.7	130	1.2	136	1.4	151
2.8	173	1	167	1.8	182
5	254	1.7	193	3.7	221
5.3	369	1.9	234	4.1	277
5.3	492	3	261	3.9	393
8.6	583	6.1	326	3.9	515
10.3	814	7.8	453	4.5	582
24.9	850	11.5	530	10.6	669
061601-10		061601-11		061601-12	
Thickness (m)	Vs (m/s)	Thickness (m)	Vs (m/s)	Thickness (m)	Vs (m/s)
2.1	150	1.3	147	1.5	138
1.4	167	1.4	164	2.6	151
1.5	187	2.3	196	2.3	182
1.8	210	1.6	234	2.9	236
3.1	254	2.4	288	3.9	328
2.7	314	2.1	324	6.1	459
2.5	366	2.7	354	6.5	663
4.6	414	3.6	446	6.8	775
10.3	472	3.3	591	15.4	920
		9.3	618		

ReMi 061602, Line 1, Canton

061602-01		061602-02		061602-03		061602-04	
Depth (m)	Vs (m/s)	Depth	Vs (m/s)	Depth	Vs (m/s)	Depth	Vs (m/s)

		(m)		(m)		(m)	
0.0	242	0.0	157	0.0	213	0.0	228
3.3	242	3.3	157	3.6	213	4.1	228
3.3	203	3.3	179	3.6	179	4.1	196
7.4	203	7.4	179	8.1	179	8.7	196
7.4	244	7.4	224	8.1	210	8.7	220
12.6	244	12.5	224	13.8	210	14.9	220
12.6	341	12.5	282	13.8	283	14.9	304
18.5	341	30.0	282	30.0	283	30.0	304
18.5	322						
30.0	322						

MASW 061702, Line 2, Canton

061702-01		061702-02		061702-03	
Thickness (m)	Vs (m/s)	Thickness (m)	Vs (m/s)	Thickness (m)	Vs (m/s)
1.1	185	0.7	205	1.7	222
1.1	205	1.2	222	1.2	245
0.7	236	0.9	239	1.8	234
1.3	234	1.6	219	2.8	216
2.5	236	1.1	231	3.2	228
2.8	231	1.2	222	1.5	248
1.9	211	2.5	236	2.3	288
1.6	259	2.6	271	2.8	285
1.7	277	1.6	308	3.4	347
1.5	317	3.2	352	4.6	427
2.6	328	2.8	368	7.2	491
2.1	265	10.6	442	21.5	551
3.8	308				
5	349				
12.3	449				
061702-04		061702-05		061702-06	
Thickness (m)	Vs (m/s)	Thickness (m)	Vs (m/s)	Thickness (m)	Vs (m/s)
1.8	216	0.9	208	1.5	228
0.7	239	0.8	216	1.1	236
1.2	231	1.2	236	0.6	231
2.3	216	2	219	2.7	222
2.2	228	2.1	228	1.6	210
2.6	242	1.4	222	0.6	198
1	268	3.7	236	1.1	239
2.3	287	3.6	262	0.7	231

3	290	3.8	332	1.4	236
3.1	324	4.3	418	2.2	297
9.8	435	3.4	507	2.4	326
		14.8	579	2.9	389
				2.2	447
				9	472
061702-07		061702-08		061702-09	
Thickness (m)	Vs (m/s)	Thickness (m)	Vs (m/s)	Thickness (m)	Vs (m/s)
1.1	202	1.6	219	1.4	216
0.7	228	1.6	231	2.2	234
0.9	242	1.7	225	1.5	228
1.1	234	1.5	216	1.7	210
0.7	236	1.3	222	2.5	231
2.4	228	2.8	234	2.6	262
1.2	254	2.1	248	3	297
2.1	282	2.5	294	3.2	325
1.8	295	2.2	332	3.6	406
2.2	321	3.5	327	2.7	432
3.2	391	4.3	378	2.4	432
2.4	402	3.1	471	3.7	458
3.8	453	6.6	521	17.5	646
12.4	558	13.2	532		
061702-10		061702-11		061702-12	
Thickness (m)	Vs (m/s)	Thickness (m)	Vs (m/s)	Thickness (m)	Vs (m/s)
2.1	222	1	208	1.8	212
1.3	234	1.1	216	0.5	229
1.8	231	1.4	242	0.7	247
1.5	216	1.9	222	1.9	234
2.7	208	1	210	2.2	225
1.3	231	2	202	0.8	242
2.2	268	2	239	2.1	264
1.5	256	2.2	271	2.7	285
2.7	303	2.7	332	2.4	303
4.2	329	2.4	386	4.1	347
4.9	432	5.1	416	3.3	390
3.9	542	3.6	476	2.1	429
17.9	613	9.6	598	3.5	447
				19.9	545

SASW 061702, Line 2, Canton

061702-01		061702-02		061702-03	
Thickness (m)	Vs (m/s)	Thickness (m)	Vs (m/s)	Thickness (m)	Vs (m/s)
2.1	222	2.6	216	2.4	134
1.8	231	3.1	242	2.2	177
1.7	248	3.8	294	1.6	208
3.4	225	5.1	350	4.9	242
3.1	268	8.1	467	6.6	299
2.4	293	10.6	646	6.8	415
3	352	13.4	922	5	519
2.7	432	25.3	991	5.9	586
9.8	473			18.6	811
061702-04		061702-05		061702-06	
Thickness (m)	Vs (m/s)	Thickness (m)	Vs (m/s)	Thickness (m)	Vs (m/s)
2.1	130	2.4	143	3	238
1.7	173	3.3	199	2.9	259
2	213	4	290	3.6	294
2.2	259	4.4	376	6.8	385
2.5	294	6.6	459	6	519
3.5	344	10	654	5.6	606
2.9	410	17.3	789	7.8	670
13.1	504			6.5	789
				23.8	860
061702-07		061702-08		061702-09	
Thickness (m)	Vs (m/s)	Thickness (m)	Vs (m/s)	Thickness (m)	Vs (m/s)
2.1	193	2.5	186	2.4	156
1	202	2.4	202	2.1	169
1.7	234	2.9	248	2.2	199
1.7	251	4.6	306	5.7	259
1.9	274	6.6	409	5.9	355
1.8	290	7	548	5.8	399
1.9	317	7.2	722	5.5	610
2.2	369	7.3	780	5.1	719
9.7	380	7.9	783	19.3	799
		29.6	1036		
061702-10		061702-11		061702-12	
Thickness (m)	Vs (m/s)	Thickness (m)	Vs (m/s)	Thickness (m)	Vs (m/s)
2.9	208	1.4	144	1.5	113
1.6	225	2.5	162	0.8	147

3.1	259	2.4	177	1.3	169
6.1	290	3.6	225	1.8	190
6.2	355	4	277	1.7	255
6.2	476	3.8	343	2.6	311
7.3	568	4.1	444	2.6	381
20.6	640	3.4	417	1.7	489
		3.7	558	10	511
		13.1	688		

ReMi 061701, Line 2, Canton

061602-01		061602-02		061602-03		061602-04	
Depth (m)	Vs (m/s)	Depth (m)	Vs (m/s)	Depth (m)	Vs (m/s)	Depth (m)	Vs (m/s)
0.0	173	0.0	173	0.0	164	0.0	171
5.1	173	5.1	173	4.7	164	2.6	171
5.1	211	5.1	205	4.7	196	2.6	196
13.4	211	10.6	205	8.0	196	9.3	196
13.4	251	10.6	241	7.9	290	9.3	256
20.7	251	17.1	241	17.1	290	17.1	256
20.7	215	17.1	343	17.1	261	17.1	283
30.0	215	30.0	343	30.0	261	30.0	283

MASW 080901, Line 1, Fore River

080901-01		080901-02		080901-03	
Thickness (m)	Vs (m/s)	Thickness (m)	Vs (m/s)	Thickness (m)	Vs (m/s)
1.4	78	1.3	56	2	72
1.9	114	2.2	91	3.9	130
2.6	157	3.7	134	5.1	199
3.4	209	5.2	198	6.3	283
4	278	6.3	258	6.9	372
5.7	375	6.3	305	7.3	473
11	473	8.9	441	16.5	526
		20.1	520		
080901-04		080901-05		080901-06	
Thickness (m)	Vs (m/s)	Thickness (m)	Vs (m/s)	Thickness (m)	Vs (m/s)
1.6	92	2	91	1.6	87
2.3	127	2.7	128	4.5	144
4.1	167	3.1	173	5.8	216
6.3	239	4.6	229	6.8	308

7.4	332	7.9	313	7.8	421
9.3	447	11.6	435	9.2	540
11	557	10.1	553	18.3	615
080901-07		080901-08		080901-09	
Thickness (m)	Vs (m/s)	Thickness (m)	Vs (m/s)	Thickness (m)	Vs (m/s)
1.6	69	1.6	81	1.2	65
2.8	111	2.4	133	2.3	104
3.8	164	4.6	196	3.8	144
6.2	232	6.2	268	4.7	199
6.6	311	6.2	349	5.1	270
7.6	398	8.2	455	6.8	372
13.4	481	12.8	588	12.1	487
080901-10		080901-11		080901-12	
Thickness (m)	Vs (m/s)	Thickness (m)	Vs (m/s)	Thickness (m)	Vs (m/s)
1.7	75	1.5	89	1.8	78
2.7	130	3.6	133	3.2	125
3.6	185	5.3	192	4.6	182
4	242	6.7	271	5.3	265
6.2	334	6.8	366	6.1	346
7.4	461	7.7	476	7.8	453
10.4	591	16.4	565	13.2	549

SASW 080901, Line 1, Fore River

080901-01		080901-02		080901-03	
Thickness (m)	Vs (m/s)	Thickness (m)	Vs (m/s)	Thickness (m)	Vs (m/s)
1.9	173	1.9	175	1.9	173
2.7	202	2	239	1.6	200
5.4	259	3.7	297	3.8	284
9.3	396	3.8	352	6.2	342
11.1	576	6	430	7.4	467
23.6	728	8.1	521	9.1	560
		10.5	645		
080901-04		080901-05		080901-06	
Thickness (m)	Vs (m/s)	Thickness (m)	Vs (m/s)	Thickness (m)	Vs (m/s)
2.6	228	1.7	160	1.4	115
1.9	135	1	248	2.7	156
4.3	280	4.2	158	4.2	216
4.9	398	7.5	346	5.7	306
5.5	502	6.9	443	5.9	372
5.3	591	14.7	613	6.9	499

11.5	709			9.2	591
080901-07		080901-08		080901-09	
Thickness (m)	Vs (m/s)	Thickness (m)	Vs (m/s)	Thickness (m)	Vs (m/s)
1.9	159	2	176	2.6	185
5.7	259	1.5	153	3.3	210
7.4	418	3.6	225	7	274
13.3	699	4.4	332	9.4	402
13.1	987	6.1	479	10.5	523
30.6	1264	12.4	565	12.1	689
				27.1	868
080901-10		080901-11		080901-12	
Thickness (m)	Vs (m/s)	Thickness (m)	Vs (m/s)	Thickness (m)	Vs (m/s)
1.6	127	2.5	170	2.4	196
2.3	153	1.4	205	2.8	228
3.5	225	3.1	274	3.8	334
5.8	360	3.3	339	6	476
5.4	487	5.4	470	6.2	610
7.3	581	5.5	580	8	743
16.1	696	14.8	714	18.8	848

ReMi 080902, Line 1, Fore River

080902-01		080902-02		080902-03		080902-04	
Depth (m)	Vs (m/s)	Depth (m)	Vs (m/s)	Depth (m)	Vs (m/s)	Depth (m)	Vs (m/s)
0.0	147	0.0	138	0.0	134	0.0	159
2.9	147	2.0	138	2.4	134	2.3	159
2.8	162	2.0	179	2.4	202	2.3	171
7.4	162	4.2	179	4.8	202	5.4	171
7.4	259	4.2	200	4.8	155	5.4	176
12.9	259	6.3	200	6.1	155	8.7	176
12.9	440	6.3	176	6.1	172	8.7	276
30.0	440	8.5	176	7.5	172	11.6	276
		8.5	303	7.5	189	11.6	312
		11.1	303	9.3	189	17.8	312
		11.1	387	9.3	224	17.8	355
		14.5	387	12.3	224	30.0	355
		14.5	463	12.3	380		
		18.0	463	16.5	380		
		18.0	548	16.5	474		
		23.4	548	21.6	474		

		23.4	603	21.6	525		
		30.0	603	30.0	525		
080902-05		080902-06		080902-07		080902-08	
Depth (m)	Vs (m/s)	Depth (m)	Vs (m/s)	Depth (m)	Vs (m/s)	Depth (m)	Vs (m/s)
0.0	155	0.0	140	0.0	150	0.0	144
2.3	155	1.8	140	2.7	150	2.3	144
2.3	169	1.8	162	2.7	164	2.3	164
5.6	169	4.1	162	6.3	164	6.0	164
5.6	201	4.1	191	6.3	195	6.0	246
10.1	201	9.2	191	10.8	195	12.8	246
10.1	244	9.2	247	10.8	344	12.8	292
13.7	244	15.3	247	15.8	344	21.6	292
13.7	278	15.3	324	15.8	412	21.6	327
19.1	278	23.4	324	18.5	412	30.0	327
19.1	344	23.4	450	18.5	446		
30.0	344	30.0	450	30.0	446		
080902-09		080902-10		080902-11		080902-12	
Depth (m)	Vs (m/s)	Depth (m)	Vs (m/s)	Depth (m)	Vs (m/s)	Depth (m)	Vs (m/s)
0.0	149	0.0	149	0.0	149	0.0	149
2.6	149	2.6	149	2.6	149	2.6	149
2.6	164	2.6	179	2.6	181	2.6	169
9.3	164	9.0	179	6.9	181	6.9	169
9.3	298	9.0	298	6.9	264	6.9	208
14.7	298	15.0	298	10.5	264	10.5	208
14.7	370	15.0	423	10.5	343	10.5	377
21.0	370	22.4	423	17.4	343	17.1	377
21.0	586	22.4	593	17.4	394	17.1	465
30.0	586	30.0	593	24.2	394	22.2	465
				24.2	426	22.2	554
				30.0	426	30.0	554

MASW 091801, Line 1, Fore River

091801-01		091801-02		091801-03	
Thickness (m)	Vs (m/s)	Thickness (m)	Vs (m/s)	Thickness (m)	Vs (m/s)
1.6	98	1.5	81	1.9	69
1.7	118	2.3	130	2.4	110
3.3	150	3.5	176	2.8	173
5.1	190	5.5	251	4.6	251
5.6	249	7.7	366	7.3	355

6.6	329	9.1	510	9.1	484
7	401	12.4	599	13.9	608
11.1	443				
091801-04		091801-05		091801-06	
Thickness (m)	Vs (m/s)	Thickness (m)	Vs (m/s)	Thickness (m)	Vs (m/s)
1.6	107	1.4	82	1.7	92
2.9	144	1.8	114	3.4	138
3.9	182	3.6	151	6.2	199
5.2	239	4.8	195	6.3	254
6.4	326	6.8	261	7.2	320
7.5	406	7.3	337	8.4	404
9.2	530	16.3	398	11	492
17.3	602			27.8	620
091801-07		091801-08		091801-09	
Thickness (m)	Vs (m/s)	Thickness (m)	Vs (m/s)	Thickness (m)	Vs (m/s)
1.1	64	1.8	78	2.3	69
2.2	87	3.6	136	4.1	141
4.9	124	4.8	187	4.2	182
6.9	182	6.4	271	4.3	236
6.9	244	8.2	389	6.6	306
6.8	303	9.9	516	9.1	409
13.2	343	19.3	631	9.9	490
				25.5	550
091801-10		091801-11		091801-12	
Thickness (m)	Vs (m/s)	Thickness (m)	Vs (m/s)	Thickness (m)	Vs (m/s)
1.8	71	1.9	75	2.4	84
2.7	114	2	115	2.7	130
3.9	159	3.5	162	3.7	173
4.1	202	5.2	219	4.9	231
5.1	255	6.2	306	8.1	306
7	343	7	401	9	375
7.4	418	7.6	488	11.7	458
22	477	14.6	608	23.5	527

SASW 091801, Line 1, Fore River

091801-01		091801-02		091801-03	
Thickness (m)	Vs (m/s)	Thickness (m)	Vs (m/s)	Thickness (m)	Vs (m/s)
1.4	151	1.1	123	1.4	115
3.5	236	2.3	216	4.1	190
6.3	352	6.4	339	5.1	311

10.6	542	8.8	504	7.5	502
11	778	10.8	732	7.7	692
11.7	1036	13	805	8.9	922
27.5	1250	29.6	941	13.3	1134
091801-04		091801-05		091801-06	
Thickness (m)	Vs (m/s)	Thickness (m)	Vs (m/s)	Thickness (m)	Vs (m/s)
3.3	199	1.6	117	2.2	138
4.2	285	1.4	164	3	213
10.8	369	4.7	244	4.8	334
11.7	502	6	355	7.1	513
13.8	709	7.7	469	9	692
22.3	997	8.1	636	11.5	736
35.9	1067	18.5	763	22.4	930
091801-07		091801-08		091801-09	
Thickness (m)	Vs (m/s)	Thickness (m)	Vs (m/s)	Thickness (m)	Vs (m/s)
3.1	169	2.4	199	2.4	177
6.3	277	1.9	173	2.7	247
11.3	432	4.3	268	4.7	337
14.5	608	4.7	385	6.7	467
13.6	842	8.6	566	7.9	663
12.2	973	8.2	757	8.9	911
35	1305	11.9	907	8.8	1061
				23.9	1305
091801-10		091801-11		091801-12	
Thickness (m)	Vs (m/s)	Thickness (m)	Vs (m/s)	Thickness (m)	Vs (m/s)
3.2	212	3.5	186	3.6	164
4.6	272	4.1	238	6.3	229
5.8	386	6.8	324	11.9	424
7.6	548	9.3	380	14.7	623
8.7	659	15.8	588	19.2	845
8.4	909	38.5	817	21.6	1049
21.7	1082			42.7	1385

ReMi 091802, Line 1, Fore River

091802-01		091802-02		091802-03		091802-04	
Depth (m)	Vs (m/s)	Depth (m)	Vs (m/s)	Depth (m)	Vs (m/s)	Depth (m)	Vs (m/s)
0.0	203	0.0	186	0.0	235	0.0	207
6.1	203	5.3	186	3.7	235	4.2	207
6.1	224	5.3	237	3.7	254	4.2	229

11.3	224	12.1	237	9.0	254	8.4	229
11.3	246	12.1	338	9.0	278	8.4	252
16.1	246	21.1	338	14.1	278	14.1	252
16.1	273	21.1	419	14.1	303	14.1	275
22.7	273	34.3	419	24.2	303	24.4	275
22.7	285	34.3	431	24.2	343	24.4	355
30.0	285	44.0	431	35.9	343	32.6	355
091802-05		091802-06		091802-07		091802-08	
Depth (m)	Vs (m/s)	Depth (m)	Vs (m/s)	Depth (m)	Vs (m/s)	Depth (m)	Vs (m/s)
0.0	246	0.0	213	0.0	201	0.0	186
3.3	246	6.2	213	6.2	201	4.8	186
3.3	264	6.2	242	6.2	252	4.8	234
13.9	264	12.5	242	12.5	252	12.5	234
13.9	276	12.5	341	12.5	273	12.5	290
24.2	276	22.4	341	22.4	273	24.4	290
24.2	320	22.4	383	22.4	320	24.4	366
30.0	320	32.6	383	30.6	320	36.3	366
30.0	484	32.6	423	30.6	375	36.3	1139
44.0	484	44.0	423	44.0	375	44.0	1139
091802-09		091802-10		091802-11		091802-12	
Depth (m)	Vs (m/s)	Depth (m)	Vs (m/s)	Depth (m)	Vs (m/s)	Depth (m)	Vs (m/s)
0.0	203	0.0	215	0.0	201	0.0	181
4.8	203	4.8	215	5.3	201	5.3	181
4.8	261	4.8	254	5.3	244	5.3	244
12.1	261	12.1	254	12.1	244	12.1	244
12.1	310	12.1	305	12.1	322	12.1	322
24.4	310	24.4	305	24.4	322	24.4	322
24.4	414	24.4	329	24.4	360	24.4	360
38.7	414	36.3	329	36.3	360	36.3	360
38.7	936	36.3	1166	36.3	1166	36.3	792
44.0	936	44.0	1166	44.0	1166	44.0	792

MASW 092503, Line 2, Fore River

092503-01		092503-02		092503-03	
Thickness (m)	Vs (m/s)	Thickness (m)	Vs (m/s)	Thickness (m)	Vs (m/s)
1.3	111	1.6	128	1.4	105
1.3	134	1.9	169	1.2	131
1.9	162	2.2	192	2.7	172
3.1	195	2.6	223	3.8	234

3.5	232	5.1	274	4.5	300
4.1	281	6.6	363	4.6	388
4.9	339	6	447	11.8	473
4.8	377	10	522		
17.1	450				
092503-04		092503-05		092503-06	
Thickness (m)	Vs (m/s)	Thickness (m)	Vs (m/s)	Thickness (m)	Vs (m/s)
1.8	107	3.2	144	1.3	110
2.4	138	3.1	182	1.4	137
3.8	190	6.9	236	2.7	186
5.2	259	7	311	4.8	234
8.6	349	7.5	386	4.3	291
8	453	8	481	4.6	357
8.1	516	18.3	585	4.7	421
16.1	558			6.2	481
092503-07		092503-08		092503-09	
Thickness (m)	Vs (m/s)	Thickness (m)	Vs (m/s)	Thickness (m)	Vs (m/s)
1.2	115	2	115	1.7	82
1.4	141	2.8	150	2.8	114
3.3	173	4.4	193	2.8	144
4	200	5.9	251	2.9	183
3.5	236	6.8	319	4.4	225
3.8	288	7.7	395	7.9	311
4	352	7.8	476	8	395
8.8	402	16.6	548	11.5	484
092503-10		092503-11		092503-12	
Thickness (m)	Vs (m/s)	Thickness (m)	Vs (m/s)	Thickness (m)	Vs (m/s)
1.3	117	1.3	104	1.6	107
1.6	144	2.7	144	2.2	147
2.8	176	3.9	196	3.5	199
3.9	213	3.8	251	4.7	262
3.5	251	4.8	297	4.7	311
5.1	310	4.7	366	7.8	406
5.5	378	7	447	9	492
12.3	476	19.8	502	14.5	560

SASW 092503, Line 2, Fore River

092503-01		092503-02		092503-03	
Thickness (m)	Vs (m/s)	Thickness (m)	Vs (m/s)	Thickness (m)	Vs (m/s)
5.09	227.8	4.8	232.9	4	271.9

5.41	255.3	3	273.4	3.3	228.7
5.7	438.5	3.7	240.7	2.03	158.2
10.4	554	3.9	285.4	6.27	315.9
14.9	748.6	4.8	385.5	9.7	439.7
17.3	898	5.3	461.1	11.5	579.2
20.6	1088.7	9.5	606	13.4	790.5
52.6	1388.5	19	721.4	33.8	1037.9
092503-04		092503-05		092503-06	
Thickness (m)	Vs (m/s)	Thickness (m)	Vs (m/s)	Thickness (m)	Vs (m/s)
5.7	337.4	4.16	244.8	4.7	271.9
2	195.3	3.04	297.1	5.4	170.8
5.2	278.4	4.2	368.2	7.8	438.6
9.8	447.4	5.7	512.5	9.5	526.2
9.6	594.3	8	696	13	674.7
9.7	728.6	8	917.6	12.9	872.9
15.4	999.7	20.9	1117	14.6	1016.9
26.6	1367.5			46.1	1249.2
092503-07		092503-08		092503-09	
Thickness (m)	Vs (m/s)	Thickness (m)	Vs (m/s)	Thickness (m)	Vs (m/s)
5.8	276.4	4.06	316.9	4	250.1
3.29	237.9	3.24	206	3	240.2
12.31	327.8	8.2	536.8	8.3	405.1
13.9	537.8	8.7	731.3	4.1	180.6
17.8	838.4	7.8	967.4	5.2	374.6
20.1	1054.2	8.7	1107.6	7.2	390.7
52.8	1355	25.3	1441	16.2	564
092503-10		092503-11		092503-12	
Thickness (m)	Vs (m/s)	Thickness (m)	Vs (m/s)	Thickness (m)	Vs (m/s)
6.9	263.6	5.4	265.7	4.3	258.7
5.6	188.2	5.6	321.6	4	307.7
11.2	437.4	5	384.7	4.8	377.6
10	581.9	4.93	447.4	6.4	416.5
13	682.3	6.57	499.4	12.1	507.6
13.6	851.5	6	615.2	16	660.3
41.7	1158.3	26.5	533.2	18.5	939.3
				41.9	1083.9

ReMi 092504, Line 2, Fore River

092504-01		092504-02		092504-03		092504-04	
Depth (m)	Vs (m/s)	Depth	Vs (m/s)	Depth	Vs (m/s)	Depth	Vs (m/s)

		(m)		(m)		(m)	
0.0	300	0.0	271	0.0	324	0.0	331
3.8	300	10.1	271	9.5	324	5.7	331
3.8	318	10.1	360	9.5	355	5.7	346
7.2	318	15.4	360	15.4	355	15.6	346
7.2	358	15.4	380	15.4	387	15.6	361
13.9	358	21.3	380	38.5	387	38.1	361
13.9	380	21.3	414	38.5	979	38.1	1015
21.3	380	36.3	414	44.0	979	44.0	1015
21.3	420	36.3	705				
40.3	420	44.0	705				
092504-05		092504-06		092504-07		092504-08	
Depth (m)	Vs (m/s)	Depth (m)	Vs (m/s)	Depth (m)	Vs (m/s)	Depth (m)	Vs (m/s)
0.0	302	0.0	302	0.0	307	0.0	288
5.7	302	5.7	302	5.7	307	5.7	288
5.7	363	5.7	363	5.7	346	5.7	327
13.9	363	13.9	363	13.9	346	13.9	327
13.9	380	13.9	385	13.9	423	13.9	432
23.5	380	23.5	385	23.5	423	23.5	432
23.5	407	23.5	483	23.5	490	23.5	496
39.4	407	46.8	483	46.0	490	46.0	496
39.4	838	46.8	1270	46.0	917	46.0	951
44.0	838	50.0	1270	50.0	917	50.0	951
092504-09		092504-10		092504-11		092504-12	
Depth (m)	Vs (m/s)	Depth (m)	Vs (m/s)	Depth (m)	Vs (m/s)	Depth (m)	Vs (m/s)
0.0	226	0.0	226	0.0	226	0.0	288
5.7	226	5.7	226	5.7	226	5.7	288
5.7	340	5.7	340	5.7	340	5.7	327
13.5	340	13.5	340	13.5	340	13.9	327
13.5	468	13.5	445	13.5	440	13.9	432
20.8	468	20.8	445	20.8	440	23.5	432
20.8	511	20.8	488	20.8	535	23.5	496
27.3	511	47.8	488	47.8	535	46.0	496
27.3	423	47.8	863	47.8	925	46.0	951
46.0	423	50.0	863	50.0	925	50.0	951

MASW 092505, Line 1, Winchester

092505-01		092505-02		092505-03	
Thickness (m)	Vs (m/s)	Thickness (m)	Vs (m/s)	Thickness (m)	Vs (m/s)

1.8	104	1.3	104	2.3	114
2.3	111	3.7	141	2.8	144
4.2	130	4.8	180	3.1	164
6.2	163	5.2	225	4.1	195
6.3	195	4.9	262	5	222
6.6	232	6.6	306	5.2	267
10.2	296	7.5	366	13.5	306
22.4	362	14	407		
092505-04		092505-05		092505-06	
Thickness (m)	Vs (m/s)	Thickness (m)	Vs (m/s)	Thickness (m)	Vs (m/s)
2.6	111	1.3	94	1.6	97
2.6	133	1.3	115	3	127
4	159	2.9	140	5.9	160
5.7	186	5	157	7.7	189
6.1	222	4.7	179	8.8	242
6	258	4.1	203	21	314
9	298	4.7	235		
		12	284		
092505-07		092505-08		092505-09	
Thickness (m)	Vs (m/s)	Thickness (m)	Vs (m/s)	Thickness (m)	Vs (m/s)
1.7	84	2.3	95	2	94
3.9	105	2.8	114	3.6	120
4.7	133	3.8	134	5.3	140
5.4	169	4.7	156	6.4	170
6.2	206	4.8	180	7.4	203
6.9	252	5.6	215	7.2	244
13.2	300	12	254	16.1	290
092505-10		092505-11		092505-12	
Thickness (m)	Vs (m/s)	Thickness (m)	Vs (m/s)	Thickness (m)	Vs (m/s)
1.5	88	1.2	71	1.9	69
2.3	107	1.9	88	4.2	94
3.1	127	2.5	105	3.2	127
3.3	146	4	124	6.1	160
4.4	162	5	149	6.4	199
5.4	186	6.7	179	8.2	234
16	222	6.2	218	8.3	274
		8.5	264	21.7	321

SASW 092505, Line 1, Winchester

092505-01	092505-02	092505-03

Thickness (m)	Vs (m/s)	Thickness (m)	Vs (m/s)	Thickness (m)	Vs (m/s)
3.2	82.1	4.2	178.3	1.98	142.7
4.9	117.7	2.77	199.3	8.72	193.2
6.8	141.6	3.46	227.2	18.1	320.9
9.6	249.6	4.77	252.5	28.8	524.9
10.1	328.1	5.9	328.6	32.9	810.9
19.4	419.9	7.1	391.5	83.5	1121.5
		13.8	438.7		
092505-04		092505-05		092505-06	
Thickness (m)	Vs (m/s)	Thickness (m)	Vs (m/s)	Thickness (m)	Vs (m/s)
2.8	128.4	5.4	126	2.56	80.5
2.29	167.5	6.2	157.4	1.74	110.2
5.31	210.3	8.6	187.8	4.3	139.9
10.4	256.6	11.9	290.1	10.6	194
11.7	223.3	12.8	359.4	10.3	265.7
27.5	371.7	14.7	475	18.5	340.2
		42.4	653.1		
092505-07		092505-08		092505-09	
Thickness (m)	Vs (m/s)	Thickness (m)	Vs (m/s)	Thickness (m)	Vs (m/s)
4	187.7	2.7	165.9	2.21	152.1
2.2	123.6	0.98	208.2	1.28	247.1
5.8	150.4	1.75	153	8.11	157.4
7.9	187.8	4.07	153.9	10.6	155
8.6	269.2	4.5	166.8	22.4	286.5
11.6	344.2	4.8	154.1	24.8	424.7
12	419.7	5.3	247.1	28.4	527.2
25.9	529.8	11.9	345.6	64.2	718.3
092505-10		092505-11		092505-12	
Thickness (m)	Vs (m/s)	Thickness (m)	Vs (m/s)	Thickness (m)	Vs (m/s)
4.43	197.9	2.9	181.7	2.28	173.1
10.37	183.3	3.4	170.5	1.34	204.6
18.3	337	4.8	155.1	1.92	153.4
35.5	547.3	6.8	183	2.86	143
39.5	736.1	18.7	249.6	3.8	159.4
46.1	962.4	22.7	419.9	7.9	349.4
52	1168	31.2	545.4	8.2	370.6
129.8	1420.9	59.5	695.1	25.7	468.7

ReMi 092506, Line 1, Winchester

092506-01	092506-02	092506-03	092506-04

Depth (m)	Vs (m/s)	Depth (m)	Vs (m/s)	Depth (m)	Vs (m/s)	Depth (m)	Vs (m/s)
0.0	108	0.0	107	0.0	107	0.0	113
3.6	108	3.6	107	3.2	107	3.5	113
3.6	119	3.6	117	3.2	115	3.5	120
7.4	119	7.8	117	7.8	115	8.4	120
7.4	145	7.8	137	7.8	131	8.4	135
12.8	145	13.7	137	14.4	131	11.4	135
12.8	194	13.6	181	14.4	178	11.4	172
30.0	194	30.0	181	30.0	178	18.0	172
						18.0	189
						30.0	189
092506-05		092506-06		092506-07		092506-08	
Depth (m)	Vs (m/s)	Depth (m)	Vs (m/s)	Depth (m)	Vs (m/s)	Depth (m)	Vs (m/s)
0.0	119	0.0	123	0.0	103	0.0	111
3.3	119	3.3	123	3.9	103	3.5	111
3.3	124	3.3	135	3.9	111	3.5	116
8.3	124	8.3	135	8.3	111	8.3	116
8.3	143	8.3	171	8.3	136	8.3	88
11.3	143	18.0	171	12.6	136	11.6	88
11.3	184	18.0	190	12.6	180	11.6	220
18.0	184	30.0	190	18.0	180	17.0	220
18.0	230			18.0	216	17.0	274
30.0	230			30.0	216	30.0	274
092506-09		092506-10		092506-11		092506-12	
Depth (m)	Vs (m/s)	Depth (m)	Vs (m/s)	Depth (m)	Vs (m/s)	Depth (m)	Vs (m/s)
0.0	121	0.0	106	0.0	119	0.0	116
3.0	121	3.0	106	3.0	119	3.0	116
3.0	131	3.0	110	3.0	125	3.0	125
7.2	131	7.2	110	7.2	125	7.2	125
7.2	110	7.2	117	7.2	112	7.2	108
12.0	110	12.0	117	13.2	112	12.8	108
12.0	200	12.0	187	13.2	228	12.8	172
17.0	200	17.0	187	16.8	228	16.8	172
17.0	207	17.0	226	16.8	282	16.8	206
30.0	207	30.0	226	30.0	282	30.0	206

MASW 092509, Line 1, Winchester

092509-01	092509-02	092509-03

Thickness (m)	Vs (m/s)	Thickness (m)	Vs (m/s)	Thickness (m)	Vs (m/s)
1.4	59	1.1	81	1.3	58
1.9	79	1.4	95	1.5	79
3.9	111	2.2	118	2.7	107
4.6	151	3.4	138	3.2	134
8.6	199	4.4	163	3.8	162
8.9	258	5	200	6.1	205
18.7	329	12.5	249	7.1	261
				10.3	304
092509-04		092509-05		092509-06	
Thickness (m)	Vs (m/s)	Thickness (m)	Vs (m/s)	Thickness (m)	Vs (m/s)
1.5	55	1.9	84	1.3	51
3.7	79	3.3	105	1.1	76
5.2	111	4.8	140	2.7	105
5.3	133	8.1	174	3.5	134
9	176	8.3	209	4.3	169
9.3	223	21.6	255	7.1	221
20	278			16	275
092509-07		092509-08		092509-09	
Thickness (m)	Vs (m/s)	Thickness (m)	Vs (m/s)	Thickness (m)	Vs (m/s)
1.4	71	1.6	71	2	74
1.8	91	2.5	95	2.5	100
2.7	117	3.8	120	4.5	134
5.2	147	5.3	143	6	170
6.9	179	6.1	179	6.4	213
8	222	7.5	221	6.7	264
10	278	8	277	13.9	317
		13.2	316		
092509-10		092509-11		092509-12	
Thickness (m)	Vs (m/s)	Thickness (m)	Vs (m/s)	Thickness (m)	Vs (m/s)
2.1	74	1.9	69	1.6	69
2.7	101	3.3	102	2.3	94
4.8	137	4.2	138	3	120
6.3	176	5.3	179	4.2	150
7.4	213	6.6	225	4.5	186
8.4	255	8.3	290	4.7	223
10.3	301	18.4	362	6.5	278
				15.2	339

SASW 092509, Line 1, Winchester

092509-01		092509-02		092509-03	
Thickness (m)	Vs (m/s)	Thickness (m)	Vs (m/s)	Thickness (m)	Vs (m/s)
3.7	147.5	3.07	133	3.4	150.4
1.91	112	3.97	192.2	9.2	200.8
2.49	126.9	5.16	107.7	15.1	252.9
5.4	170.1	10.4	265.7	20.1	503.4
6.9	234.4	12.6	346.1	23.2	685.1
8.7	252.1	10.8	421.9	49	887.9
18.9	294.6	32	517.3		
092509-04		092509-05		092509-06	
Thickness (m)	Vs (m/s)	Thickness (m)	Vs (m/s)	Thickness (m)	Vs (m/s)
3.5	189	4.6	138.8	4.7	159.2
2.69	105.3	5.8	147.6	10.4	156.9
4.01	152.6	14.7	220.3	15.6	218.6
2.2	121.3	13.2	360	18.2	342.2
4.7	208	11.5	421.9	18.2	398.2
4.8	267.4	22.2	510.3	26.5	511.1
14.1	313.7			38.4	661.6
092509-07		092509-08		092509-09	
Thickness (m)	Vs (m/s)	Thickness (m)	Vs (m/s)	Thickness (m)	Vs (m/s)
4.2	159.2	3.1	152.3	3.7	159
3.5	123.8	3.2	135.9	3	112.1
5.1	144.5	6.7	137.8	4.8	145.2
6.5	153	8.3	184.9	4.3	123.6
8	274.6	10.4	278.4	6.4	229.9
7.9	349.4	22.3	341.8	8.3	290.1
18.8	416.4			17.5	342.6
092509-10		092509-11		092509-12	
Thickness (m)	Vs (m/s)	Thickness (m)	Vs (m/s)	Thickness (m)	Vs (m/s)
4.3	150.4	5.8	158	5.8	155
3.8	164	4.2	144.5	7.3	133
4.6	149.7	5.7	134.7	10	150.4
9	224.5	7.5	247.6	15.5	136.5
13.9	345.9	9.2	317.3	18.3	177.2
15.2	454.3	21.6	371.7	19.2	262.3
15.5	578.2			23.3	314.7
41.7	720.1			62.6	338.4

ReMi 092510, Line 1, Winchester

092510-01	092510-02	092510-03	092510-04

Depth (m)	Vs (m/s)	Depth (m)	Vs (m/s)	Depth (m)	Vs (m/s)	Depth (m)	Vs (m/s)
0.0	132	0.0	113	0.0	121	0.0	117
4.4	132	4.5	113	6.1	121	6.3	117
4.4	143	4.5	99	6.1	107	6.3	95
8.1	143	9.9	99	8.4	107	8.3	95
8.1	124	9.9	198	8.4	128	8.3	107
10.2	124	19.8	198	11.1	128	11.4	107
10.2	112	19.8	252	11.1	226	11.4	212
12.2	112	30.0	252	19.8	226	19.8	212
12.2	309			19.8	236	19.8	218
19.8	309			30.0	236	30.0	218
19.8	383						
30.0	383						
092510-05		092510-06		092510-07		092510-08	
Depth (m)	Vs (m/s)	Depth (m)	Vs (m/s)	Depth (m)	Vs (m/s)	Depth (m)	Vs (m/s)
0.0	93	0.0	107	0.0	103	0.0	111
5.6	93	5.7	107	5.7	103	5.7	111
5.6	104	5.7	125	5.7	91	5.7	109
9.6	104	9.8	125	9.8	91	9.8	109
9.6	173	9.8	181	9.8	119	9.8	133
14.1	173	14.1	181	14.1	119	14.1	133
14.1	229	14.1	242	14.1	186	14.1	205
19.8	229	19.8	242	19.8	186	19.8	205
19.8	260	19.8	264	19.8	189	19.8	212
30.0	260	30.0	264	30.0	189	30.0	212
092510-09		092510-10		092510-11			
Depth (m)	Vs (m/s)	Depth (m)	Vs (m/s)	Depth (m)	Vs (m/s)		
0.0	145	0.0	133	0.0	164		
5.7	145	5.7	133	5.7	164		
5.7	116	5.7	107	5.7	137		
9.8	116	9.8	107	9.8	137		
9.8	127	9.8	113	9.8	131		
14.1	127	14.1	113	13.8	131		
14.1	244	14.1	190	13.8	277		
19.8	244	19.8	190	30.0	277		
19.8	310	19.8	200				
30.0	310	30.0	200				

MASW 111301, Line 2, Winchester

111301-01		111301-02		111301-03	
Thickness (m)	Vs (m/s)	Thickness (m)	Vs (m/s)	Thickness (m)	Vs (m/s)
1.9	118	2.3	125	1.8	110
2.4	147	3.2	156	2.1	138
2.6	169	4.4	187	3.2	170
4.8	200	7.2	236	4	200
6.5	255	7	285	5.1	238
6.7	319	7.6	336	6.5	293
17.1	395	10.3	388	13.3	366
111301-04		111301-05		111301-06	
Thickness (m)	Vs (m/s)	Thickness (m)	Vs (m/s)	Thickness (m)	Vs (m/s)
2	120	1.7	98	1.9	123
3.2	150	3.1	130	1.9	146
4.2	182	3.5	167	3.1	173
7.4	236	5	216	3.8	200
6.8	287	7.2	288	5.6	255
6.8	342	15.5	353	6	313
17.6	391			13.7	383
111301-07		111301-08		111301-09	
Thickness (m)	Vs (m/s)	Thickness (m)	Vs (m/s)	Thickness (m)	Vs (m/s)
1.9	125	2	124	1.5	84
1.9	149	1.9	141	2.2	118
2.9	180	3	160	3.1	150
4.1	215	3.9	213	4.1	193
4.7	261	5	251	4.1	238
4.5	303	5.4	300	4.7	287
6.5	363	14.8	355	10.3	323
9.5	435				
111301-10		111301-11		111301-12	
Thickness (m)	Vs (m/s)	Thickness (m)	Vs (m/s)	Thickness (m)	Vs (m/s)
1.8	118	2.3	130	1.1	75
1.5	147	2.2	159	2.1	107
2.5	176	2.8	183	2.9	141
4.1	218	4	229	3.6	179
4.6	275	4.4	283	4.2	231
4.9	334	4.4	340	5.8	294
10.6	389	9.9	393	6	369
				16.3	454

SASW 111301, Line 2, Winchester

111301-01		111301-02		111301-03	
Thickness (m)	Vs (m/s)	Thickness (m)	Vs (m/s)	Thickness (m)	Vs (m/s)
2.2	150	3.7	154	2.6	153
2.6	191	2.6	178	3.3	187
4	264	3.6	248	4.5	236
8	305	4.1	288	4.6	294
9.3	399	5.2	343	5.6	359
14.4	593	10.4	406	6.4	471
19.9	682	12.4	488	10.8	591
23.1	998			22.2	783
42.5	1052				
111301-04		111301-05		111301-06	
Thickness (m)	Vs (m/s)	Thickness (m)	Vs (m/s)	Thickness (m)	Vs (m/s)
3.7	170	1.9	126	3.4	173
3.6	212	3	173	3.4	190
4.1	262	3.4	241	5	271
7.4	317	7.2	329	9.4	337
7.5	421	6.7	409	9.2	424
9.8	542	10.1	499	7.7	498
12	566	27.7	593	15.9	587
15.9	682				
38	969				
111301-07		111301-08		111301-09	
Thickness (m)	Vs (m/s)	Thickness (m)	Vs (m/s)	Thickness (m)	Vs (m/s)
3.1	147	3.8	167	3.5	161
2	165	3.1	187	2.2	158
3.5	228	4.8	231	1.4	170
8.1	296	7.7	291	2.8	192
11.2	383	8.8	401	3.1	191
14.1	462	9.9	516	3.2	231
		15.9	631	4.9	281
				14.9	347
111301-10		111301-11			
Thickness (m)	Vs (m/s)	Thickness (m)	Vs (m/s)		
2.4	134	3.2	147		
2.8	169	3.1	190		
6.5	268	4.5	242		
9.7	398	5	291		
15	627	4.5	360		
16.3	848	6.2	441		

31.3	912	15.5	515

ReMi 111302, Line 2, Winchester

111302-01		111302-02		111302-03		111302-04	
Depth (m)	Vs (m/s)	Depth (m)	Vs (m/s)	Depth (m)	Vs (m/s)	Depth (m)	Vs (m/s)
0.0	122	0.0	147	0.0	172	0.0	133
3.3	122	2.6	147	2.4	172	3.8	133
3.3	134	2.6	167	2.4	188	3.8	160
5.6	134	5.6	167	5.6	188	7.0	160
5.6	193	5.6	192	5.6	227	7.0	238
8.9	193	10.1	192	9.8	227	12.0	238
8.9	279	10.1	268	9.8	266	12.0	272
20.1	279	20.1	268	25.0	266	24.2	272
20.1	310	20.1	290	25.0	557	24.2	503
30.0	310	30.0	290	32.0	557	34.0	503
30.0	1061	30.0	1235	32.0	674	34.0	653
44.0	1061	30.0	1235	40.0	674	40.0	653
44.0	1235						
30.0	1235						
111302-05		111302-06		111302-07		111302-08	
Depth (m)	Vs (m/s)	Depth (m)	Vs (m/s)	Depth (m)	Vs (m/s)	Depth (m)	Vs (m/s)
0.0	133	0.0	133	0.0	133	0.0	137
3.8	133	3.8	133	3.8	133	3.8	137
3.8	160	3.8	160	3.8	160	3.8	160
7.0	160	7.0	160	7.0	160	7.0	160
7.0	193	7.0	193	7.0	217	7.0	247
13.4	193	13.4	193	11.8	217	12.6	247
13.4	307	13.4	327	11.8	317	12.6	366
22.6	307	25.4	327	29.0	317	25.6	366
22.6	319	25.4	341	29.0	360	25.6	417
34.6	319	38.4	341	37.2	360	35.0	417
34.6	868	38.4	972	37.2	589	35.0	707
40.0	868	40.0	972	40.0	589	40.0	707
111302-09		111302-10					
Depth (m)	Vs (m/s)	Depth (m)	Vs (m/s)				
0.0	135	0.0	133				
3.8	135	3.6	133				
3.8	162	3.6	159				

7.0	162	6.8	159
7.0	247	6.8	224
12.6	247	13.4	224
12.6	331	13.4	290
25.6	331	25.6	290
25.6	387	25.6	373
36.2	387	35.0	373
36.2	625	35.0	853
40.0	625	40.0	853

Downhole Vs profile, Line 1, Canton

depth(m)	Vs(m/s)
0	0
1.5	259
3.0	244
4.6	183
6.1	183
7.6	183
9.1	201
10.7	238
12.2	238
13.7	238
15.2	274
16.8	238
18.3	274
19.8	274
21.3	274
22.9	274
24.4	274

Crosshole1 Vs profile, Line 1, Canton

depth(m)	Vs(m/s)
0	0
1.5	245
3.0	136
4.6	154
6.1	159
7.6	187
9.1	201

10.7	216
12.2	184
13.7	225
15.2	257
16.8	283
18.3	258
19.8	229
21.3	290
22.9	300
24.4	283
25.9	262
27.4	233
29.0	231
30.5	307
32.0	575
33.5	2023
35.1	2131
36.6	3465
36.6	4166

Crosshole2 Vs profile, Line 1, Canton

depth(m)	Vs(m/s)
0	0
0.9	232
2.1	228
3.0	208
4.0	251
4.9	165
6.1	186
7.0	209
7.9	281
9.1	255
10.1	277
11.0	283
11.9	340
13.1	322
14.0	405
14.9	461
15.8	316
17.1	431

18.0	423
18.9	382
20.1	349
21.0	321
21.9	257
22.9	267
24.1	329
25.0	482
25.9	469
27.1	435
28.0	459
29.0	468
29.9	494
31.1	575
32.0	542
32.9	840
34.1	493
35.1	518

SCPT Vs profile, Line 1, Canton

depth(m)	Vs(m/s)
0	0
3.0	292
4.5	191
6.0	168
7.5	162
9.0	194
10.5	236
12.0	228
13.5	215
14.5	231
16.5	240
18.0	266
19.5	255
21.0	268
22.5	292
24.0	304
25.5	253
27.0	265
28.5	251

30.0	265
31.1	433

SCPT Vs profile, Line 2, Canton

depth(m)	Vs (m/s)
0	0
3.0	276
4.5	245
6.0	176
7.5	191
9.0	180
10.5	185
12.0	255
13.5	244
15.0	256
18.0	279
21.0	261
24.5	293

Crosshole Vs profile, Fore River

depth(m)	Vs(m/s)
0	288
1.5	288
3.0	221
4.6	191
6.1	189
7.6	251
9.1	229
10.7	179
12.2	196
13.7	183
15.2	186
16.8	153
18.3	213
19.8	232
21.3	255
22.9	208
24.4	243
25.9	230

27.4	249
29.0	265
30.5	276
32.0	261
33.5	339
35.1	410
36.6	648
38.1	542
39.6	581
41.1	586
42.7	657
44.2	552
45.7	592
47.2	629
48.8	546
50.3	739
51.8	1479
53.3	1477
54.3	1723
54.9	1374

SCPT Vs profile, Fore River

depth(m)	Vs(m/s)
2.4	179
3.4	179
4.4	157
5.4	218
6.3	191
7.3	228
8.3	336
9.3	249
10.3	239
11.3	228
12.3	244
13.3	291
14.3	269
15.3	224
16.3	199
17.3	281
18.3	222

19.2	284
20.2	251
21.2	213
22.2	203
23.2	196
24.2	321
25.2	333
26.2	302
27.2	267
28.2	355
29.2	292
30.2	386
31.2	280
32.1	422
33.1	374
34.1	369
35.1	369
36.1	374
37.1	386
38.1	309
40.1	343
41.1	294
42.1	464
43.1	378
43.8	480